GE Research &
Development Center

Specific Anion and Corrosion Potential Effects on Environmentally Assisted Cracking in 288°C Water

P.L. Andresen

Physical Metallurgy Laboratory
93CRD215, December 1993

Class 1

Technical Information Series

Corporate Research and Development

Technical Report Abstract Page

Title	Specific Anion and Corrosion Potential Effects on Environmentally Assisted Cracking in 288°C Water		
Author(s)	P.L. Andresen	**Phone**	(518)387-5929 8*833-5929
Component	Physical Metallurgy Laboratory		
Report Number	93CRD215	**Date**	December 1993
Number of Pages	71	**Class**	1
Key Words	stress corrosion cracking, stainless steel, high temperature water, water chemistry, anion effects, corrosion potential, mechanisms, crack chemistry		

This report summarizes the environmentally assisted cracking data, experimental and analytical modeling of crack chemistry, and fundamental understanding and prediction of the effects of water chemistry on crack growth in high temperature BWR water. Corrosion potential is shown to be of fundamental importance, in that it properly accounts for the varying crack growth response to a range of oxidant and reductant concentrations. Since cracks and crevices create a deaerated, low potential environment, an elevated (external) corrosion potential creates a difference in potential from crack mouth to tip which causes anion concentration within the crack, as well as pH shifts (often acidic). A potential gradient is not essential to high crack growth rates since they can be observed in fully deaerated water if, e.g., the environment is sufficiently acidic. Thus, most cracking "*thresholds*" (e.g., *threshold* potential) are not absolute, but applicable only to a specific set of material, water chemistry, and loading conditions.

The role of anion specificity appears to be primarily related to the ability of an anion to shift pH within the crack since, e.g., SO_4^{2-} provides the charge balance necessary to support the elevated H^+ activity which defines acidity. Shifts to high pH are also possible and deleterious; in this instance, cations (e.g., dissolved species such as Ni^{2+} or impurities such as Na^+) are necessary to provide charge balance for the excess OH^-. The thermodynamic and kinetic stability of species in the deaerated crack is important since, e.g., chromate can reduce to chromia. Complexing may also occur. In certain pH and potential regimes, repassivation can be impeded by sulfide formation and adsorption, both in high alloy and low alloy materials.

The crack chemistry that forms interacts with the crack tip material to cause a specific crack growth rate. Thus, identical crack growth rates can be achieved in, e.g., non-sensitized stainless steel as in sensitized stainless steel if a somewhat more aggressive water chemistry is used. The crack chemistry issues are similar for high alloy (304/316 stainless steel and Alloy 600/182/82) and low alloy / carbon steels, although the latter are strongly influenced by dissolution of MnS in the crack. The crack growth response of these BWR structural materials varies, although their sensitivity to water chemistry is strongly a function of Cr content.

Manuscript received November 10, 1993

Specific Anion and Corrosion Potential Effects on Environmentally Assisted Cracking in 288°C Water

Peter L. Andresen

Mechanism of Crack Advance

The slip oxidation mechanism is widely recognized as providing the best quantitative explanation of environmentally assisted crack advance in ductile alloys in hot water [1-5]. In this mechanism crack advance is related to dissolution (separated anodes and cathodes) or (direct chemical) oxidation reactions at the crack tip where a thermodynamically stable oxide is ruptured by increasing strain in the underlying matrix (Figure 1). The film rupture rate is related to the strain rate in the metal matrix, which is controlled by creep processes under constant load or applied strain rates under monotonically increasing or cyclic load conditions. Equation 1 relates the average crack velocity, V_t, to the crack tip strain rate, $\dot{\varepsilon}_{ct}$, where A and n account for the material and environment at the crack tip:

$$\overline{V}_t = A\,(\dot{\varepsilon}_{ct})^n \qquad (1)$$

Various important issues have been discussed previously [1-5], such as (1) the limits to the validity of this relationship, e.g., at high crack tip strain rates ($\approx 10^{-2}$ s^{-1}) where a bare surface is continuously maintained; (2) the contributions of the mechanical component of crack advance under cyclic loading; (3) the effects of crack blunting and crack branching, etc. The model has been quantified for the steady state and transient compositions of the environment at the crack tip as a function of the conditions in the bulk (external) solution; the oxidation rates for the material/environment system expected at a strained crack tip; and the oxide fracture strain and the crack tip strain rate, defined in terms of engineering parameters such as K, ΔK, R, frequency, etc. These issues have been discussed in detail elsewhere for stainless steels [1-5], low alloy and carbon steels [1-8], ductile nickel alloys [2-4,9-11], and irradiated stainless steels [12-13]. Additionally, short crack behavior and the transition to long crack behavior [14], concerns for crack chemistry similitude [14], treatment of thickness- and time-varying properties, and treatment of distributions in properties and statistical approaches [1-13] have also been addressed. Finally, the validity and practical use of a prediction model has been summarized for various materials and components [1-14].

Mechanism of Water Chemistry Effects on Crack Advance

The result of predictive modeling is the ability to accurately account for the isolated, individual effects, e.g., of stress intensity (Figure 2), corrosion potential (Figure 3), and solution conductivity (Figure 4), as well as their interactions (Figure 5). These figures all show pronounced effects on environmentally assisted cracking in stainless steel of water chemistry; similar effects are observed in nickel-base alloys (Figures 6 and 7). If the effects of water chemistry and material condition are not accounted for, there is an enormous spread in the data (Figure 8).

These laboratory observations on the importance of water chemistry are also reflected in incidence of stress corrosion cracking in plant components (Figures 9 and 10).

The effects of various water chemistry parameters on environmentally assisted cracking can be understood in terms of the crack chemistry (primarily pH) and the contribution to ionic mass transport in the crack of variables such as corrosion potential, conductivity (anion activity), flow rate, etc. (Figure 11). The steady state and transient crack chemistry can be determined in terms of the competition among the three components of liquid mass transport: ordinary diffusion, potential driven ion migration, and convection:

$$J_i = -D_i \cdot \nabla C_i - Z_i \mu_i F C_i \cdot \nabla \phi + C_i \cdot V \qquad (2)$$

where J_i is the flux, D_i is the diffusion coefficient, C_i is the activity, Z_i is the charge per ion, μ_i is the ionic mobility, F is Faraday's constant, $\nabla\phi$ is the potential gradient, and V is the velocity (convection) field.

The effects of differences among iron- and nickel-base structural alloys on these mass transport processes are small, since they often exhibit similar corrosion potential behavior. For a given crack chemistry, the crack growth rate varies with Cr content (and other parameters), as will be discussed later. Also, the MnS inclusions in low alloy and carbon steel dissolve and have a strong influence on the crack chemistry and crack growth rates. The role of various parameters in creating crack chemistry and influencing environmentally assisted crack growth rates is summarized below.

1. **Corrosion potential** is known to be a more fundamental parameter than oxidant/reductant concentrations, since it properly accounts for the wide ranging response to different oxidant and reductant concentrations (Figure 12), including under irradiated conditions. This is demonstrated most clearly in the crack growth rate data on specimens coated or alloyed with noble metals [15] (Figure 13) where the changes in growth rate parallel the shifts in corrosion potential, not the dissolved oxygen concentration.

Note that the term *electrochemical potential* is occasionally used to represent the corrosion potential. A *corrosion potential* is a mixed potential representing a kinetic balance of 2 or more anodic and cathodic reactions. An *electrochemical potential* is for a single, half cell reaction (e.g., $O_2 + 2H_2O + 4e^- = 4OH^-$), and can represent the standard potential for a single reaction, the reversible potential (i.e., including the effects of temperature, fugacity and activity of various species, etc.), and polarization behavior (e.g., from activation (Tafel) or concentration polarization of a reaction).

2. **Potential gradient in the crack.** Since dissolved oxygen is very efficiently reduced in cracks and crevices in high temperature water, a low potential, deaerated environment exists (even in high irradiation fluxes). This creates the difference in potential from crack mouth to tip that causes anion concentration, as well as pH shifts (often acidic), within the crack. Estimates from crack simulation experiments (Figure 14) and analysis of cracking data (in which the tradeoff between dissolved oxygen and conductivity is evaluated) show that in reasonably pure water the crack tip anion concentration is increased by ≈30X at a corrosion potential of ≈0 V_{she} (the crack tip potential in water of at least moderate purity (<1 μS/cm) is ≈ –0.5 V_{she}):

$$C_{ct} \approx C_{ext} \cdot (10)^{\frac{\Delta\phi}{0.4}} = C_{ext} \cdot (316)^{\Delta\phi} \quad (3)$$

where the external anion activity (solution conductivity), C_{ext}, is increased to crack tip anion activity, C_{ct}, condition by a factor that is exponentially related to the potential difference, $\Delta\phi$, from crack mouth to tip. Material dependencies among iron- and nickel-base alloys are generally small, since the $\Delta\phi$ values are similar.

This interaction between the external (crack mouth) corrosion potential and the external solution conductivity to create a specific crack chemistry has also been demonstrated in crack growth measurements. These analyses rely on the realistic assumption that the observation of similar crack growth rates (under identical loading conditions) implies similar crack chemistries. In fully deaerated (e.g., sulfate) environments, accelerated crack growth rates (equivalent to those in aerated solutions) can be achieved if the impurity level is elevated by 20 to 50X above that used in the aerated tests (Figures 15 - 17).

Thus, the rate at which cracks grow is controlled by the crack chemistry not, e.g., by the external potential per se, and a given crack chemistry can be achieved by different combinations of potential and conductivity; i.e., a high potential, moderately low conductivity condition can give the same crack chemistry as a very low potential, but high conductivity environment.

Another way to view this interaction is that lower corrosion potentials not only decrease the crack growth rates but also provide an increasing tolerance to impurities. For example, Figure 18 shows no increase in growth rate at 10 μM H_2SO_4 (8.9 μS/cm) at a corrosion potential of -0.5 V_{she}; this is a dramatic increase in tolerance to impurities compared to the pronounced effect of much lower H_2SO_4 concentrations shown in later figures (e.g., Figures 26 and 28).

This, coupled with the observations of high growth rates in deaerated water presented above, provides evidence that crack tip dissolution reactions are primarily coupled to *local* cathodic reactions, not to the cathodic oxygen reduction reactions at the crack mouth, since this would require than the ionic dissolution current (e.g., Ni^{2+} and OH^-) flow over the entire length of the crack. While ionic currents clearly flow in the crack and cause a more concentrated, pH-shifted chemistry, there is no requirement that *crack growth* be limited to or directly controlled to a highly physically separated cathodic reaction site. Additionally, in the high resistivity crack solution, the amount of ionic current that would have to flow to account for the full range of observed crack growth rates would require very large potential gradients in the crack (on the order of hundreds or thousands of volts). These concepts and observations contradict proposed models of crack advance that are based on electrochemical reactions that are coupled from crack tip to crack mouth [16].

3. **The pH of the crack solution**, not the anion activity per se, apparently controls the environmental cracking response. While high crack growth rates can be achieved in fully deaerated water provided the pH is shifted sufficiently (Figures 15 - 17), Kassner has shown that this is not observed if neutral or slightly basic impurities (e.g., Na_2SO_4) are used [17-18]. This is expected only if pH is important, since the sulfate activity is unchanged. Note that under *aerated* conditions, neutral impurities can affect crack growth rate because, in addition to anion concentration, the potential gradient causes acidification (or alkalinization). Kassner also showed that, in buffered mixtures of borate and sulfuric acid, that intergranular cracking and high crack growth

rates were observed if the solution was acidic, but as the borate to sulfate ratio was changed and the pH increased, no intergranular cracking was observed (Figure 19).

While most emphasis has been on acidification, high crack growth rates can also occur if the pH is raised (Figure 20). The effect of corrosion potential in concentrating OH^- in the crack is similar to any other anion. However, the net effect of a potential gradient in producing a high pH crack chemistry is lessened by the potential driven migration of cations out of the crack. In the presence of, e.g., Na_2SO_4, this causes acidification, since the Na^+ moves out of the crack under the potential gradient and is displaced by a constant source of H^+ (from metal dissolution and hydrolysis, i.e., $Ni^{2+} + 2H_2O \rightarrow NiOH + 2H^+$) in the crack. However, for an *increase* in pH to occur, there must be a corresponding increase in the concentration of a non-H^+ cation to provide charge balance for OH^-, just as there must be a non-OH^- anion present for acidification to occur (if only H^+ and OH^- are present, the solution remains at neutral pH).

Because the potential gradient acts to drive cations out of the crack, the ease with which the concentration of OH^- can be increased in the crack is more limited than for acidification. For acidification, the potential gradient acts on anions (e.g., Cl^- into the crack) and cations (e.g., Na^+ out of the crack) to maximize the pH shift. However, for alkanization, the potential gradient has counteracting effects; i.e., it drives OH^- anions into the crack, but drives the non-H^+ cations (e.g., Na^+, required to sustain an alkaline pH shift) out of the crack. Detailed analysis of this situation must account for differences in mobility between the cations and OH^-, as well as the contribution of metal dissolution and metal ion solubility vs. pH (metal ions become more soluble with increasing pH above a certain value, Figure 21).

4. **Oxide solubility.** The effect on crack growth rate of crack chemistry (pH) best correlates with the effects on oxide solubility (Figure 21). In neutral water at lower temperatures, metal oxide solubilities are not as low as at high temperature, and water chemistry effects are much less pronounced below than above about 200°C [19], as will be discussed later. In addition to explaining the effects of temperature, oxide solubility also explains the effects of increased crack growth rate as the pH is either raised or lowered, since the oxide solubility increases in both cases.

5. **The role of anion specificity** can be primarily related to the ability of a given anion to support pH shifts within the crack. Anions such as Cl^- or SO_4^{2-} provide the charge balancing capability required for increased activity of H^+ (acidification). Anions such as nitrate and chromate are not thermodynamically stable in the low redox potential environment in a crack (Figure 22), and thus should not have an effect on crack tip pH or growth rates. This is observed for nitrate (Figure 23), although it appears that moderate chromate levels (as additions or releases from stainless steel surfaces) may affect crack growth rates (Figure 24). This may occur because of kinetic limitations in reducing chromate to chromia as in sulfate environments, which should reduce to HS^- at low potentials (in deaerated water), but apparently do not do so to any appreciable extent.

The anion specificity issue is complicated by other factors than thermodynamic and kinetic stability of species in the low redox potential crack. Chloride and fluoride are probably complexing agents in high temperature water; when complexed, the effective "solubility" of metal "ions" increases, despite the lack of an actual increase in metal ion activity, as would occur,

e.g., from a shift in pH. Another complicating factor is the possible effects of oxidizing anions (e.g., nitrate or chromate) on the corrosion potential. The buffering capability of species like borate, phosphate, and carbonate must also be taken into account.

In certain pH and potential regimes, repassivation can be impeded or completely prevented by sulfide formation and adsorption, both in high alloy (Figure 25) and low alloy materials [20]. This appears to be limited to higher pHs (and thus lower potentials) than is typical of BWR operation, and correlates with the formation of S^{2-} (Figure 22).

Based on available crack growth rate data [1-10,17-19,21-29], the effects of sulfate (Figures 26 and 27) and chloride (Figures 28 and 29) can be considered of similar aggressiveness, while fluoride (Figure 30), phosphate (Figure 31), and carbonate (Figure 32) are somewhat less so, and chromate (Figure 24) even less so. Nitrate (Figure 23) appears not to be harmful. Non-ionic species, such as silica (which ionizes in water only to about 1% [30]), have little effect on crack growth (Figure 33).

6. **The minimum anionic level** that should have an effect on crack chemistry and growth rate is related to the concentration of OH^- in neutral water (assuming the impurity is being added to pure water). In 288°C water, the activity of OH^- is 2.34×10^{-6} M. Under the action of a potential gradient, there will be a continuous migration of anions (OH^- and, e.g., Cl^-) into the crack, (also cations out of the crack), and at steady state a counter-balancing flow of anions out of the crack by ordinary diffusion (where the flux is a function of the anion activity gradient). Dissolution in the crack / crevice (even without crack growth) of iron- and nickel-base alloys in high temperature water, followed by hydrolysis ($Ni^{2+} + 2H_2O \rightarrow NiOH + 2H^+$), provides a continuous source of H^+ in the crack; thus (in moderately pure water) the OH^- which migrates into the crack largely recombines with H^+ (although even in pure water, some is charge balanced by the limited solubility of metal cations). Thus, much of the ionic current in the crack is carried mostly by OH^- moving into the crack, and H^+ moving out of the crack; these species recombine in the crack to maintain the dissociation constant of 288°C water of 5.5×10^{-12}, and one of them can increase in concentration only if some non-OH– or non-H^+ species exists to maintain charge balance in the solution.

Even at low concentrations, non-OH^- anions (such as Cl^-) migrate into the crack and are able to provide charge balance for excess H^+. To date, there has been no analytical modeling performed to identify what this *''threshold''* anion concentration is, but it should be related to the OH^- activity in water on the basis of ''charge carrying capability'' (or normality - not molarity, and certainly not ppb or conductivity). Crack micro-sampling techniques for direct determination of crack chemistry are just being developed [22], and are long overdue.

Crack growth observations [21-32] (Figures 26 - 35) indicate that impurity concentrations below 10^{-7} N are important; this corresponds (Table 1) to 4.8 ppb sulfate (10^{-7} N equals 0.5×10^{-7} M H_2SO_4), 3.6 ppb chloride, and 2.0 ppb fluoride. More importantly, analyses of BWR component data (Figures 9 and 10) show a strong effect of conductivity (specific anions were not measured) on environmental cracking of various BWR components. While the response shown in Figure 9 suggests that cracking doesn't occur at conductivities below about 0.2 μS/cm, it's clear that lower conductivity merely extends the time required for cracks to reach a specific, detectable depth, as indicated in Figure 10.

7. **Caveats to Anion Specificity and Minimum Anion Level.** There are a variety of caveats that must be recognized in evaluating the experimental data on the effects of impurities. First, most experiments have been performed using SSRT specimens, which is an accelerated test that can be insensitive to subtle impurity effects. Additionally, few experiments have been performed under well controlled conditions, i.e., corrosion potential measured and constant during the test and from test-to-test; unnotched specimens; excellent *''background''* water purity (the effect of 10^{-7} N chloride is difficult to identify or interpret if the outlet autoclave water contains 10^{-6} N of other impurities); etc.

Even with highly controlled water chemistry and using CT specimens instrumented for continuous, high resolution crack monitoring, evaluation of impurity effects is complicated by the ability to reproduce the corrosion potential and perhaps subtleties of solution chemistry, as well as the resultant crack growth rates. In particular, the crack growth rate of highly susceptible (e.g., sensitized type 304 stainless steel) in pure water at typical BWR corrosion potentials (e.g., 0 to +0.15 V_{she}) can be particularly difficult to reproducibly establish. Andresen has observed that in *ultra high purity water* (i.e., <0.07 μS/cm outlet conductivity), the crack growth rate can be unaffected by potential (at least between −0.5 V_{she} and ≈ 0.1 V_{she}) in some instances (Figure 36), but in other cases (even on nominally identical materials), the crack growth rate can increase significantly on shifting from −0.5 V_{she} to ≈ 0.1 V_{she} (Figure 37).

In one instance careful studies were performed to evaluate this phenomenon, and Andresen found that fairly small changes in water chemistry and corrosion potential could give rise to moderately large changes in crack growth rate, especially if sufficient time was given for the higher rate to appear and stabilize (Figure 37). Apparently, the potential gradient causes the crack solution pH to increase with time, causing higher crack growth rates; in ultra high purity water, acidification is not possible. This suggests that some of the earlier work on impurity effects [21] may over-state the effect of impurities on crack growth rate. It also makes interpretation of the existing data and the specification of optimal experimental procedures difficult.

This ambiguity applies primarily to susceptible materials like sensitized type 304 stainless steel and perhaps sensitized Alloy 600 and Alloy 182 weld metal, since relatively small changes in crack chemistry are required to influence crack growth. No similar difficulties were observed for non-sensitized type 304/316 stainless steel [21,22], where crack growth rate effects are only observed at moderately high conductivity (Figures 27 and 29).

8. **Transient response** to shifts in impurity level is also important since changes in the solution conductivity in operating plants typically represents the single largest variation among plant operating parameters that control environmental cracking. If an anionic impurity is introduced into the external solution, it will move into the crack via ordinary diffusion and potential-driven migration according to Equations 2 and 3. Under typical BWR conditions, the extent of its concentration in the crack is limited to 20 to 50X (Equation 3), as discussed previously.

Both experimental measurements and analytical modeling confirm that this process is reversible, i.e., that if the impurity is removed from the external solution, its concentration in the crack will decrease to zero (except perhaps for chemical entrapment or incorporation into the oxide films). If the corrosion potential is also decreased, a rapid decrease in impurity concentration in the crack and in crack growth rate is observed (Figures 26 - 32). If the corrosion potential is

maintained constant (as is typically the case), then the diffusion of the impurity from the crack is slower, and the crack growth rate decreases more slowly. Other examples, and a more detailed discussion of this issue, are presented in references [1-5,30,31]. This has also been observed in specimens exposed to BWR recirculation water; an example is shown in Figure 38.

Thus, elevated solution conductivity does not cause a permanent increase in crack growth rate, although it does have a short term effect that persists longer than the external conductivity transient (the time required to return to the original crack growth rate is longer than the time required to achieve an elevated crack growth rate). If particularly severe conductivity transients occur early in life (in one instance, to 50 μS/cm), its effect on cracking becomes quite pronounced relative to its effect on average plant conductivity (Figure 9), since cracks can nucleate early in life and grow to depths where relatively high stress intensities exist that can cause continued growth at moderate rates after the conductivity decreases.

9. **Temperature** has a strong effect on environmental cracking (Figures 39 and 40) [19], and evaluation of the literature data shows that impurity effects are particularly pronounced above ≈150 to 200°C. This corresponds to the temperature where the temperature activated response of crack growth deviates from linearity, with the crack growth rate in very pure water peaking at ≈150 to 200°C, then decreasing precipitously above 250 to 280°C. This has been attributed to the increasingly dominant effect of (low) metal oxide solubility with temperature. Indeed, if the water chemistry is sufficiently poor (so that oxide solubility is no longer a limiting factor due to the acidify of the crack tip solution), the apparent activation energy of ≈10 kcal/mole observed at lower temperature extends to temperatures above 300°C (Figure 40).

10. **"Thresholds".** The broad use of the concept of a "threshold" is misleading because these values are inter-dependent values which are not absolutes, but apply only for a very limited, specific set of material, water chemistry, and loading conditions. For example, a commonly used *threshold* potential of –0.3 V_{she} clearly does not apply if a sufficient high concentration of acidic impurity is present (Figures 15 - 17).

11. **A material - environment interdependence** exists, in that a specific crack chemistry and crack tip material combine to cause a specific crack growth rate. For example, identical crack growth rates can be achieved in, e.g., non-sensitized stainless steel as in sensitized stainless steel if a somewhat more aggressive water chemistry is used (Figure 4, also Figures 26 - 29). Expressed differently, the tolerance to impurities changes with material; in particular, higher Cr level (especially above ≈18%) give a greatly increased tolerance to impurities (Figure 41). This is particularly clear when comparing the crack length vs. time response of sensitized (Figures 26 and 28) vs. non-sensitized (Figures 27 and 29) stainless steel. Thus, the combination of more resistant (e.g., non-sensitized and/or higher Cr) materials and the shift to lower corrosion potentials can greatly increases the tolerance to BWR impurities.

The crack chemistry that forms under specific water chemistry conditions is apparently not strongly influenced by the type of material (sensitized and non-sensitized stainless steel, nickel-base alloys and weld metals, or carbon and low alloy steels), since they exhibit *similar* corrosion potentials (both inside and outside the crack) in high temperature water, and the mass transport processes and kinetics are identical. The subsequent crack growth rate response varies with material, and appears to vary most strongly with the Cr content of the material. Thus, sensitized

type 304 stainless steel and sensitized Alloy 600 or 182 weld metal exhibit similar crack growth rates and sensitivity to water chemistry, while non-sensitized type 304/316 stainless steel, non-sensitized Alloy 600, and Alloy 82 weld metal are less susceptible under the same conditions.

12. **Crack Initiation vs. Crack Growth.** There is very little data on crack initiation, per se, in high temperature water. Indeed, it is recognized that crack initiation is inherently linked to an arbitrary value of crack detectability, which might be 10 to 15% of wall thickness for ultrasonic inspection, to perhaps a 0.1 mm by periodic visual examination, to about 1 to 10 μm by continuous potential drop monitoring. Since long crack / crevice chemistries develop even in very short cracks [14], the behavior of even very small cracks can be similar to long cracks. Much of "initiation" data were obtained by slow strain rate testing, where both initiation (short crack) and crack growth are important.

Andresen [33] performed interrupted SSRT experiments on sensitized stainless steel, and observed that strain- or time-to-crack initiation was lower in acidic environments than in neutral or slightly basic environments (Figure 42). This is consistent with the crack growth data (discussed earlier, e.g., Figure 19) in that pH is important; in the absence of an acidification (or, more generally, pH shifting) mechanism (as would be the case if no crack exists), the crack growth data also show little or no effect of neutral or slightly basic impurities (e.g., Na_2SO_4, but do show an effect of acidic impurities (e.g., H_2SO_4). Note that since oxide rupture controls environmental crack advance, initiation and growth can occur by the same processes, although rates of oxide rupture and the local chemistry vary.

The effects of exposure to aggressive chemistry, especially early in life, can be very significant. Figure 9 shows that the incidence of cracking is much higher (than indicated by using *average* conductivity) in instances where large conductivity transients occurred. Similarly, Figure 43 shows that exposure to impure water shifts the initiation of cracking by many order of magnitude in time.

13. **Mechanical loading** controls environmentally assisted cracking by altering the rate at which the protective oxide is ruptured at the crack tip. Formulations have been developed to relate the applied strain rate in SSR tests, stress intensity in SCC tests, and stress intensity amplitude, frequency, and load ratio in corrosion fatigue tests [1-13]. One important influence of variations in loading is that the difference in response (or factor-of-improvement) observed for changes in material or water chemistry will be dependent on the loading conditions. Figure 2 shows the divergence at low stress intensity for difference water chemistry conditions, which would apply equally well for differences in material condition. Figures 44 and 45 show the differences in factor of improvement for different loading conditions and for different changes in water chemistry.

14. **Application of Laboratory Data to BWRs.** One important issue relates to the applicability of laboratory data to plant components and exposures. As experimental procedures have improved, most laboratory data can be considered very representative of plant response. Additionally, predictive models provide methods for handling the growth of cracks through complex residual stress profiles (e.g., in welded components), as well as the time-varying effects of water chemistry, fluence, etc. [1-13]. The single largest difference is in the area of flow rate, where very few laboratories reproduce the high flow rates that exist in many locations in BWRs. This

has two primary effects. First, high flow rates can significantly affect the corrosion potential in the low oxygen regime. At low flow rate, the stagnant boundary layer at the surface of a metal is comparatively thick, and the mass transport of oxidants to the surface is lower than at high flow rate. Thus, e.g., the conditions under which low corrosion potentials are achieved in the laboratory can be different than in-plant. This concern applies primarily to the lower corrosion potential regime (e.g., $< 0\ V_{she}$), and results in non-conservatism in the laboratory data.

The second effect of high flow rate is on crack chemistry. When properly oriented relative to the crack, external fluid flow may have a large effect on the crack chemistry via convective flushing. This has been shown most dramatically in low alloy steels (Figure 46), where the sulfur-rich environment created by dissolution of MnS in the crack is removed at high flow rate. Of course, in this case the effect of high flow rate is exaggerated by the geometry of the crack (CT specimen with 3-sides of the crack open to the environment).

Basis for Water Chemistry Guidelines

The knowledge of crack chemistry and the resultant environmental cracking susceptibility is incomplete; accordingly, establishing guidelines for plant operation is complex, and existing guidelines [35,36] require updating as new insights and data become available. However, it is possible to establish sensible guidelines based on reasonably accurate knowledge of the mechanism of impurity effects coupled with observation of crack chemistry and crack growth rates in the laboratory and field.

I. **Guidelines should be based on the concentration in normality** of the (anionic) species, since this is a measure of their charge-carrying and charge-balancing capability. Specification in terms of ppb or conductivity may be more convenient, but this should be done for individual anions after accounting for their differences in atomic weight and/or mobility. When using a conductivity-based specification, it is also crucial to differentiate between the acid and salt forms of the impurity, since the mobility of H^+ vastly changes the conductivity for a given impurity concentration (Figure 47).

In attempting to balance the deleterious effects of impurities with the uncertainty in the observed data (and achievability in a plant), my preliminary recommendation for steady state operation for sensitized type 304 stainless steel or Alloy 182 weld metal under normal water chemistry conditions ($\simeq 0.1\ V_{she}$) is 10^{-7} N (total) for sulfate (4.8 ppb) plus chloride (3.6 ppb), and perhaps an *additional* 2×10^{-7} N for the total of fluoride (3.8 ppb), phosphate (19.2 ppb, assuming $H_2PO_3^{2-}$), and carbonate (12.2 ppb, assuming HCO_3^-). We have no basis for concern for nitrates up to 100 ppb (0.683 μS/cm HNO_3) [22], nor for chromate levels less than about 12 ppb (1×10^{-7} M, 0.10 μS/cm).

For potentials below $\simeq 0\ V_{she}$, the impurity levels can be increased by about a factor of two for every $0.12\ V_{she}$ decrease in potential (based on Equation 3). Similarly, impurity levels about 3 to 5 times higher can typically be tolerated for non-sensitized stainless steel and Alloy 82 weld metal (based on the observation of little or no enhancement in crack growth at about 25 ppb sulfate, or about 10 ppb chloride).

II. **Guidelines should reflect the interaction between corrosion potential and anion activity** (as just indicated) in producing a crack chemistry, and the **continuum in crack growth response** from very low in pure water, to *progressively higher* in more aggressive water chemistries. For example, Figure 3 shows that there is no threshold potential or conductivity at which cracking suddenly starts or stop. Figure 5 shows that a specific crack growth rate objective can be met by combinations of corrosion potential, conductivity, and stress intensity. These data support the use of weighted guidelines that acknowledge the interaction in corrosion potential and impurity level, and the continuum in crack growth response. Figure 48 provides approximate response to impurities based on crack growth rate predictions.

III. **Time-based response to impurities must be accounted for**, as summarized earlier. The effect of short term exposures to high conductivities can be very significant, as indicated in the anomalously high incidence of cracking in shroud head bolts where there was exposure to high conductivity transients (Figure 9). A time-conductivity weighting approach should be used which penalizes conductivity values above 0.3 to 0.5 μS/cm, and severely penalizes conductivity values above 0.7 to 1.0 μS/cm. Plant and laboratory data support an exposure limit of <1 day at 0.3 to 0.5 μS/cm, and an exposure limit of <8 hours to conductivity values above 0.7 to 1.0 μS/cm. Note that this should particularly apply to temperatures above 150 to 200°C, where the effect of impurities is particularly high (Figure 39) [19].

Guidelines could perhaps be weighted so that deviations from the average conductivity (anion activity) by more than 3X (or perhaps above ≈0.25 μS/cm, or ≈ 5×10^{-7} N) be penalized by a time-weighted factor that recognizes the increased likelihood of developing a "long" crack (i.e., a crack greater than about 0.010 inch where an occluded chemistry and/or a moderate stress intensity can exist). Without having considered it closely, some formula like $(\kappa/0.2)^2 \cdot (\text{hours}/4)^2$ might be appropriate, since it non-linearly penalizes both high conductivity and long time.

IV. **Intentional impurity additions** of, e.g., NaOH to reduce the conductivity associated, e.g., with chromate should receive careful consideration prior to implementation. Since sensitized materials can crack in ultra high purity water (where the crack solution can only increase in pH), the addition of non-H^+ cations to the system can only provide a greater opportunity for alkanization. Nonetheless, there appears to be more flexibility or maneuverability in the high pH regime than in the low pH regime. This may be true because the minimum in oxide solubility apparently falls above neutral in high temperature water (Figure 21), and also because the alkanization process is not as efficient as the acidification process (as described above in the section on *"pH of the crack solution"*).

Areas of Future Research

A variety of issues have been identified that point to the need for further research in the area of water chemistry effects on environmentally assisted cracking. Water chemistry effects are particularly important, since they represent the *easiest* way to mitigate environmental cracking and, in many cases, the *only* way.

A. Characterize the minimum levels of anionic impurities necessary to increase crack growth rates for several materials, several impurities, and several corrosion potentials.

While the data are relatively unambiguous for non-sensitized type 304/316 stainless steel, more work is certainly required for sensitized type 304 stainless steel and Alloy 182 weld metal, and perhaps sensitized Alloy 600 and Alloy 82 weld metal. The response of low alloy and carbon steel to impurity effects is much less well characterized than the other materials.

The most critical impurities to evaluate include sulfate, chloride, and chromate, although more data is needed for fluoride, phosphate, and others. It is critical to evaluate the response as a function of carefully controlled, measured, and maintained corrosion potential. It is already very clear that the level of impurities that can be tolerated at $< -0.3\ V_{she}$ is much higher than at $0.1\ V_{she}$. Details of the difference in response in very pure water between 0, 0.1, and $0.2\ V_{she}$ is not fully clear, and therefore the combined effects of impurity levels at these potentials is less clear.

B. Clarify the possible advantages and problems of intentional additions of NaOH, LiOH, ammonia, etc. to reduce crack growth rate.

C. Employ the emerging capability of crack solution micro-sampling to quantitatively characterize the high temperature crack chemistry associated with different external anion levels, corrosion potentials, materials, etc. Combine with analytical modeling to evaluate the differences in response of the alkanization process (in pure water or, e.g., with NaOH) and the acidification process, and their effects on crack growth.

D. Clarify the possible roles of kinetic stability of species like sulfate (HS^- should be stable in the crack), chromate (Cr_2O_3 should be stable in the crack), nitrate (ammonia should be stable in the crack), etc. Clarify the possible role of complexing in high temperature water, as well as the effect of S^{2-}, HS^-, and other sulfur and non-sulfur species on repassivation kinetics.

References

[1] F.P. Ford, D.F. Taylor, P.L. Andresen, and R.G. Ballinger, "Environmentally Controlled Cracking of Stainless Steel and Low Alloy Steels in Light Water Reactor Environments", NP-5064M, Final Report, EPRI, February 1987.

[2] F.P. Ford and P.L. Andresen, "Development and Use of a Predictive Model of Crack Propagation in 304/316L, A533B/A508 and Inconel 600/182 Alloys in 288°C Water", *Proc 3rd Int Conf on Environmental Degradation of Materials in Nuclear Power Systems - Water Reactors*, Traverse City, August 1987, TMS-AIME, pp.789-800, 1988.

[3] P.L. Andresen and F.P. Ford, "Life Prediction by Mechanistic Modelling and System Monitoring of Environmental Cracking of Fe and Ni Alloys in Aqueous Systems", Materials Science and Engineering, A103, pp.167-183, 1988.

[4] F.P. Ford, P.L. Andresen, H.D. Solomon, G.M. Gordon, S. Ranganath, D. Weinstein, and R. Pathania, "Application of Water Chemistry Control, On-Line Monitoring and Crack Growth Rate Models for Improved BWR Materials Performance", Proc. Fourth Int. Symp. on Environmental Degradation of Materials in Nuclear Power Systems - Water

Reactors, NACE, pp. 4-26 to 4-51, 1990.

[5] P.L. Andresen, R.P. Gangloff, L.F. Coffin and F.P. Ford, "Applications of Fatigue Analysis: Energy Systems", *Proc, Third Int Conf on Fatigue and Fatigue Tresholds*, U of Va, June 1987, Eng Matls Advisory Services, W. Midlands, UK, 1987.

[6] F.P. Ford, P.L. Andresen, D. Weinstein & S. Ranganath, "SCC of Low Alloy Steels in High Temperature Water", Proc. Fifth Int. Symp. on Environmental Degradation of Materials in Nuclear Power Systems - Water Reactors, ANS, 1991, p.561.

[7] F.P. Ford and P.L. Andresen, "Corrosion Fatigue of A533B/A508 Pressure Vessel Steels in Water at 288°C", Proc. Third Intl. Atomic Energy Agency Specialists Mtg on Subcritical Crack Growth, Moscow, USSR, May 1990, NRC NUREG/CP-0112 (ANL-90/22), Vol. 1, p.105-124.

[8] F.P. Ford and P.L. Andresen, "Stress Corrosion Cracking of A533B/Pressure Vessel Steels in Water at 288°C", Proc. Third Intl. Atomic Energy Agency Specialists Mtg on Subcritical Crack Growth, Moscow, USSR, May 1990, NRC NUREG/CP-0112 (ANL-90/22), Vol. 2, p.37-54.

[9] P.L. Andresen, "Fracture Mechanics Data & Modeling of Environmental Cracking of Nickel-Base Alloys in High Temperature Water", Paper #44, Corrosion/91, NACE, Houston, March 1991.

[10] P.L. Andresen, "Development of Data and Predictive Models for Environmental Cracking of Nickel Alloys in 288°C Water", Final Report on EPRI Contract RP2006-17, May 1991.

[11] K.S. Brown, P.L. Andresen and G.M. Gordon, "Modeling of Creviced Alloy 600 Shroud Head Bolt SCC Field Experience", Proc. Life Prediction of Corrodible Structures, Hawaii, November 1991, NACE.

[12] P.L. Andresen, F.P. Ford, S.M. Murphy, J.M. Perks, "State of Knowledge of Radiation Effects on Environmental Cracking in Light Water Reactor Core Materials", Invited Review Paper, Proc. Fourth Int. Symp. on Environmental Degradation of Materials in Nuclear Power Systems, NACE, 1990, pp. 1-83 to 1-121, 1990.

[13] P.L. Andresen, "Irradiation Assisted Stress Corrosion Cracking", in Book on Stress Corrosion Cracking, July 1991, Ed. R. Jones, ASM, to be published, March 1992.

[14] Peter L. Andresen, Ioannis P. Vasatis & F. Peter Ford, "Behavior of Short Cracks in Stainless Steel at 288°C", Paper #495, Corrosion/90, NACE, Houston, 1990.

[15] P.L. Andresen," Effect of Pd-Coating & Pd-Alloying on the Stress Corrosion Crack Growth Rate of Stainless Steel in 288°C Water", Proc. Sixth Int. Symp. on Environmental Degradation of Materials in Nuclear Power Systems - Water Reactors, TMS-AIME, 1993.

[16] D.D. Macdonald and M. Urquidi-Macdonald, "An Advanced Coupled Environment Fracture Model for Predicting Crack Growth Rate in LWR Heat Transport Circuits", Proc.

Fifth Int. Symp. on Environmental Degradation of Materials in Nuclear Power Systems - Water Reactors, ANS, 1991, p. 345.

[17] W.E. Ruther, W.K. Soppet, G. Ayrault, and T.F. Kassner, "Effect of Sulfuric Acid, Oxygen and Hydrogen in High Temperature Water on Stress Corrosion Cracking of Sensitized Type 304 Stainless Steel", *Corrosion* 40, p.518 (1984).

[18] W.E. Ruther, W.K. Soppet and T.F. Kassner, "Effect of Temperature and Ionic Impurities at Very Low Concentrations on Stress Corrosion Cracking of Type 304 Stainless Steel", *Corrosion* 44, p.791 (1988).

[19] P.L. Andresen, "Effects of Temperature on Environmental Crack Growth Rates of Stainless Steel and Alloy 600", Paper #92089, Corrosion/92, New Orleans, NACE. To be published in Corrosion Journal in 1993.

[20] P. Combrade, M. Foucault, P. Marcus, J.M. Grimal, A. Gelpi, "Effect of Sulfur on the Protective Layers on Alloy 600 and 690 in Low and High Temperature Environments", Proc. Fourth Int. Symp. on Environmental Degradation of Materials in Nuclear Power Systems, NACE, 1990, pp. 5-79, 1990.

[21] P.L. Andresen, "Effects of Specific Anionic Impurities on Environmental Cracking of Austenitic Materials in 288°C Water", Proc. Fifth International Symposium on Environmental Degradation of Materials in Nuclear Power Systems - Water Reactors, ANS, 1992, p.209-182.

[22] P.L. Andresen, Unpublished data, GE CRD, Schenectady, NY, May 1993.

[23] M.E. Indig, G.M. Gordon, and R.B. Davis, "The Role of Water Purity on Stress Corrosion Cracking", *Proc. 1st Int. Symp. on Environmental Degradation of Materials in Nuclear Power Systems - Water Reactors*, Traverse City, AIME, p.243-248 (1987).

[24] B.M. Gordon, M.E. Indig, R.B. Davis, A.E. Pickett, and C.W. Jewett, "Environmentally Assisted Cracking Resistance of BWR Structural Materials in Hydrogen Water Chemistry", *Proc. 2nd Int. Symp. on Environmental Degradation of Materials in Nuclear Power Systems - Water Reactors*, Monterey, ANS, p.583-592 (1986).

[25] R.A. Carnahan and C.W. Jewett, "An In-Plant Monitoring Method to Relate Water Chemistry to Plant Materials Performance", Paper #30, *EPRI Seminar on BWR Corrosion, Chemistry and Radiation Control*, EPRI, Palo Alto (1984).

[26] L.G. Ljungberg, D. Cubicciotti and M. Trolle, "The Effect of Sulfate on Environmental Cracking in Boiling Water Reactors Under Constant Load or Fatigue", *Corrosion* 46, p.641 (1990).

[27] L.G. Ljungberg, D. Cubicciotti and M. Trolle, "Effect of Impurities on IGSCC in High Temperature Water", *Corrosion* 44, p.66 (1988).

[28] L.G. Ljungberg, D. Cubicciotti and M. Trolle, "Effects of Some Seldom Noticed Water Impurities on Stress Corrosion Cracking of BWR Construction Materials", *Corrosion* 45, p.66 (1989).

[29] L.G. Ljungberg, "Study on Environmental Cracking in Simulated BWR Water", Project RP2293-1, EPRI, Palo Alto (1991).

[30] P.L. Andresen, "The Effect on Crack Growth Rate of Dissolved Silica in Sensitized Stainless Steel in 288°C Water", GE CRD Report G628, August 1992.

[31] P.L. Andresen, "Transition and Delay-Time Behavior of High Temperature Crack Propagation Rates Resulting from Water Chemistry Changes", *Proc. 1st Int. Symp. on Environmental Degradation of Materials in Nuclear Power Systems - Water Reactors*, ANS, 1986, p.84-92.

[32] P.L. Andresen, "Modeling of Water and Material Chemistry Effects on Crack Tip Chemistry and the Resulting Crack Growth Kinetics", *Proc 3rd Int. Symp. on Environmental Degradation of Materials in Nuclear Power Systems - Water Reactors*, AIME, p.301-312, 1988.

[33] P.L. Andresen, "Effect of Material and Environmental Variables on SCC Initiation in Slow Strain Rate Tests on Type 304 Stainless Steel", *Symp. on Environmental Sensitive Fracture: Evaluation and Comparison of Test Methods,* April 1982, STP 821, ASTM, Philadelphia, 1984, p.271-287.

[34] "BWR Water Chemistry Guidelines", NP-3589 SR-LD, EPRI, April 1985.

[35] "BWR Hydrogen Water Chemistry Guidelines", NP-4947 SR, EPRI, October 1988.

Table 1. Concentration, ppb, and Conductivity Relationships for Various Acids

	Sulfate		Chloride		Fluoride		Chromate		Nitrate		Carbonate*		Phosphate*	
µM	ppb	µS/cm	ppb	µS/cm	ppb	µS/cm	ppb	µS/cm	ppb	µS/cm	ppb	µS/cm	ppb	µS/cm
0.01	0.96	0.0582	0.355	0.0550	0.19	0.0549	1.16	0.0578	0.62	0.0563	0.61	0.0558	0.96	0.0561
0.02	1.92	0.0621	0.71	0.0581	0.38	0.0577	2.32	0.0611	1.24	0.0580	1.22	0.0569	1.92	0.0574
0.03	2.88	0.0666	1.07	0.0600	0.57	0.0594	3.48	0.0647	1.86	0.0598	1.83	0.0580	2.88	0.0589
0.05	4.80	0.0769	1.77	0.0641	0.95	0.0631	5.80	0.0727	3.10	0.0639	3.05	0.0605	4.80	0.0623
0.07	6.72	0.0887	2.48	0.0687	1.33	0.0673	8.12	0.0814	4.34	0.0684	4.27	0.0631	6.72	0.0662
0.1	9.6	0.109	3.6	0.077	2.0	0.076	11.6	0.0954	6.2	0.076	6.1	0.067	9.6	0.073
0.2	19.2	0.185	7.1	0.108	3.8	0.104	23.2	0.145	12.4	0.107	12.2	0.083	19.2	0.100
0.25	24.0	0.226	8.86	0.126	4.75	0.120	27.8	0.164	15.5	0.125	15.3	0.091	24.0	0.116
0.3	28.8	0.267	10.6	0.145	5.7	0.138	34.8	0.194	18.6	0.143	18.3	0.099	28.8	0.133
0.4	38.4	0.351	14.2	0.184	7.6	0.175	46.4	0.241	24.8	0.182	24.4	0.115	38.4	0.167
0.5	48.0	0.435	17.7	0.224	9.5	0.213	58.0	0.287	31.0	0.221	30.5	0.130	48.0	0.203
0.7	67.2	0.606	24.8	0.306	13.3	0.292	81.2	0.377	43.4	0.303	42.7	0.157	67.2	0.277
1.0	96.1	0.863	35.5	0.432	19.0	0.411	116	0.508	62.0	0.427	61.0	0.194	96.0	0.390
2.0	192.1	1.721	71.0	0.857	38.0	0.814	232	0.926	124.0	0.846	122	0.293	192	0.770
3.0	288.2	2.581	106.4	1.281	57.0	1.218	348	1.333	186.0	1.266	183	0.371	288	1.153
5.0	480.3	4.301	177.3	2.133	95.0	2.023	580	2.138	310.0	2.108	305	0.496	480	1.918
7.0	672.4	6.020	248.2	2.985	133.0	2.832	812	2.39	424.0	2.951	427	0.599	672	2.684
10.0	960.6	8.600	354.5	4.264	190.0	4.045			620.0	4.215				
20.0	1921.2	17.200	709.0	8.527	380.0	8.088			1240.0	8.428				
50.0	4803.0	43.000	1772.5	21.318	950.0	20.220			3100.0	21.070				

* Approximate values

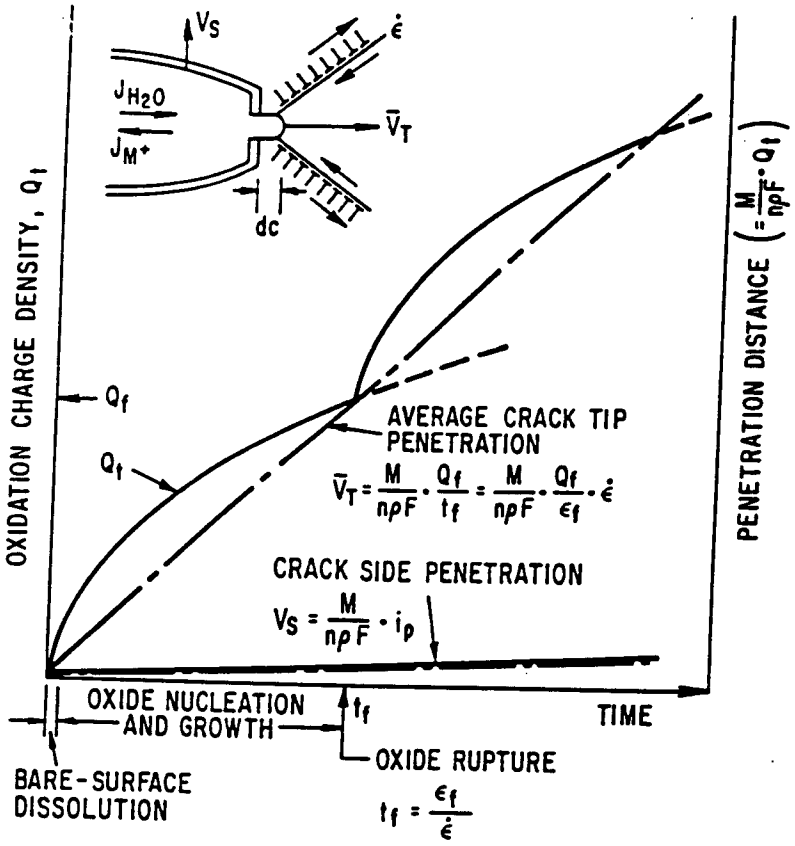

Figure 1. Schematic oxidation charge density/time relationships for a strained crack tip and unstrained crack sides.

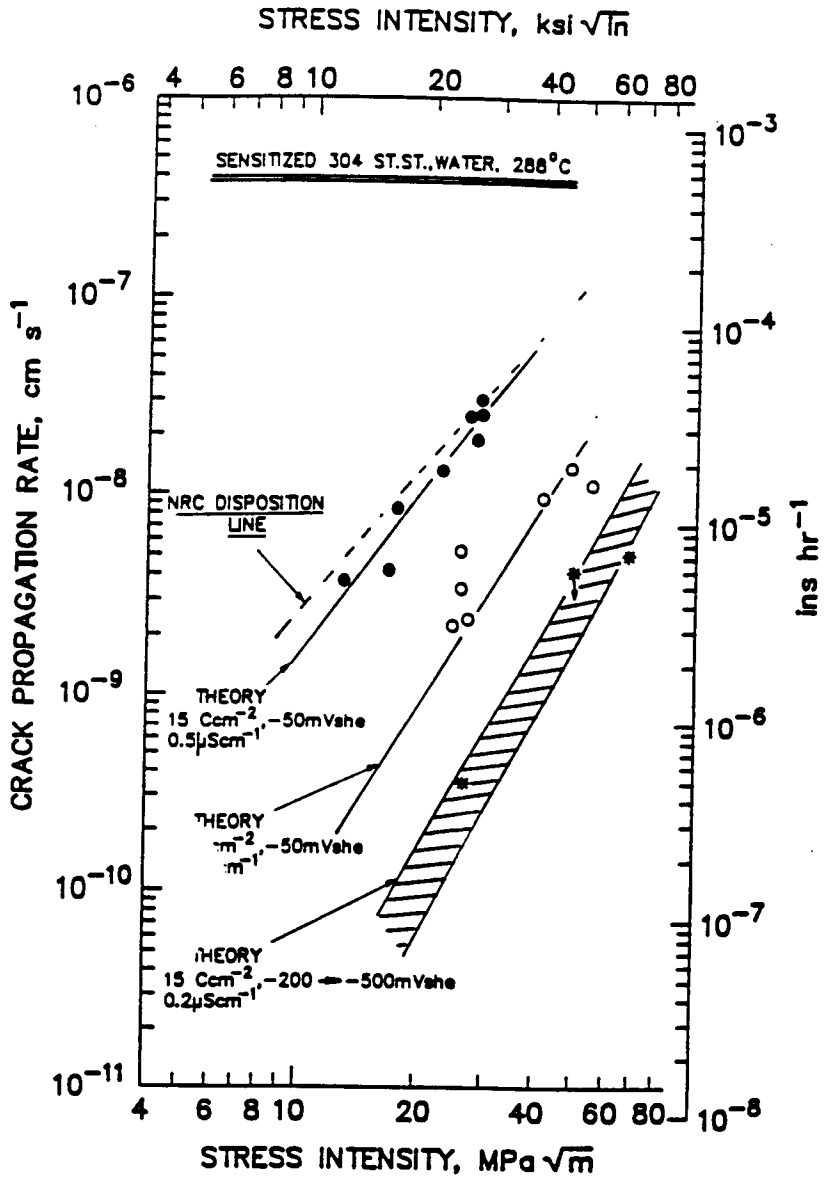

Figure 2. Relationship between the empirically derived NRC disposition line for sensitized type 304 stainless steel in oxygenated water at 288°C and the predicted velocity vs. stress intensity for different water chemistries or degrees of sensitization.

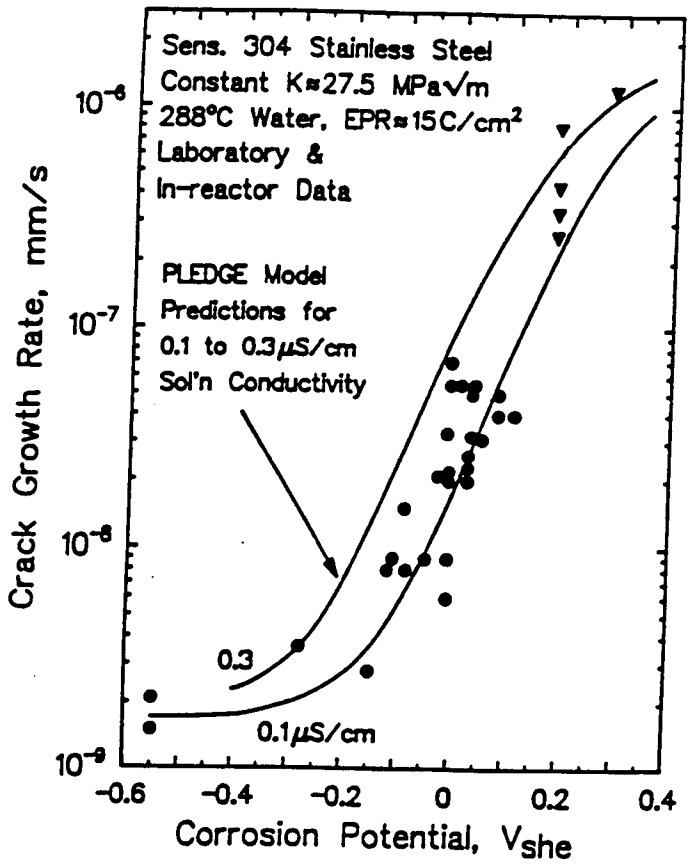

Figure 3. Comparison of observed vs. predicted crack growth rate as a function of corrosion potential for sensitized type 304 stainless steel at constant load. Data points at elevated corrosion potentials and growth rates correspond to irradiated water chemistry conditions in test or commercial reactors [1-5].

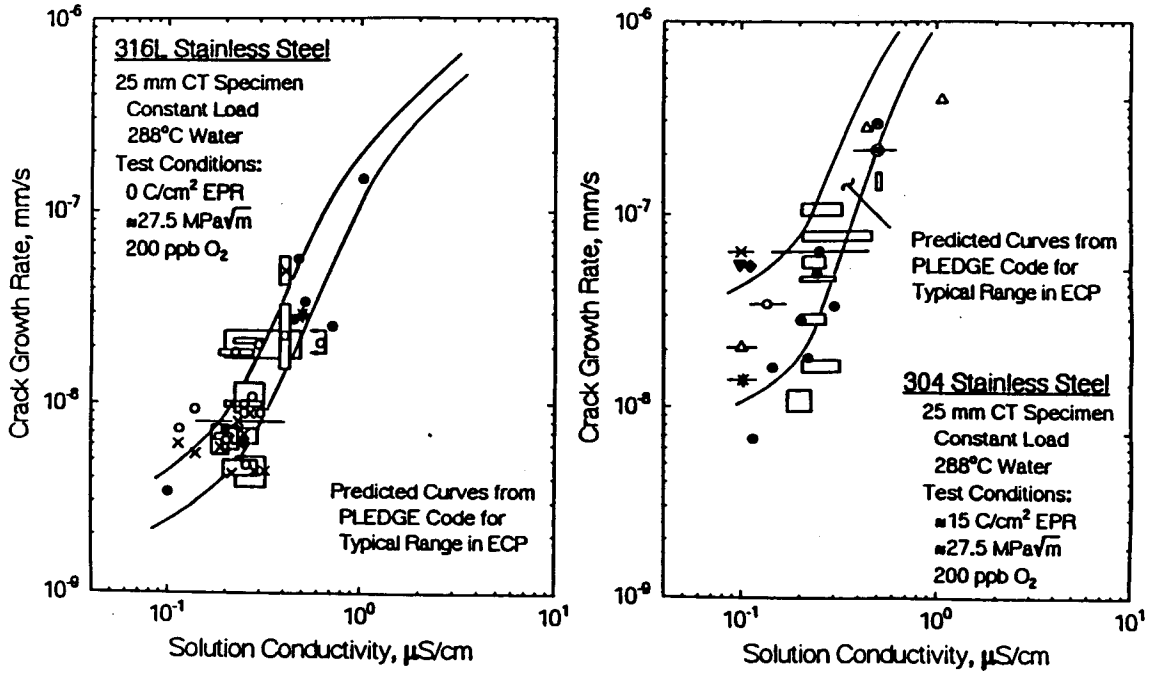

Figure 4. Comparison between observed and predicted crack growth rate vs. solution conductivity for statically loaded (a) type 316L and (b) sensitized type 304 stainless steels in 288°C water containing 200 ppb O_2 [1-5].

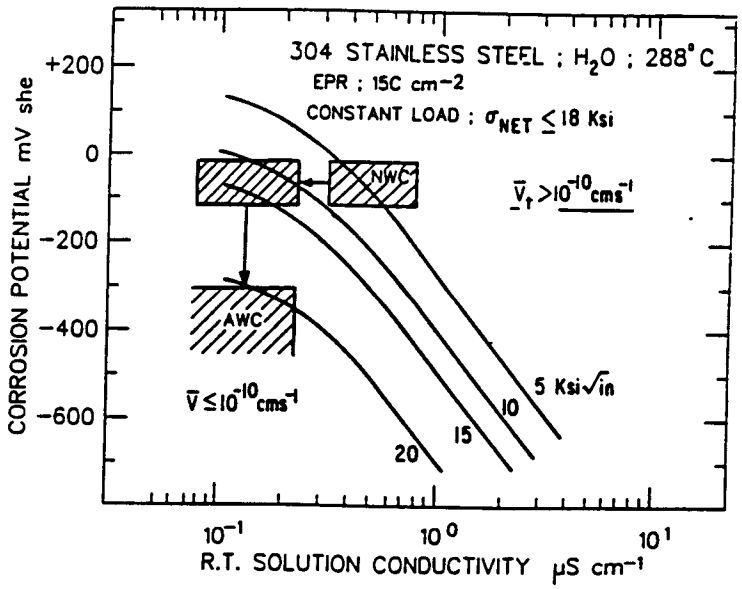

Figure 5. Combinations of corrosion potential, solution conductivity and stress intensity values which will give crack growth rates on sensitized type 304 stainless steel which are either greater or less than 10^{-10} cm/s. The hatched areas represent BWR operating conditions of normal water chemistry (NWC), improved water purity, and alternate or hydrogen water chemistry (AWC).

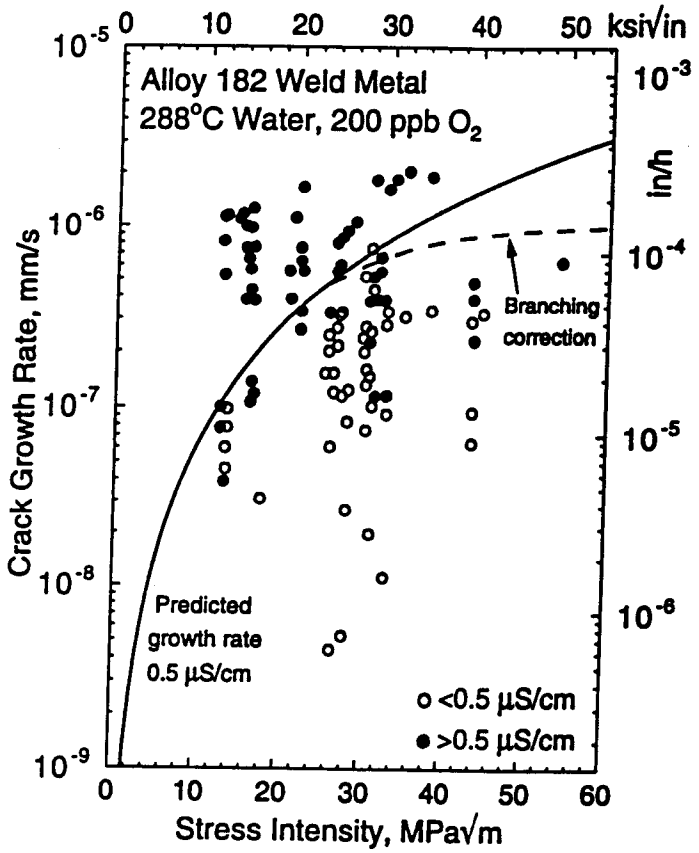

Figure 6. Delineation of Alloy 182 weld metal crack growth rate data in 288°C water based on a solution conductivity greater than or less than 0.5 µS/cm.

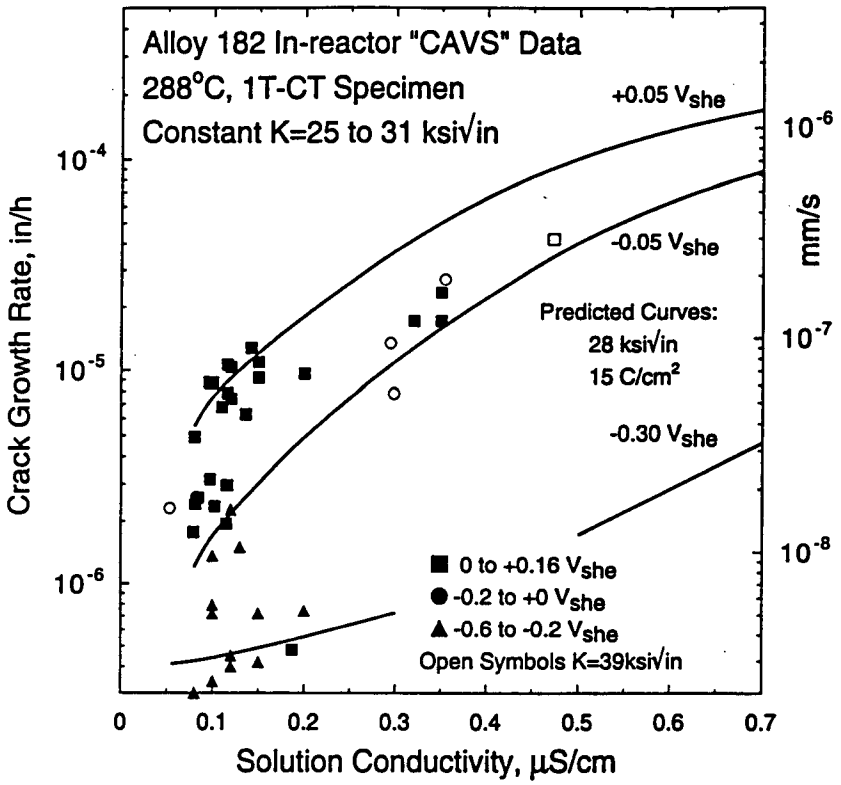

Figure 7. Comparison of the predicted and observed crack growth rates vs. solution conductivity for in-plant GE "CAVS" data on Alloy 182 weld metal tested at constant load in BWR water of varying chemistry (corrosion potential).

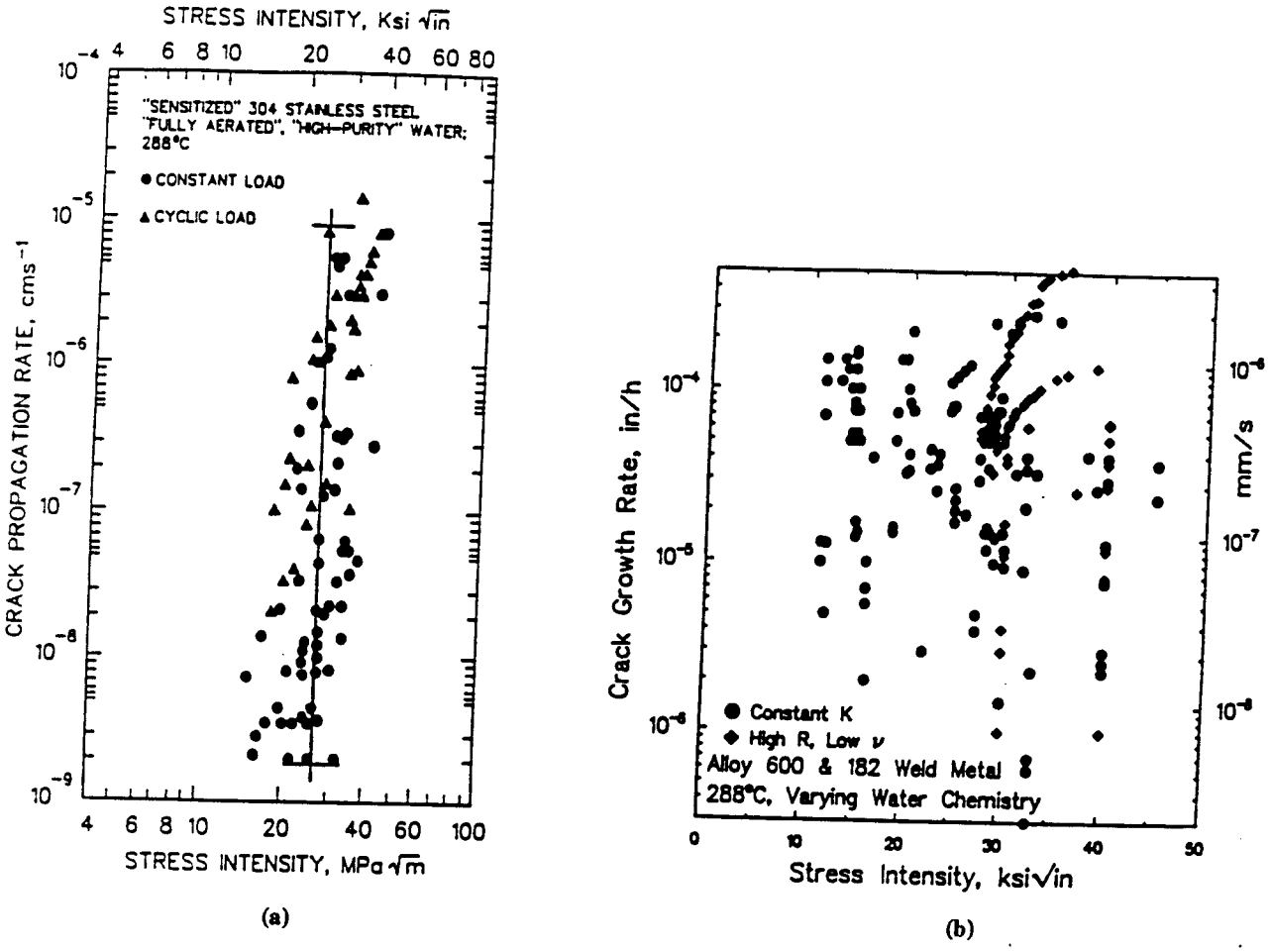

Figure 8. Crack growth rate vs. stress intensity in 288°C water for (a) sensitized type 304 stainless steel and (b) Alloy 600 and Alloy 182 weld metal. Data are from many sources, many of which provide only nominal water and material chemistry conditions. This inadequate definition results in orders of magnitude spread in crack growth rate that can mistakenly be interpreted, e.g., for a very high dependence on stress intensity.

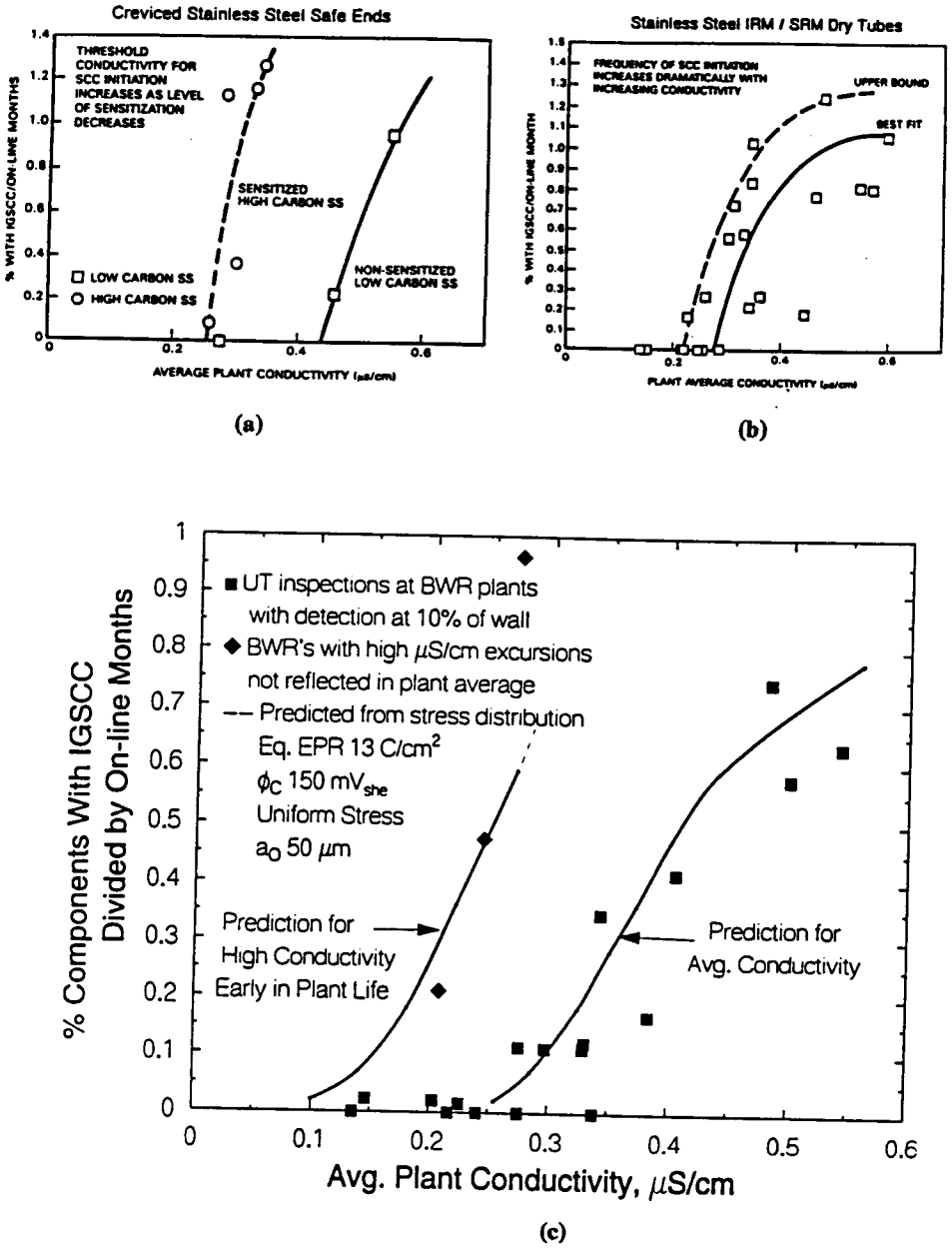

Figure 9. The effects of average plant water purity are shown in field correlations of the core component cracking behavior for (a) stainless steel IRM/SRM instrumentation dry tubes, (b) creviced stainless steel safe ends, and (c) creviced Inconel 600 shroud head bolts, which also shows the predicted response vs. conductivity.

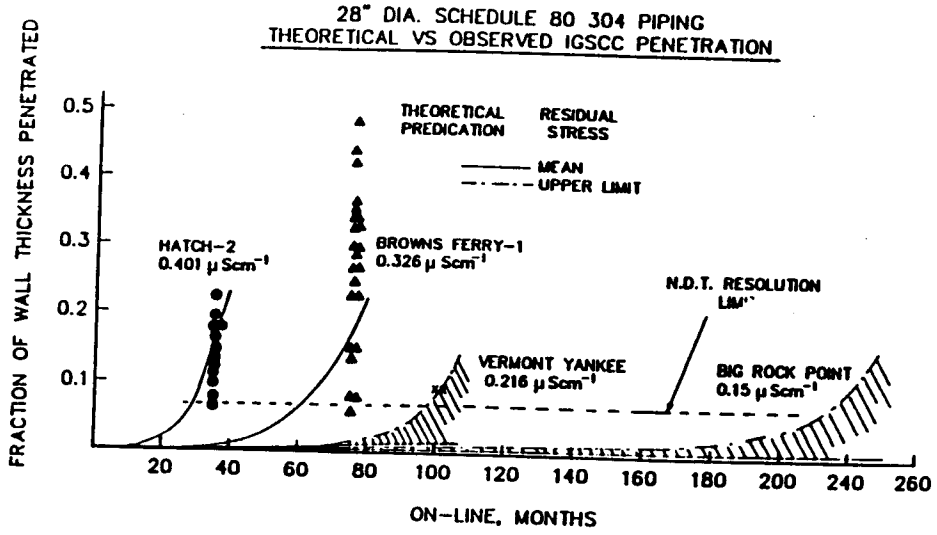

Figure 10. Crack depth vs. operating time for weld sensitized, 711 mm (28 inch) diameter, schedule 80 stainless steel piping (EPR = 15 C/cm^2) in 288 °C water containing 200 ppb oxygen. Data are from various BWR plants operating at the specified mean solution conductivity. Predictions account for the complex variation in residual stress vs. wall thickness and associated stress intensity vs. crack depth/time [2,3].

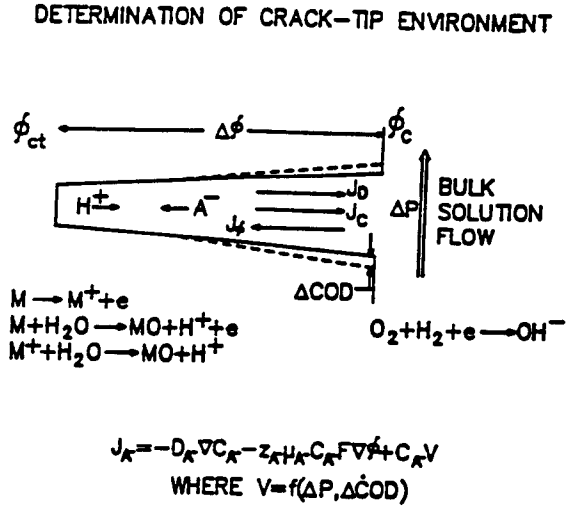

Figure 11. Schematic of a crack and the associated mass transport and thermodynamic criteria which govern the crack tip environment.

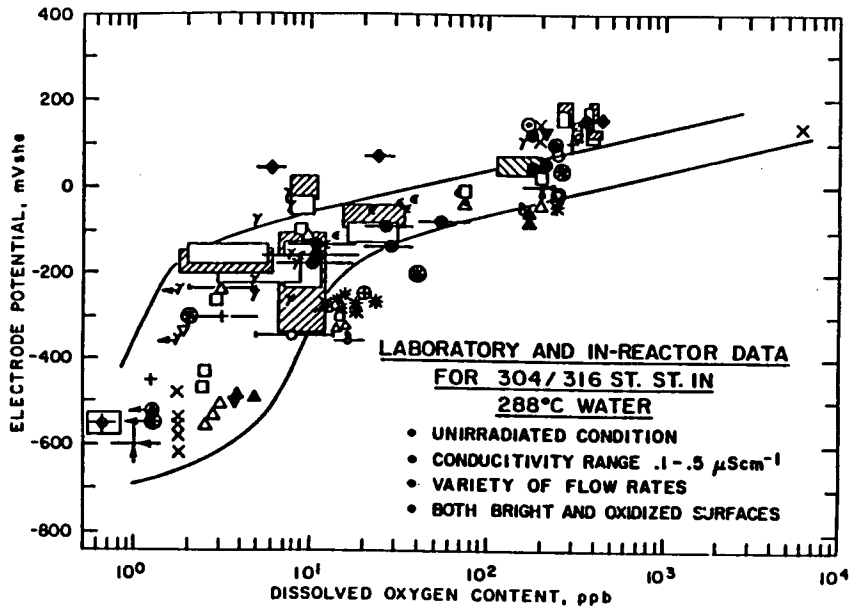

Figure 12. Corrosion potential/dissolved oxygen content relationships for unirradiated stainless steel in water at 288°C.

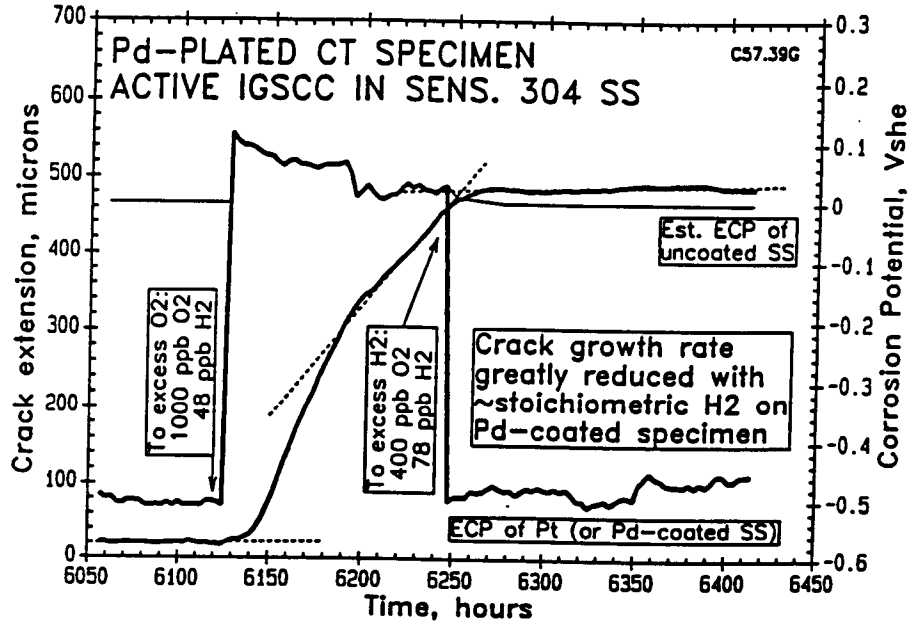

Figure 13. Crack length and corrosion potential vs. time for Pd-coated CT specimen c57.39g showing a low corrosion potential and crack growth rate in 1 μM H_2SO_4 (0.863 μS/cm) under excess hydrogen. On changing to excess oxygen at 6124 hours, the corrosion potential and growth rate increase dramatically; returning to excess hydrogen at 6244 hours causes the corrosion potential and growth rate to again drop.

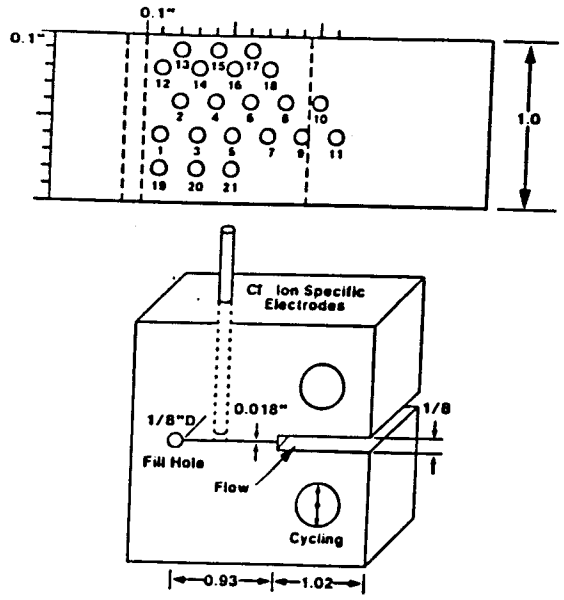

(a)

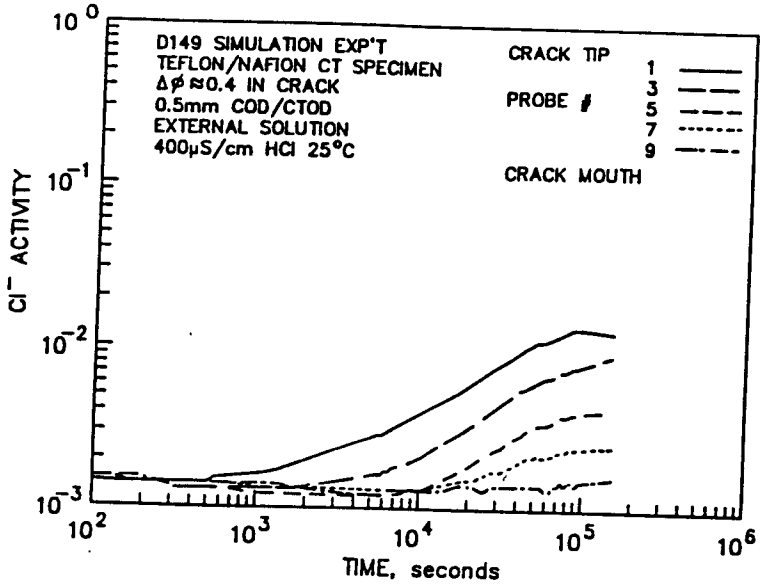

(b)

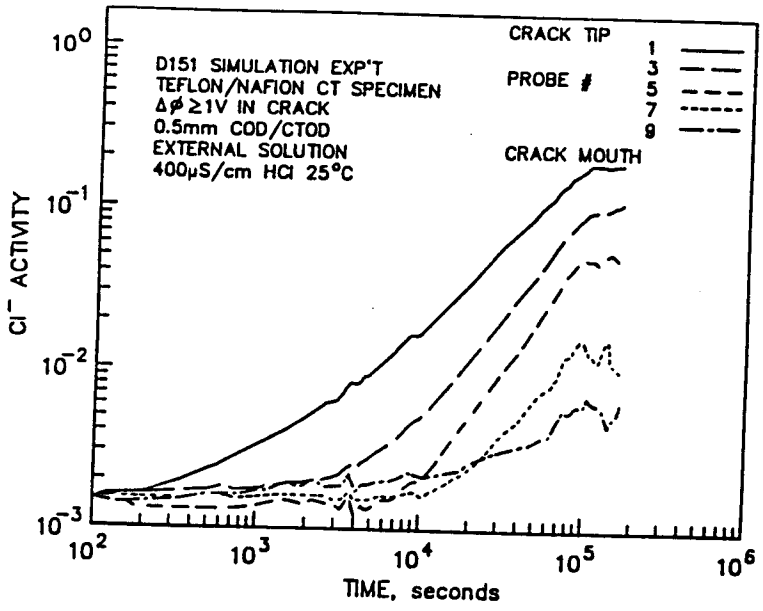

(c)

Figure 14. (a) Schematic of the Teflon^R specimen used in the room temperature crack chemistry simulation experiments. (b) The effect of potential field driven ion transport on the chloride activity vs time for locations from the crack tip (probe #1) to mouth (probe #9) in 1-dimensional experiments. For $\Delta\phi \approx 0.4$ V, the anion activity at the crack tip is ≈10X, as expressed in Equation 3.

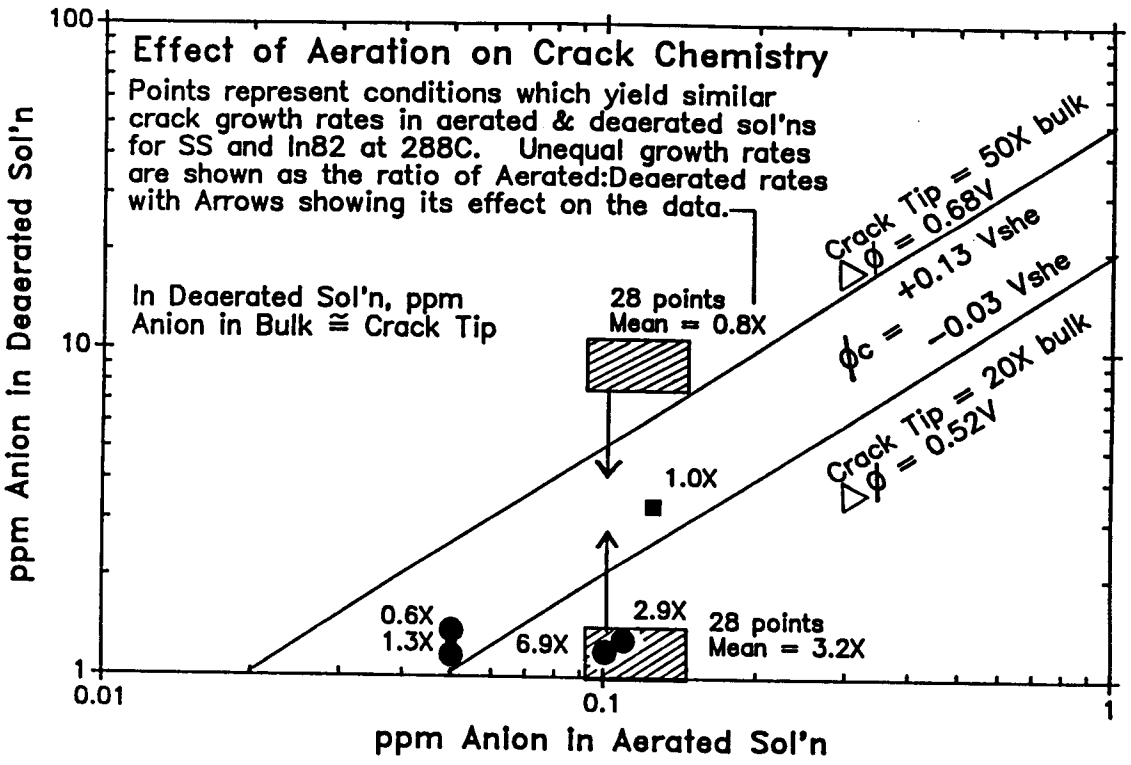

Figure 15. The inter-relationship between corrosion potential and solution conductivity in establishing a crack tip anion activity is shown by comparing crack growth rates in aerated vs. deaerated solutions. If the growth rates under two conditions are similar, then it is inferred that the crack tip chemistries are similar. Each point represents a pair of datum obtained at similar crack growth rates and loading conditions in 288°C water. Since perfect matches, requiring identical crack growth rates under aerated and deaerated conditions, were generally unavailable, the labels (e.g., 2.9X) indicate the ratio of the crack growth rate in aerated vs. deaerated solutions. The arrows indicate where points would shift if the growth rate match were perfect.

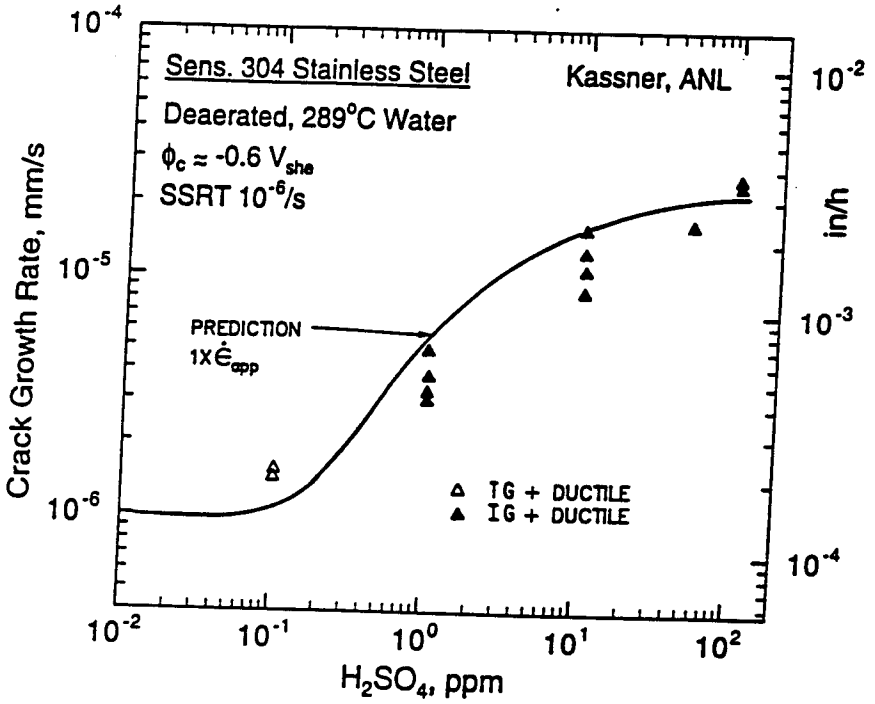

Figure 16. The effect of H_2SO_4 additions on the crack growth rate of sensitized 304 stainless steel tested in deaerated, 289°C water in slow strain rate experiments at 1 x 10^{-6} s^{-1} [17,18].

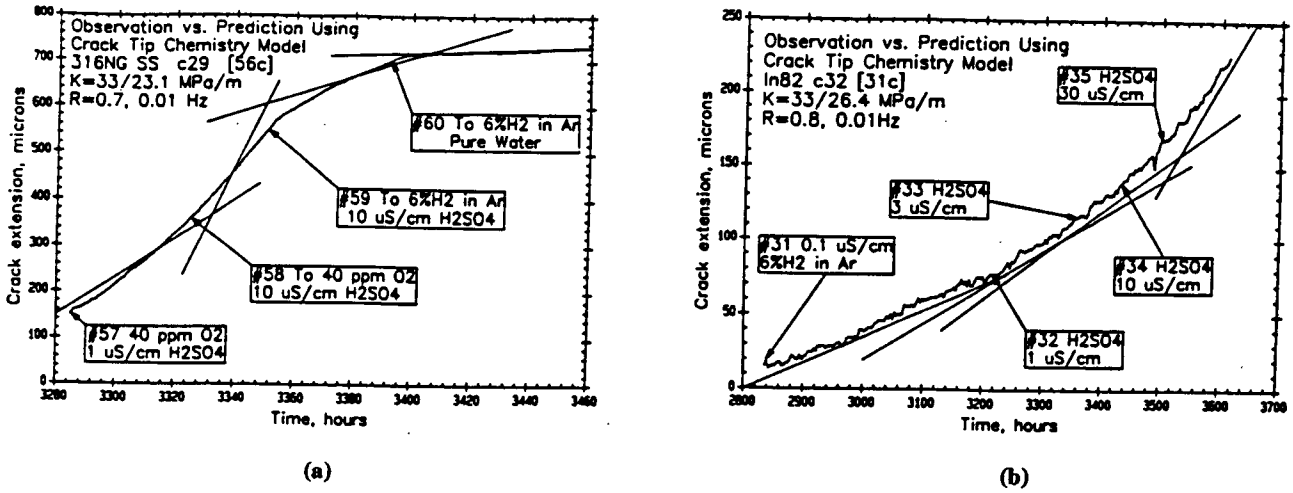

Figure 17. The crack extension vs. time response of (a) non-sensitized 304L stainless steel and (b) Alloy 82 weld metal to changes in water chemistry showing elevated crack growth rates in the non-sensitized material in deaerated water at high conductivities. This illustrates the inter-relationship between solution conductivity and corrosion potential in creating a specific crack tip solution chemistry and thus a specific crack growth rate. The straight line segments represent predictions of crack growth rate behavior for the various conditions shown.

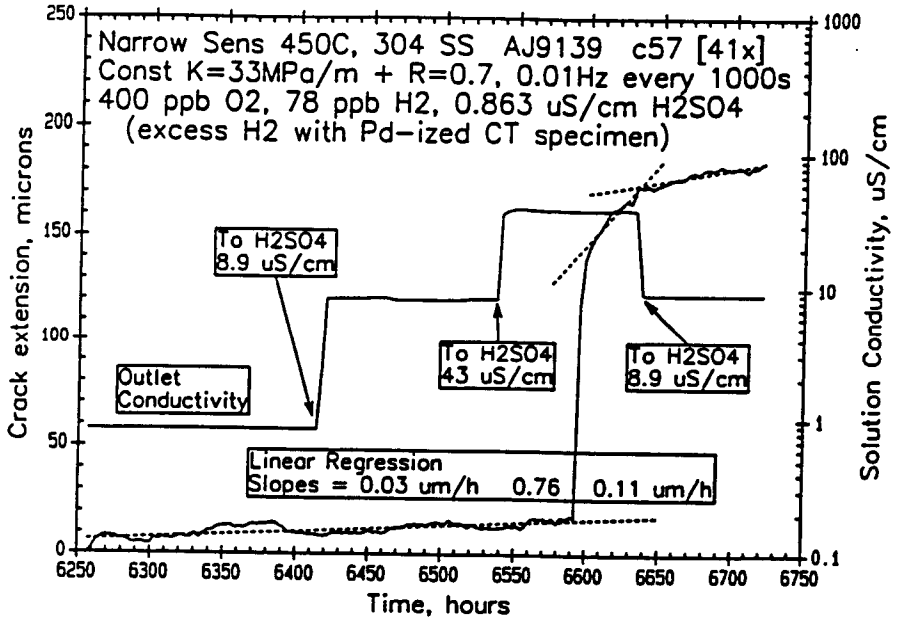

Figure 18. Crack length vs. time for CT specimen c57.41x showing that accelerated crack growth can be achieved at the thermodynamically lowest potentials (characteristic of fully deaerated water, or catalytic surfaces in excess hydrogen) provided sufficient H_2SO_4 is added. This also shows that low corrosion potentials provide a large tolerance to impurities since, at high corrosion potentials, effects on crack growth of ≈0.1 μM H_2SO_4 are readily observed.

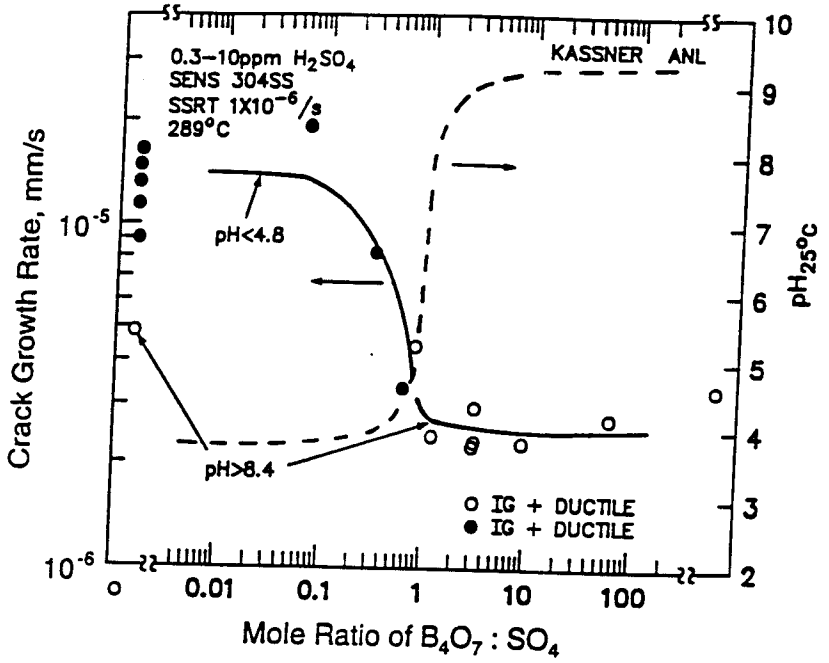

Figure 19. Influence of the borate:sulfate mole ratio on the crack growth rate of sensitized 304 stainless steel tested in deaerated, 289°C water in slow strain rate experiments at 1 x 10^{-6} s^{-1} [17,18].

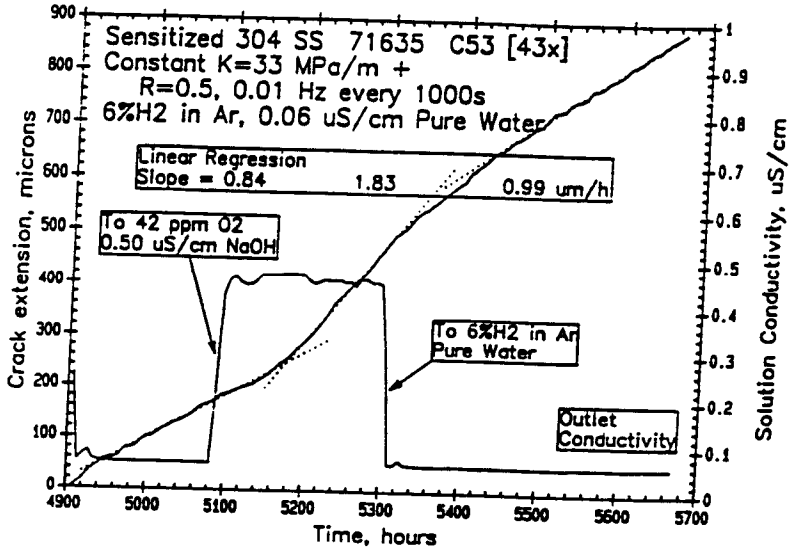

Figure 20. Crack extension vs. time for sensitized type 304 stainless steel (c53.38x & c53.43x) in 288°C water showing the effect of various concentrations of OH^- as NaOH.

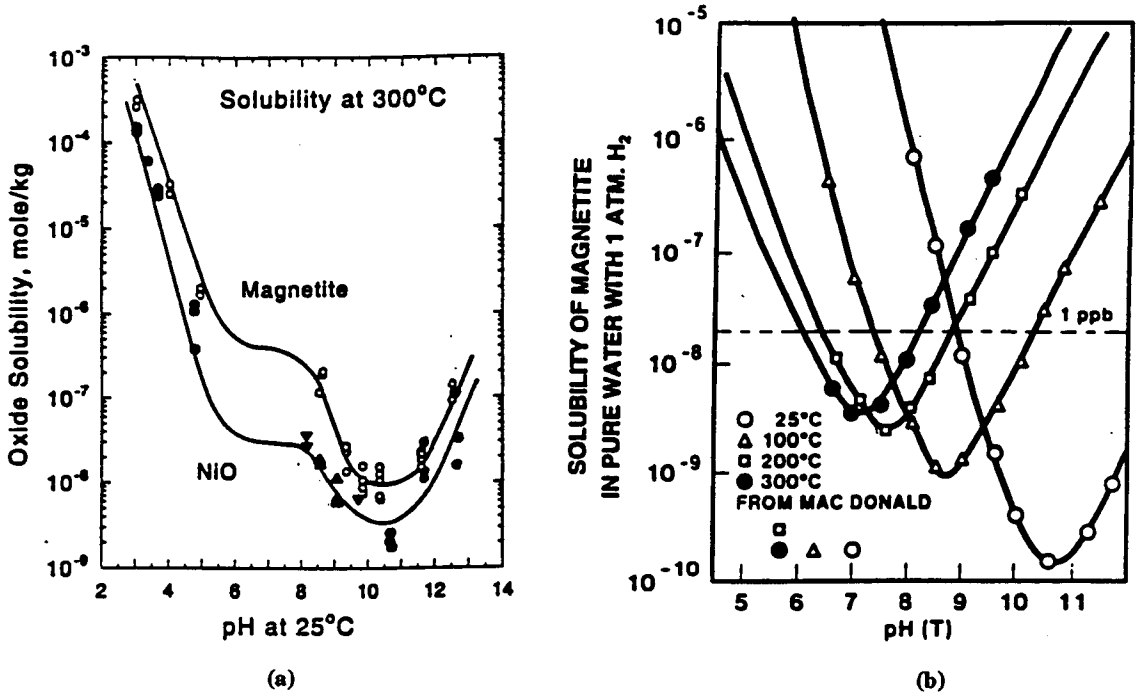

Figure 21. (a) The effect of temperature and pH_T on the calculated solubility of iron oxide in pure water containing 1 atmosphere H_2 [32]. Solubility comparison at a constant pH (or for solution of fixed composition) shows that, for $pH_T < 8$, the solubility decreases with temperature. (b) Experimental solubilities of iron and nickel oxides at 300°C and 780 mole/kg H_2 with least squares fit plotted against $pH_{25°C}$, in contrast to pH_T in (a). Compared to chromium oxide, the solubilities of iron and nickel oxides are similar. In contrast to the calculated solubilities in (a), a "plateau" is observed at $\approx pH_{25°C}$ of 5 — 7, which sometimes is reported to span a larger pH range.

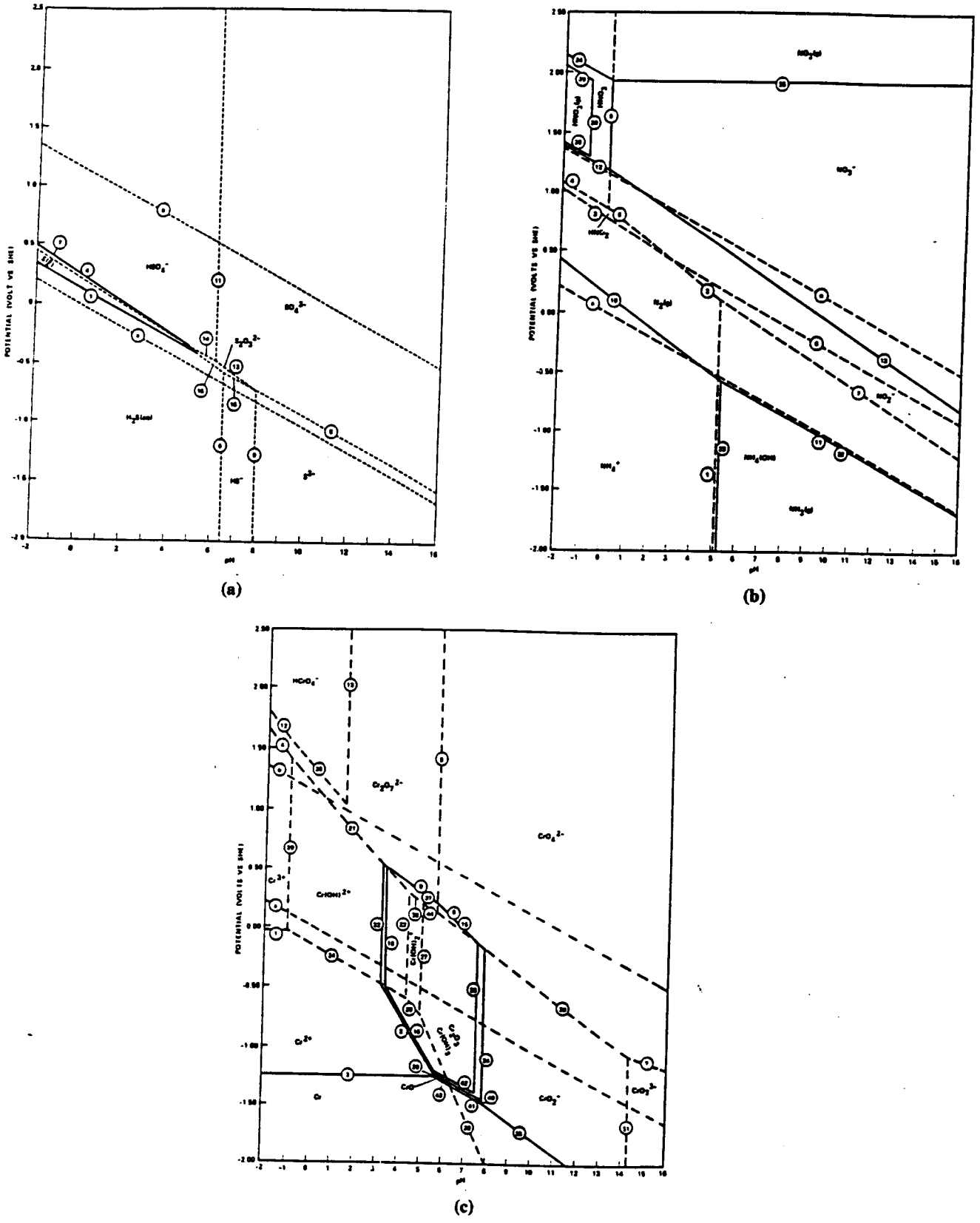

Figure 22. Pourbaix (pH vs. potential) diagram at 250°C for the (a) S – H_2O, (b) N – H_2O, and (c) Cr – H_2O systems.

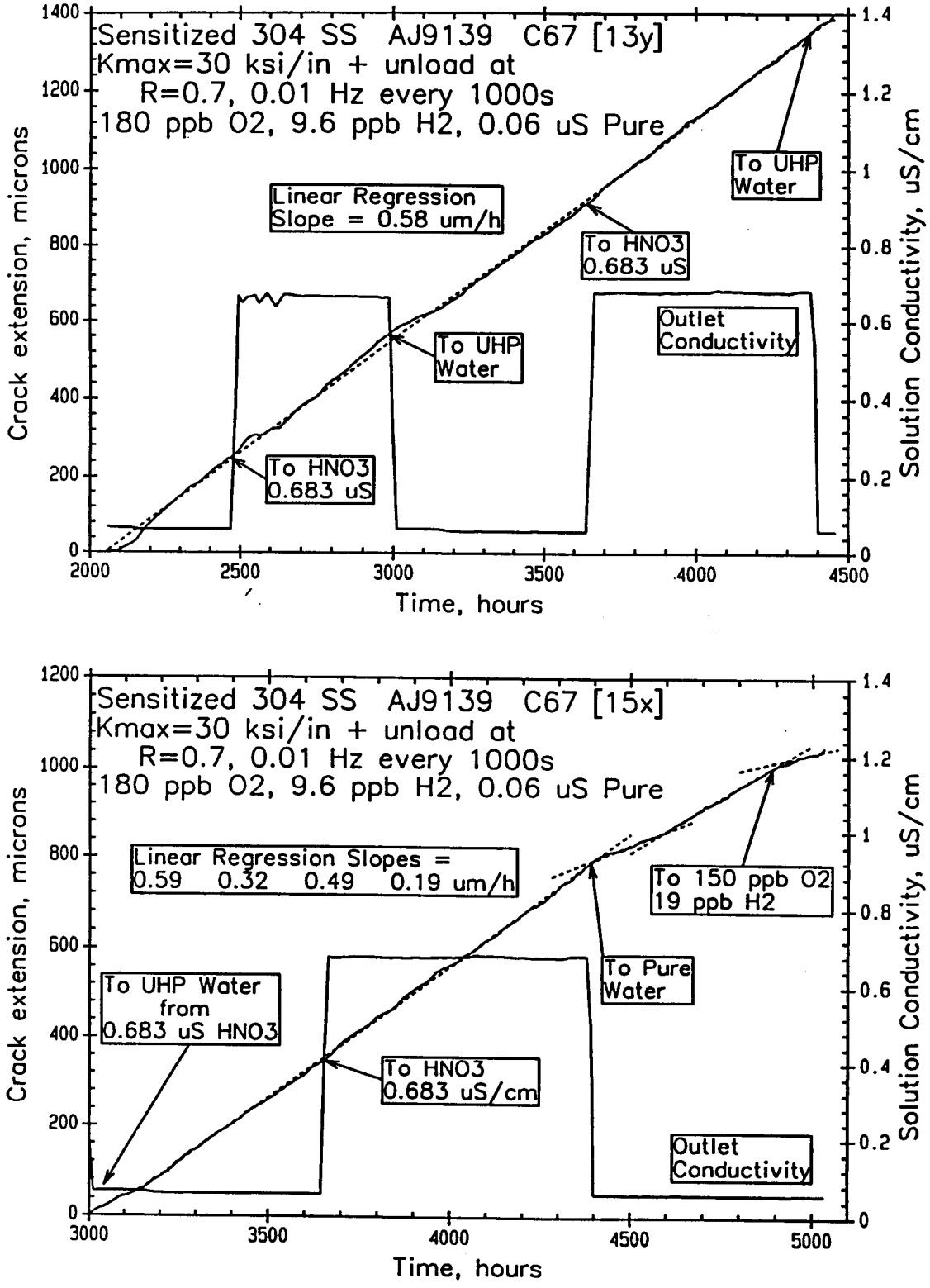

Figure 23. Crack length vs. time for CT specimens of sensitized type 304 stainless steel showing the minimal effect of 100 ppb nitrate (as HNO_3) on the crack growth rate in 288°C water.

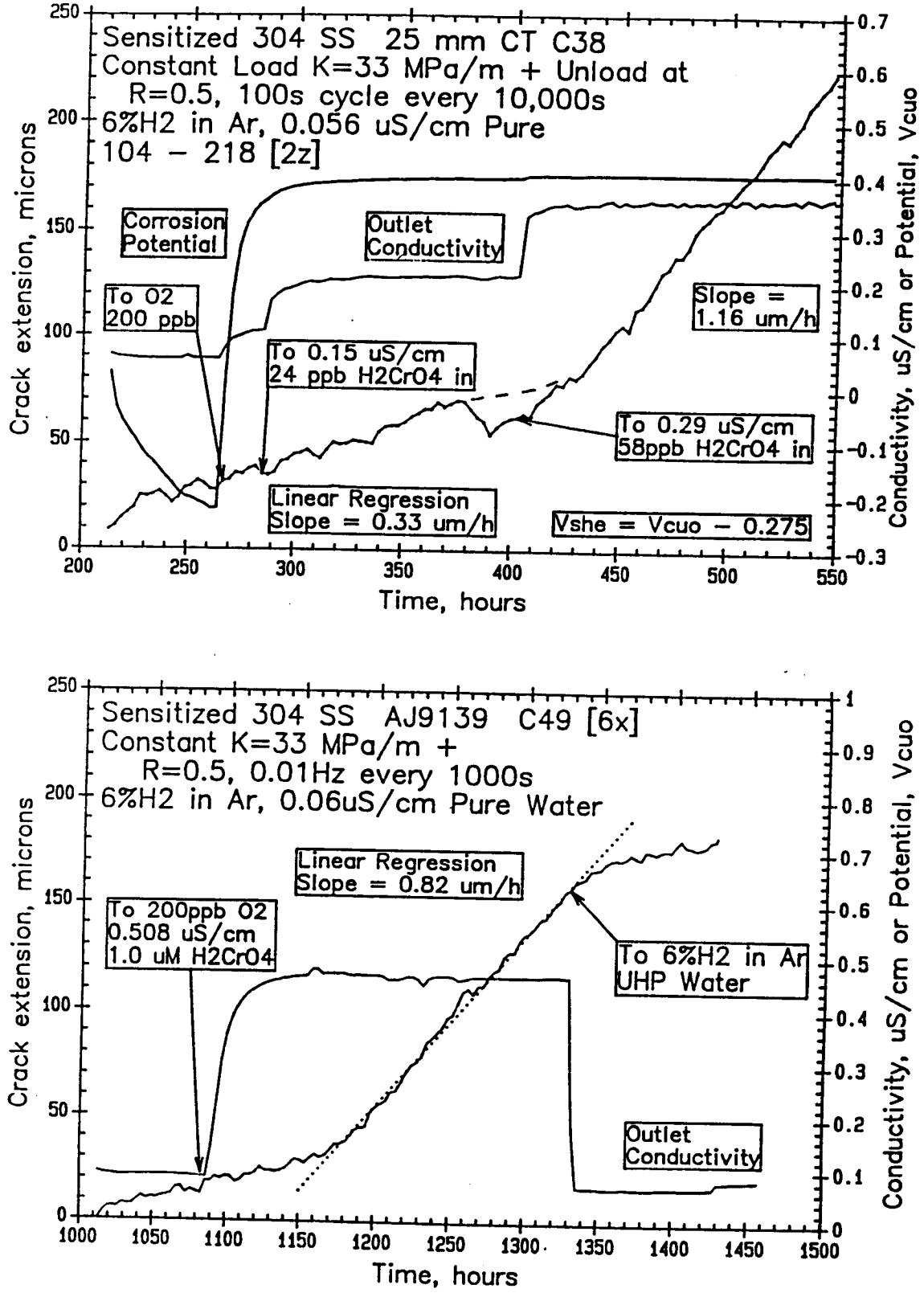

Figure 24. Crack length vs. time for CT specimens of sensitized type 304 stainless steel showing the effect of chromate (as H_2CrO_4) on the crack growth rate in 288°C water.

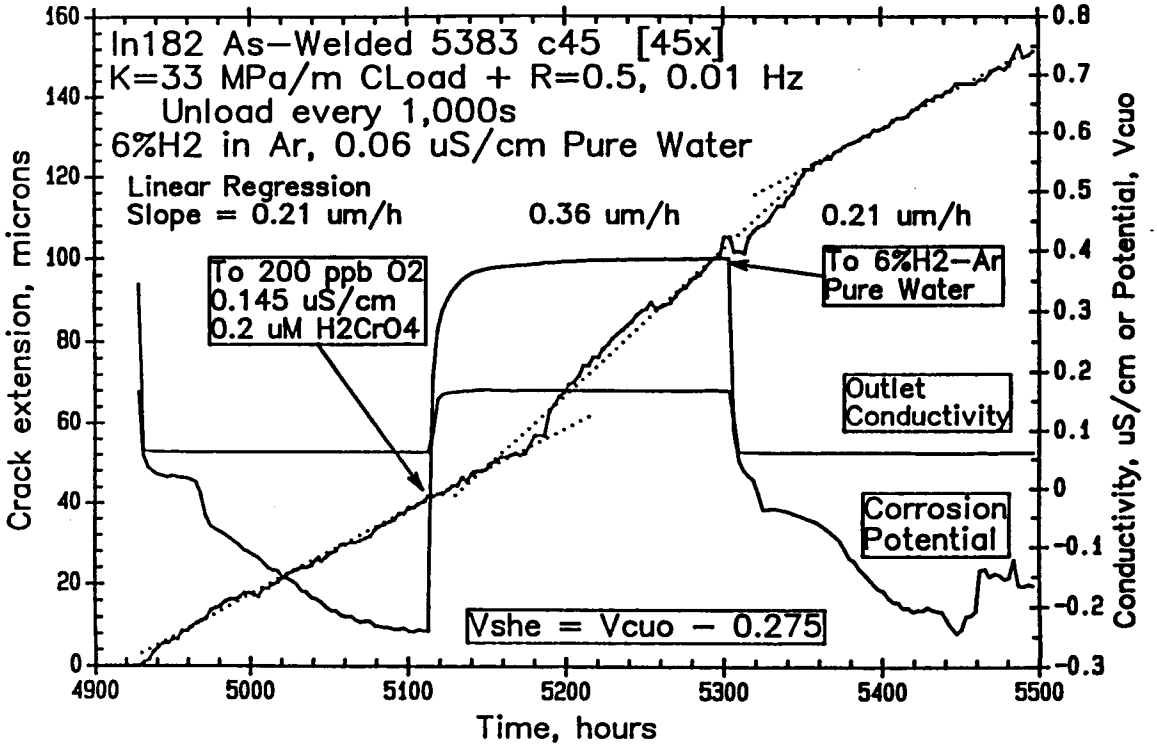

Figure 24 continued.

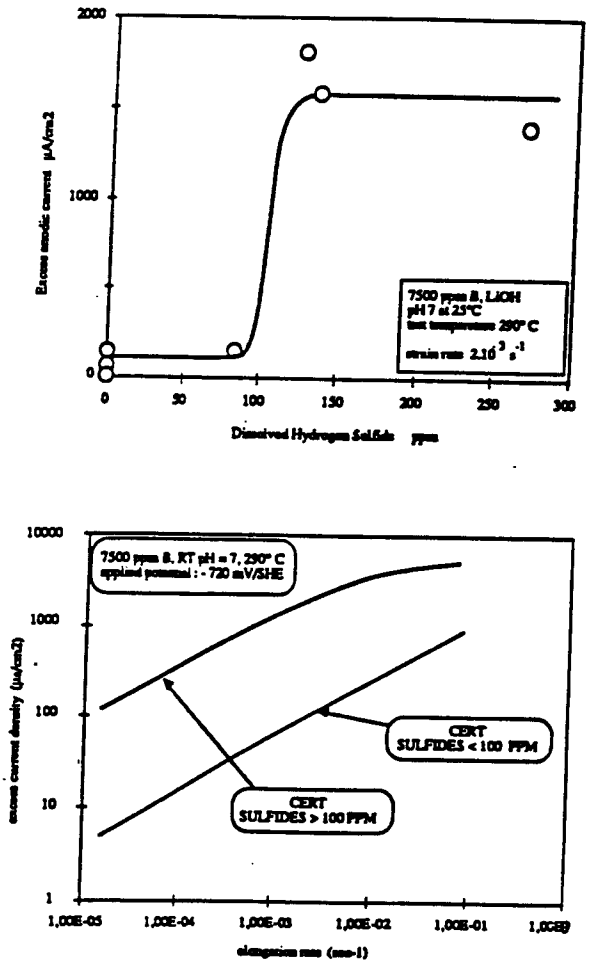

Figure 25. The effects of sulfide concentration on the excess anodic current density (metal dissolution rate) and slow strain rate behavior of Alloy 600 showing a steep threshold at ≈100 ppm sulfide [20].

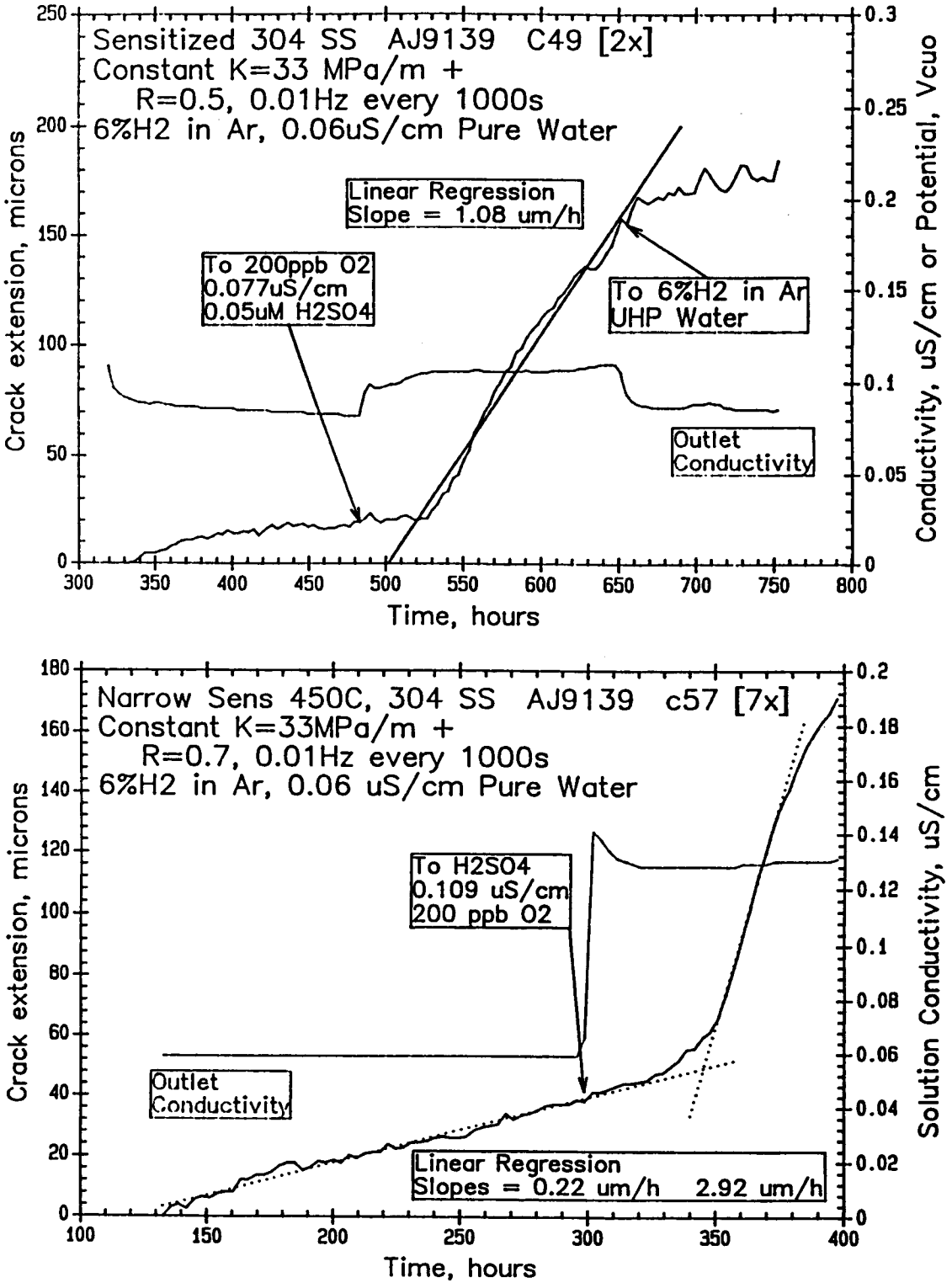

Figure 26. Crack length vs. time for CT specimens of sensitized type 304 stainless steel showing the effect of sulfate (as H_2SO_4) on the crack growth rate in 288°C water. Also, the factor of enhancement as a function of H_2SO_4 concentration for sensitized type 304 stainless steel. The enhancement factor is computed by dividing the steady state crack growth rate in impure water to that in pure water. The data represent an upper bound on the factor of enhancement since a lower bound value for the crack growth rate in pure water was employed.

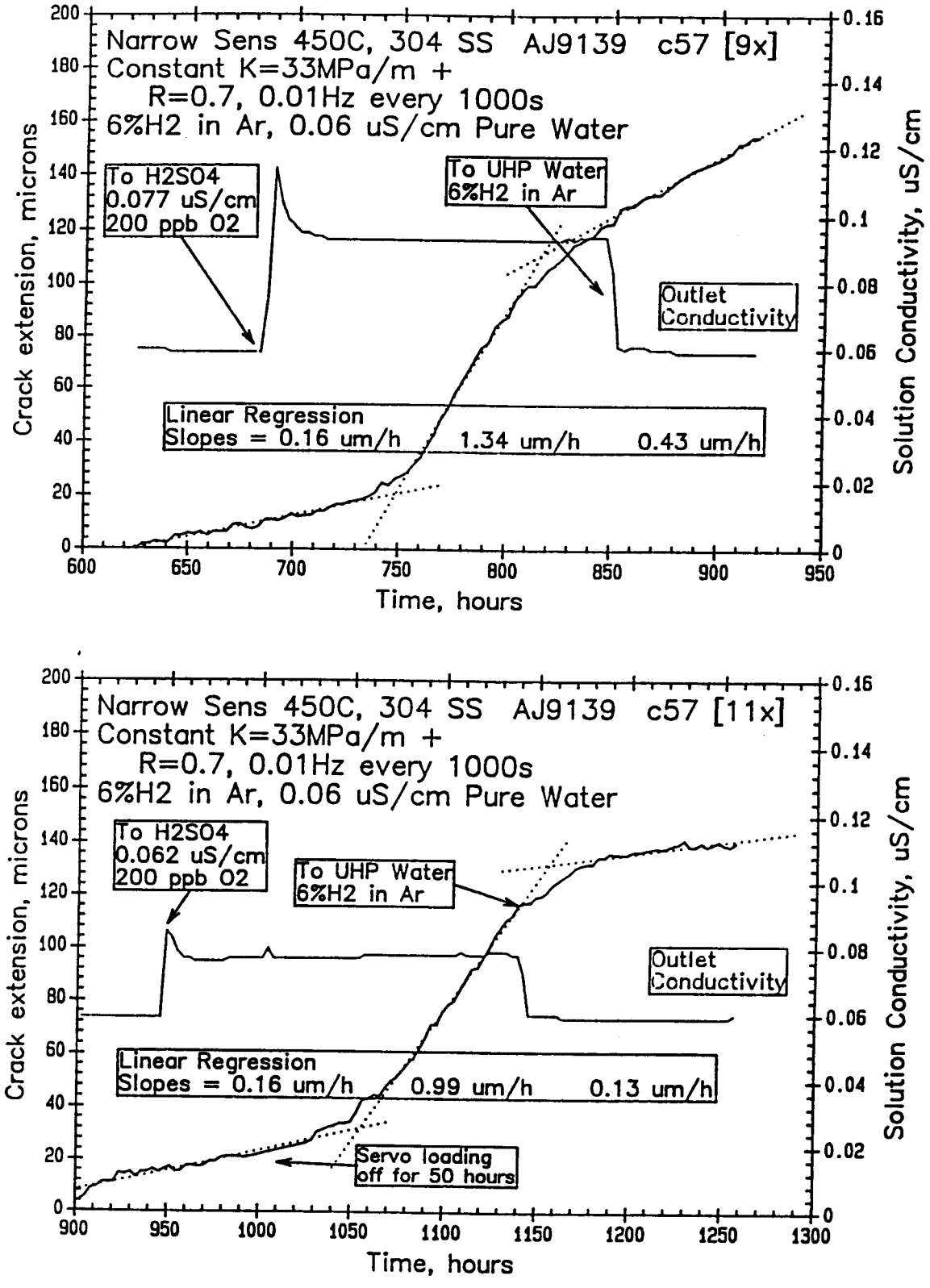

Figure 26 continued.

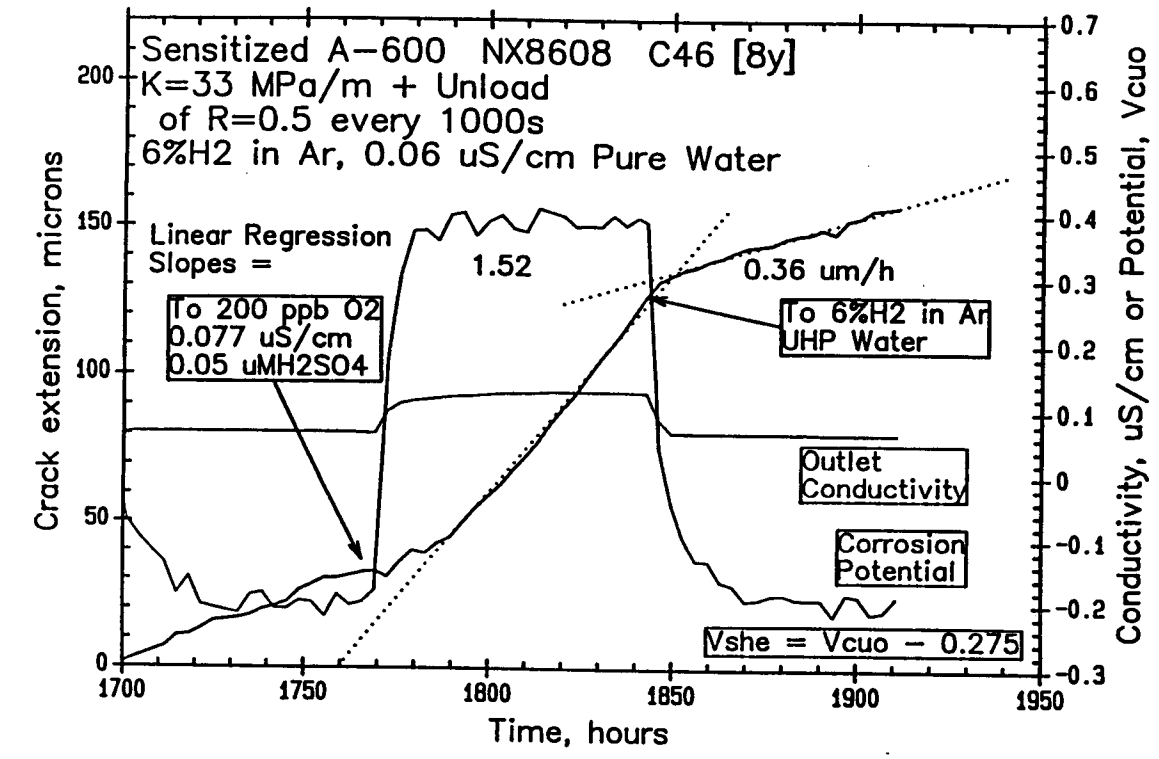

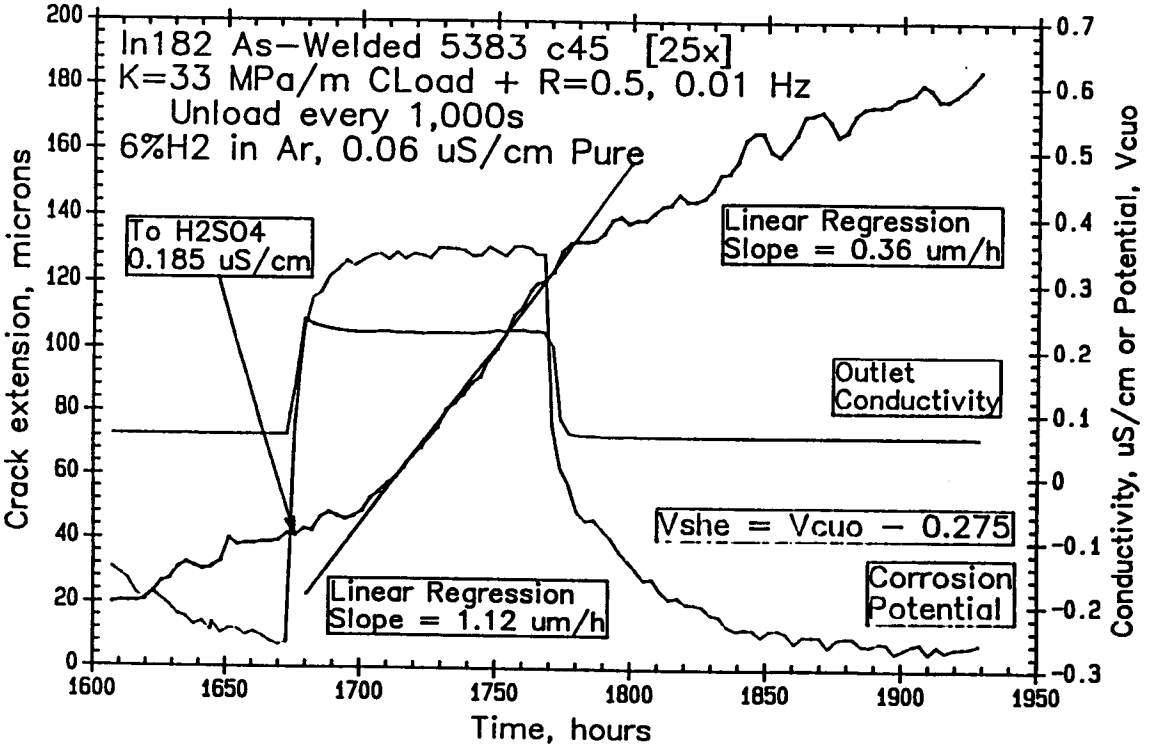

Figure 26 continued.

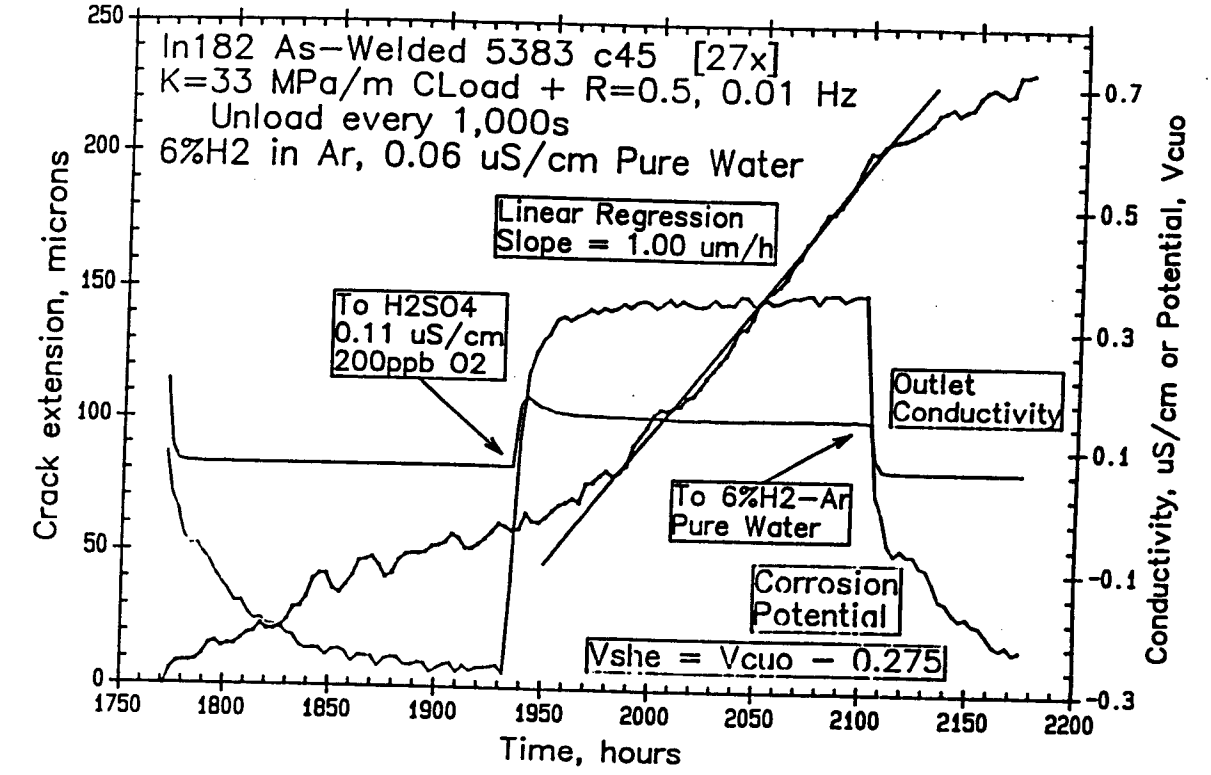

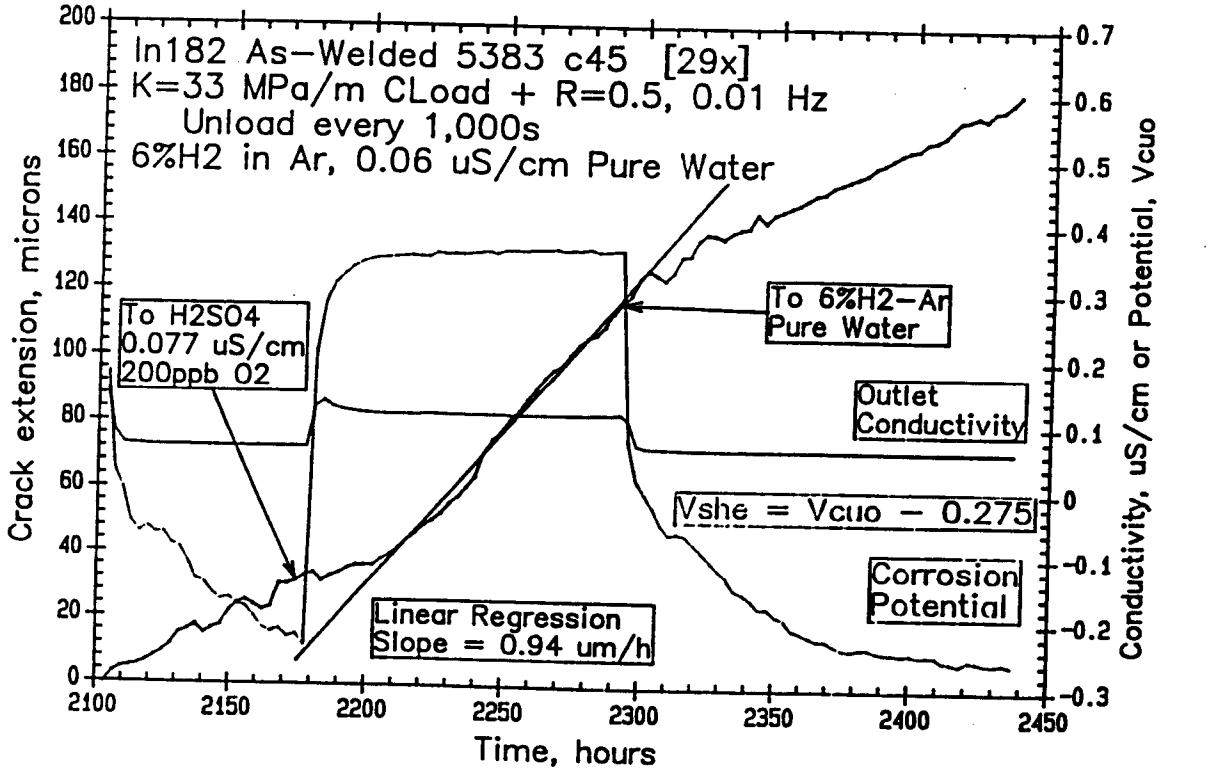

Figure 26 continued.

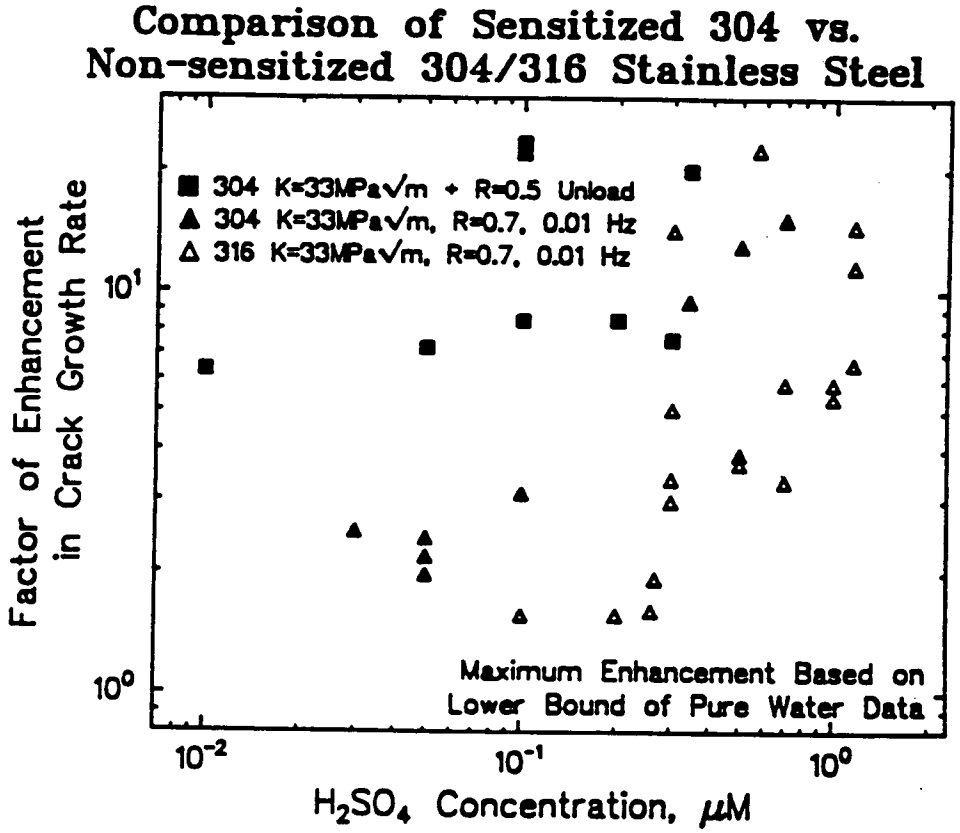

Figure 26 continued.

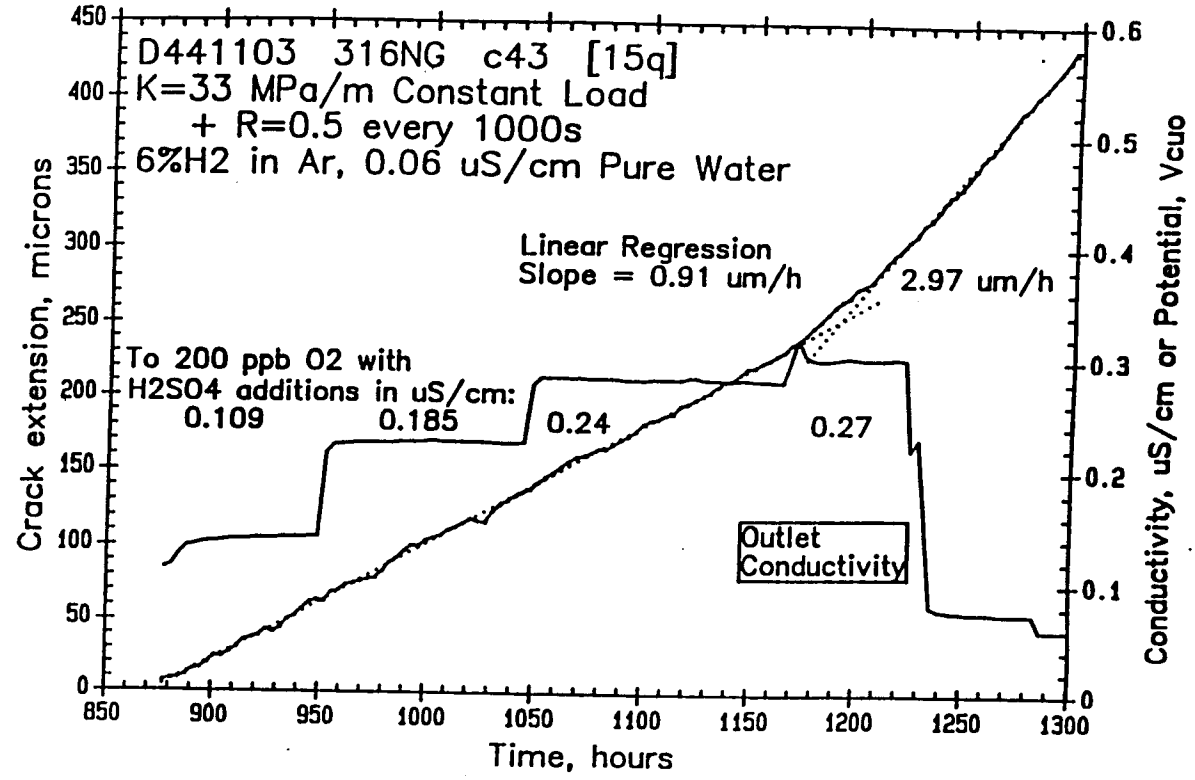

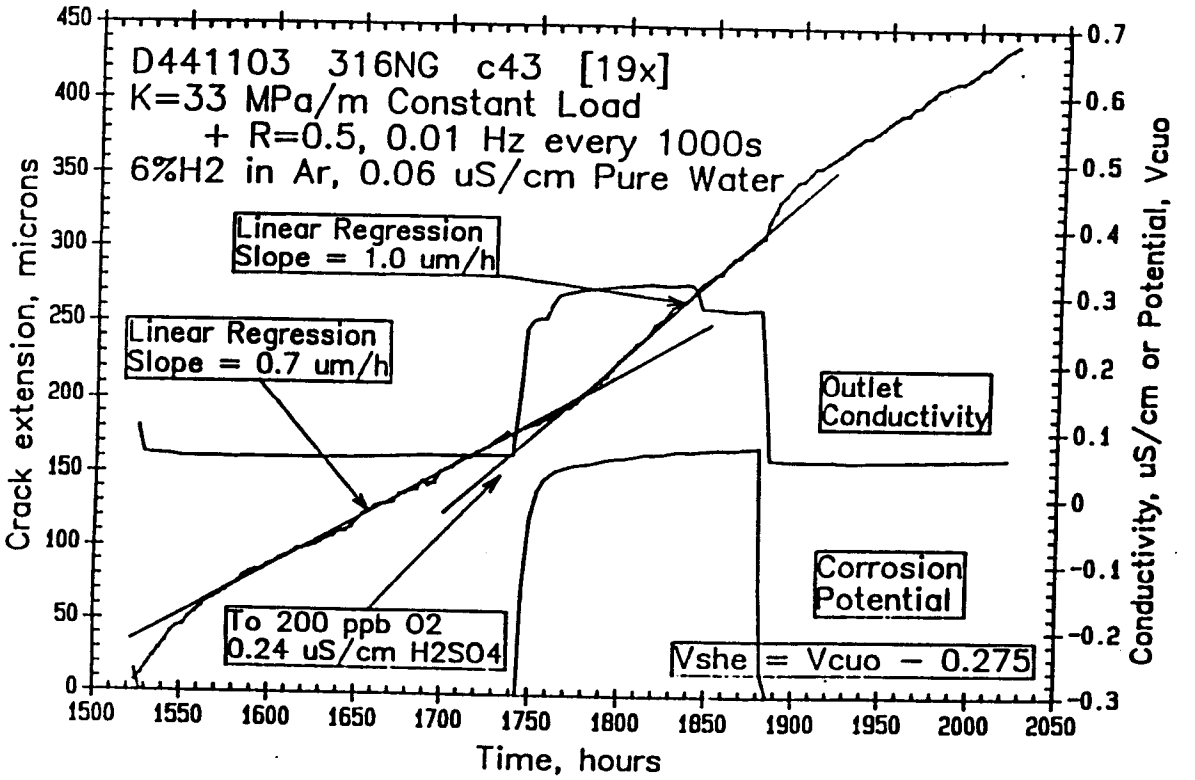

Figure 27. Crack length vs. time for CT specimens of non-sensitized stainless steel showing the effect of sulfate (as H_2SO_4) on the crack growth rate in 288°C water.

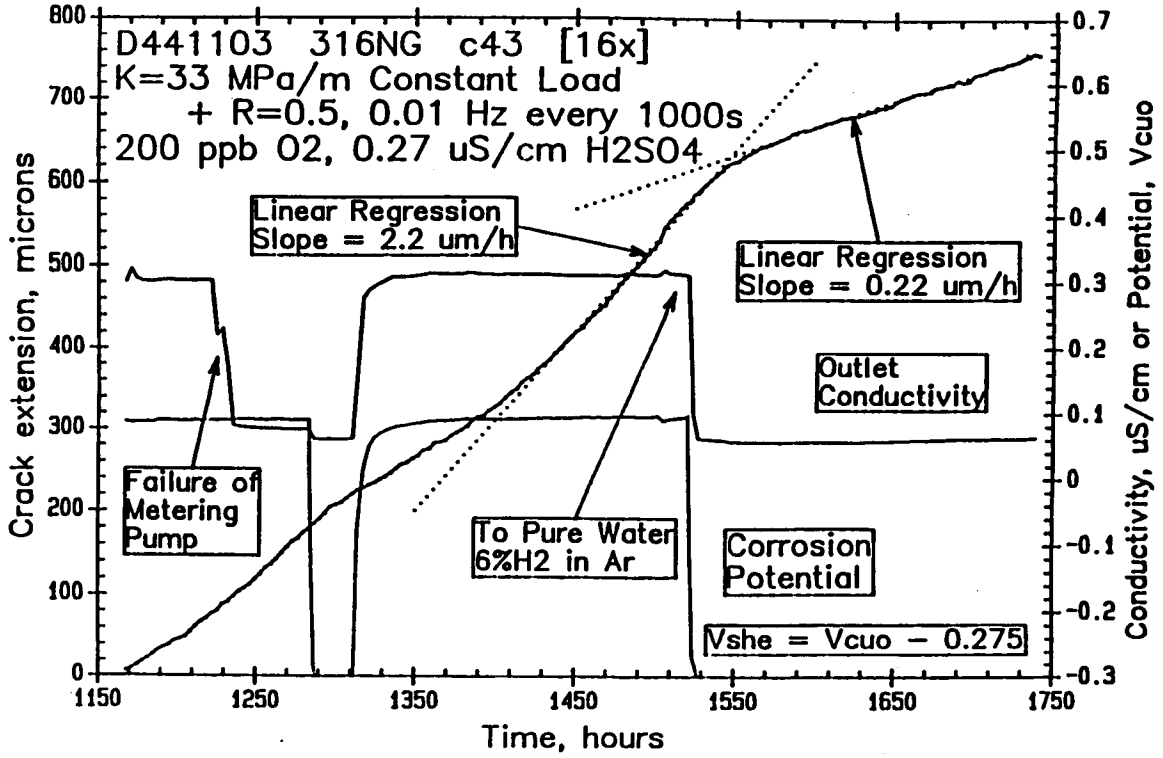

Figure 27 continued.

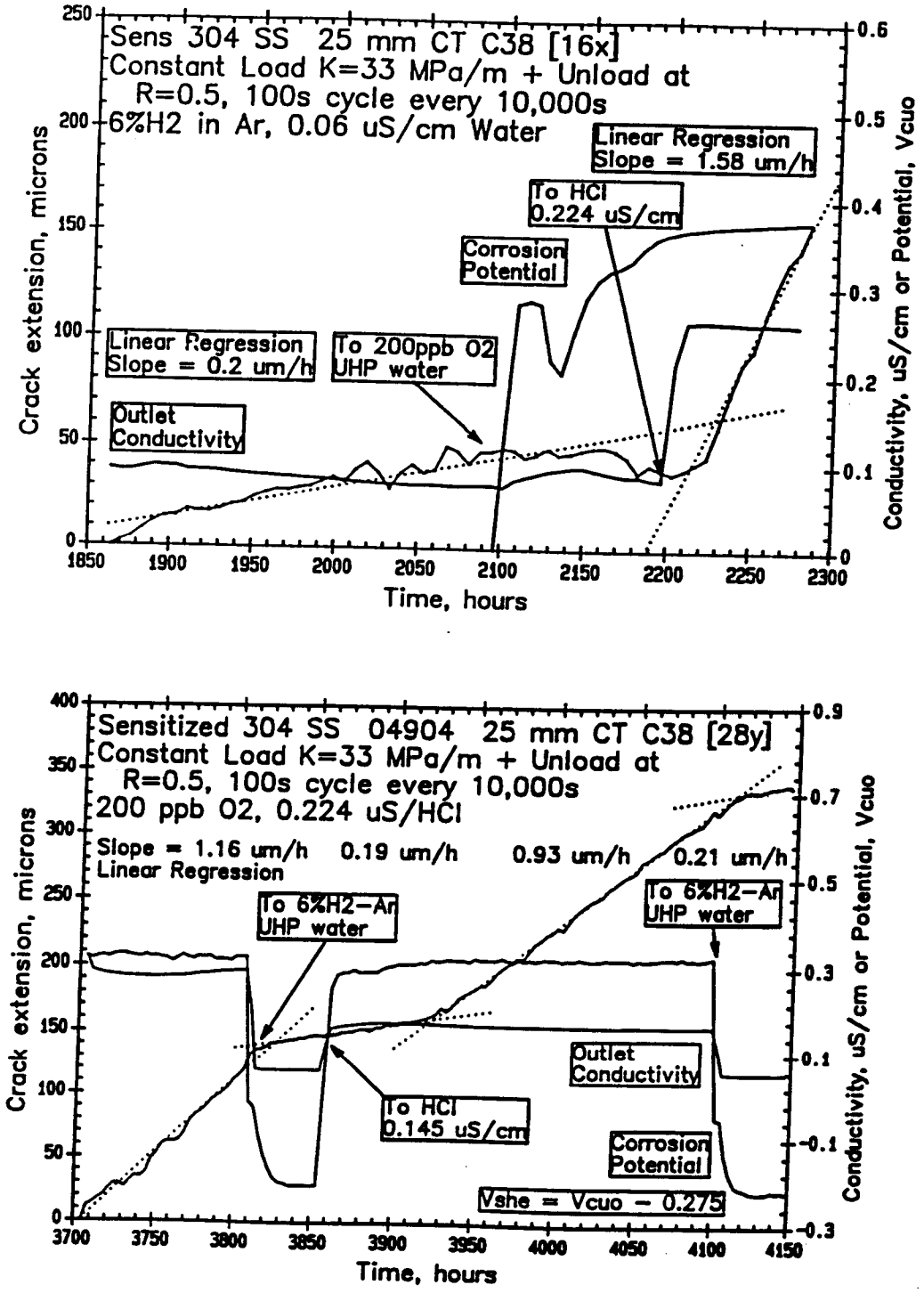

Figure 28. Crack length vs. time for CT specimens of sensitized type 304 stainless steel showing the effect of chloride (as HCl) on the crack growth rate in 288°C water. Also, the factor of enhancement as a function of HCl concentration for sensitized type 304 stainless steel. The enhancement factor is computed by dividing the steady state crack growth rate in impure water to that in pure water. The data represent an upper bound on the factor of enhancement since a lower bound value for the crack growth rate in pure water was employed.

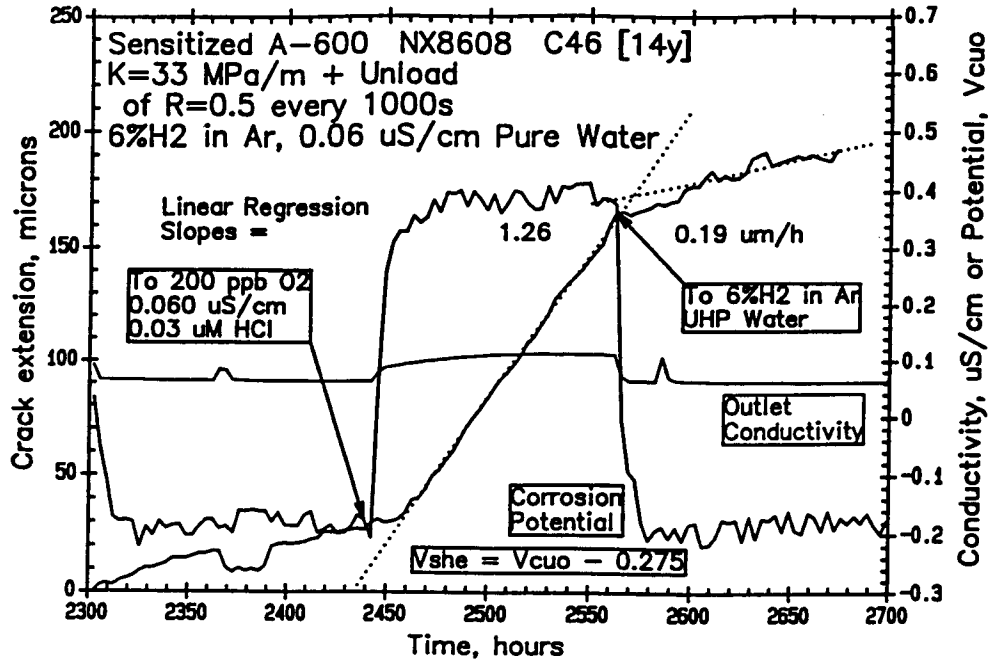

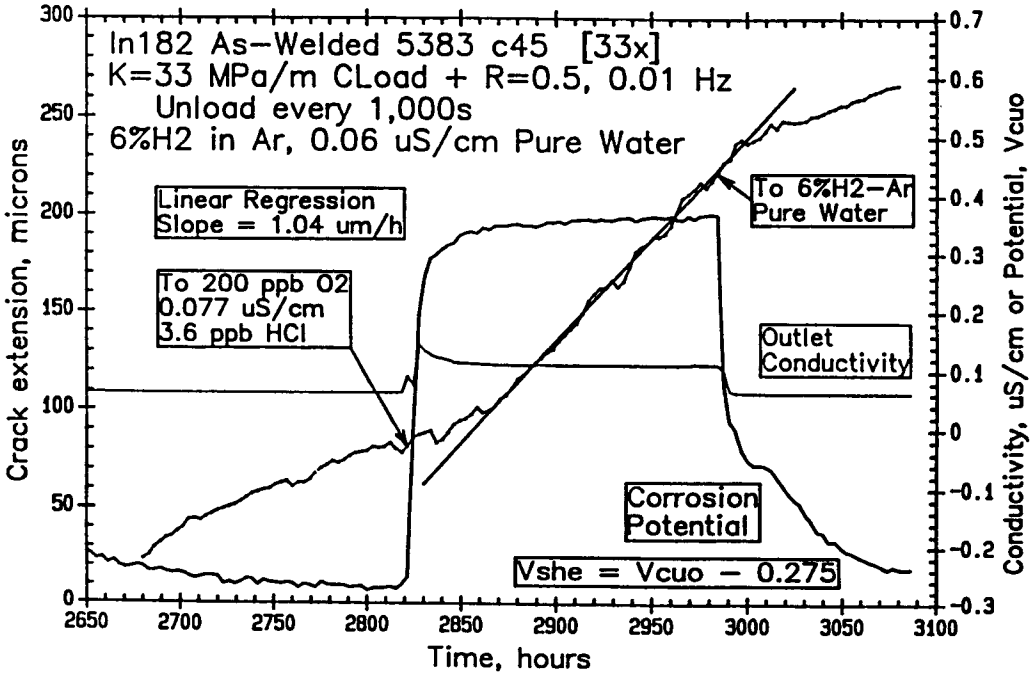

Figure 28 continued.

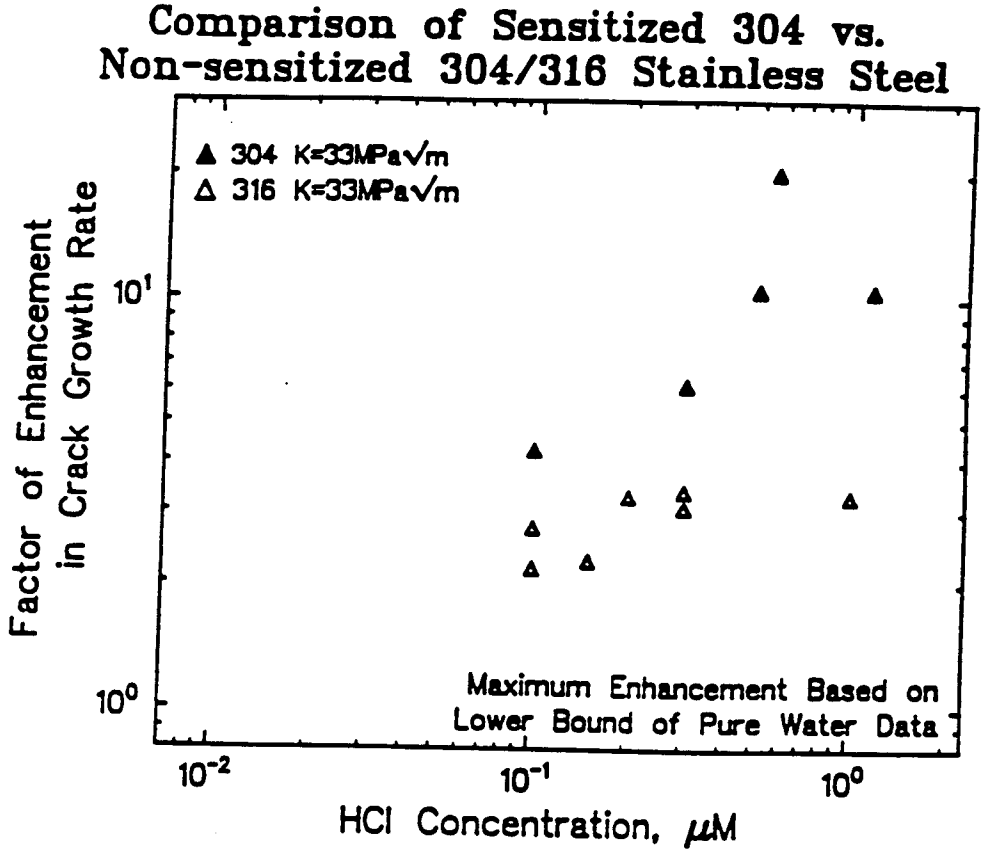

Figure 28 continued.

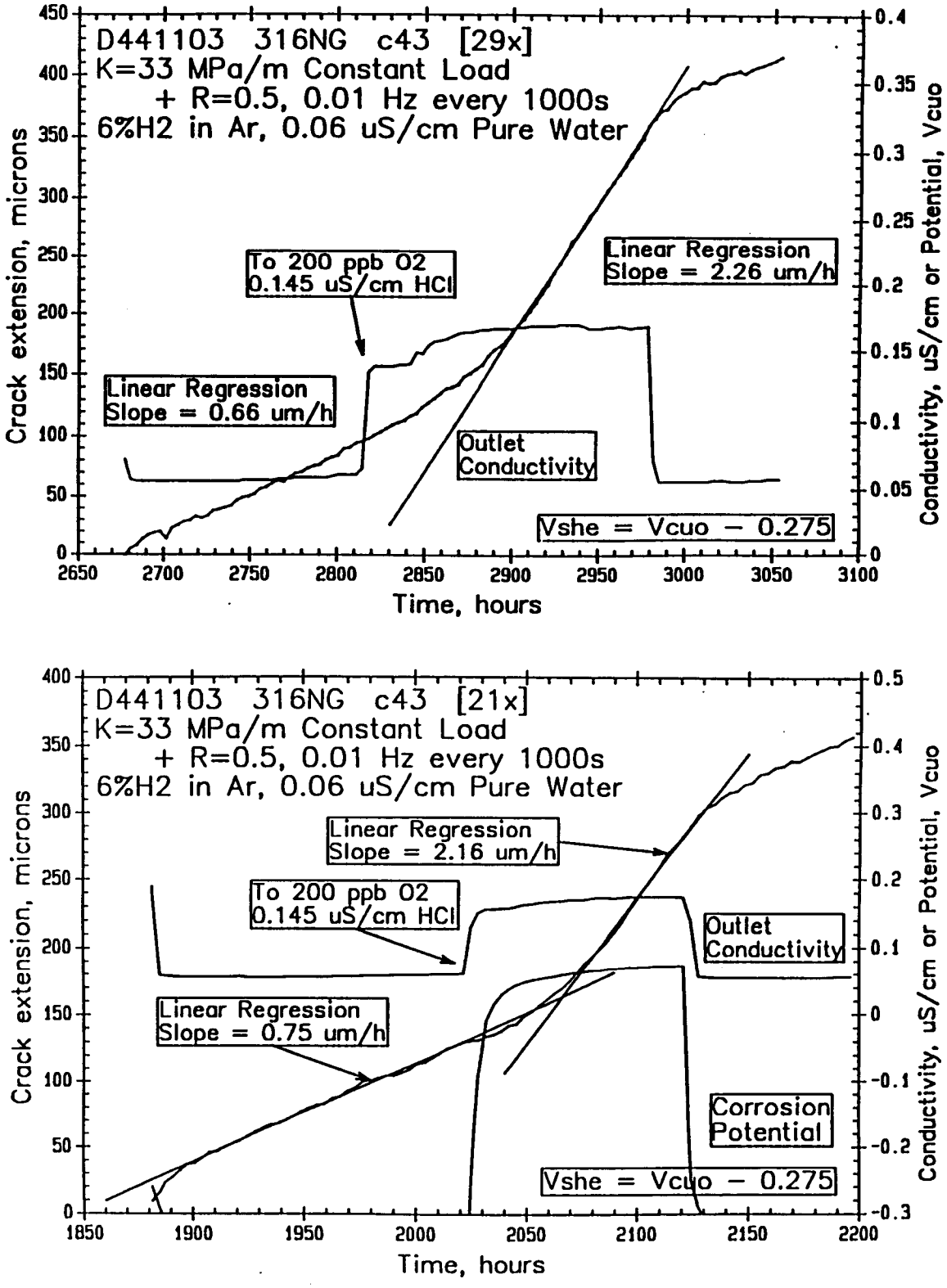

Figure 29. Crack length vs. time for CT specimens of non-sensitized stainless steel showing the effect of chloride (as HCl) on the crack growth rate in 288°C water.

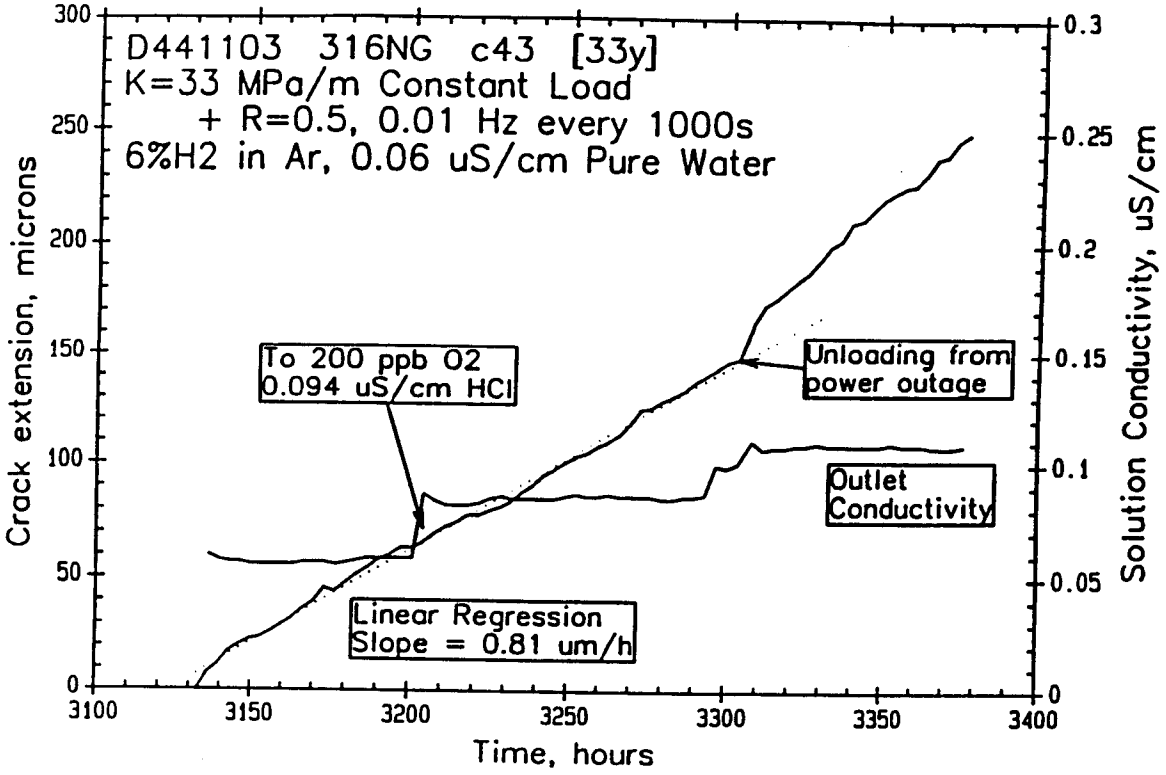

Figure 29 continued.

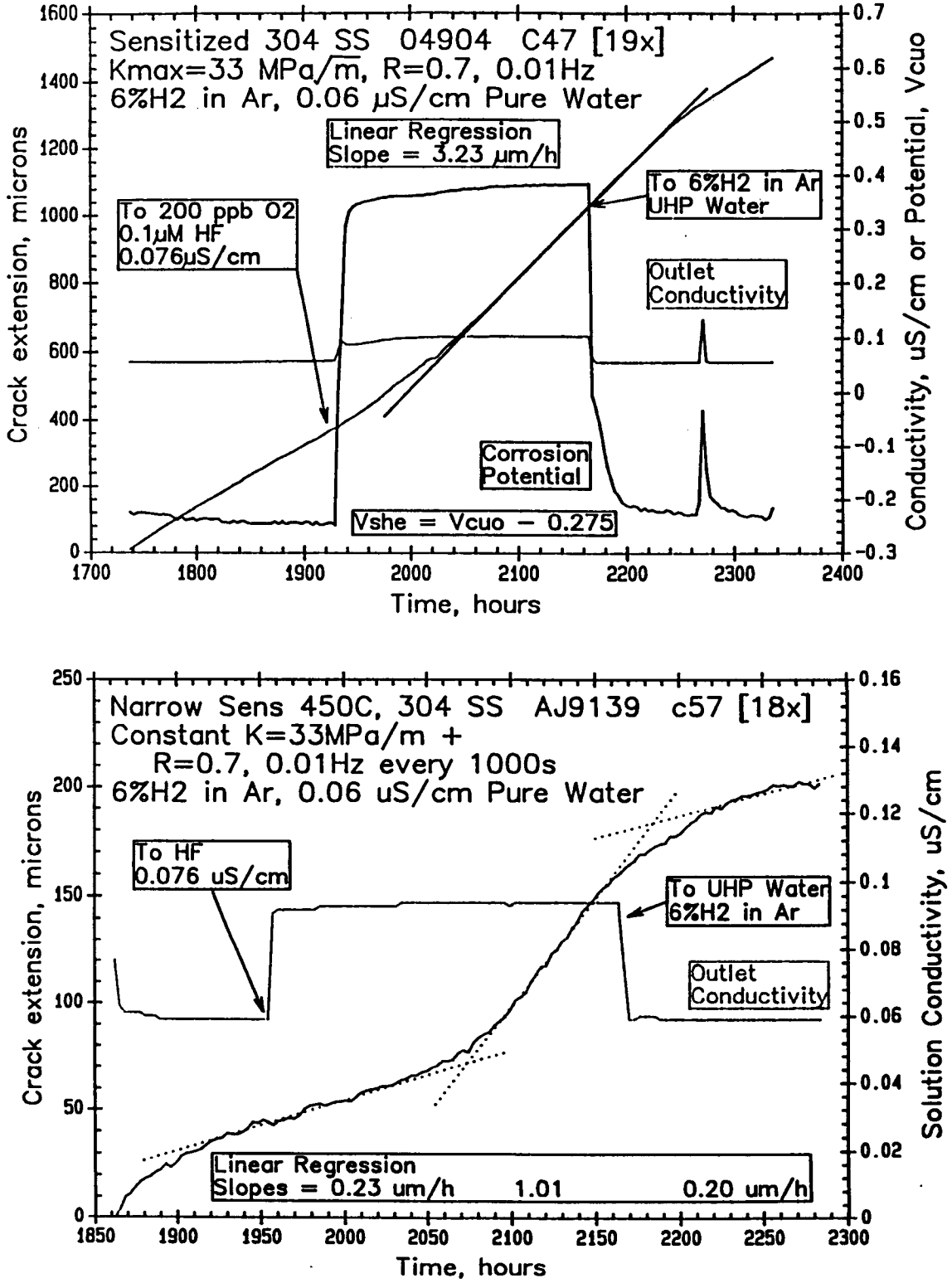

Figure 30. Crack length vs. time for CT specimens of sensitized type 304 stainless steel showing the effect of fluoride (as HF) on the crack growth rate in 288°C water.

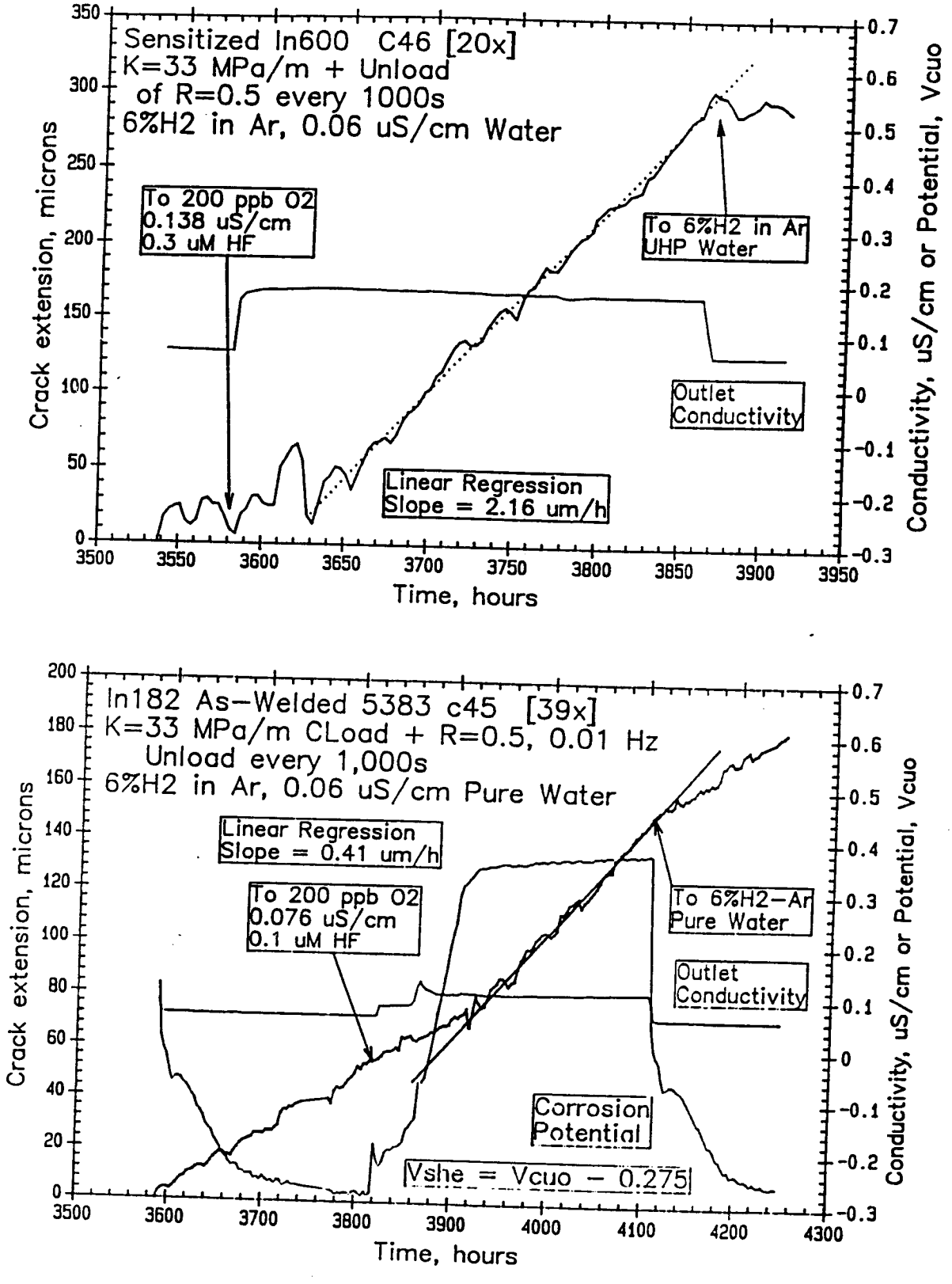

Figure 30 continued.

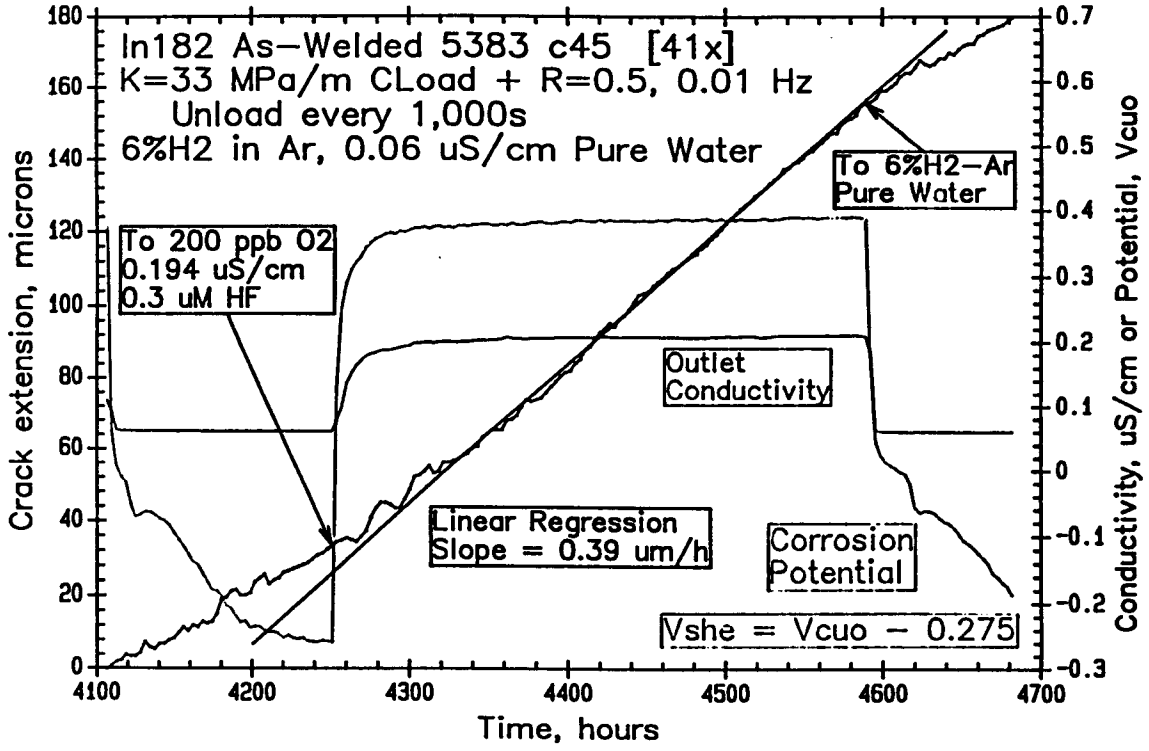

Figure 30 continued.

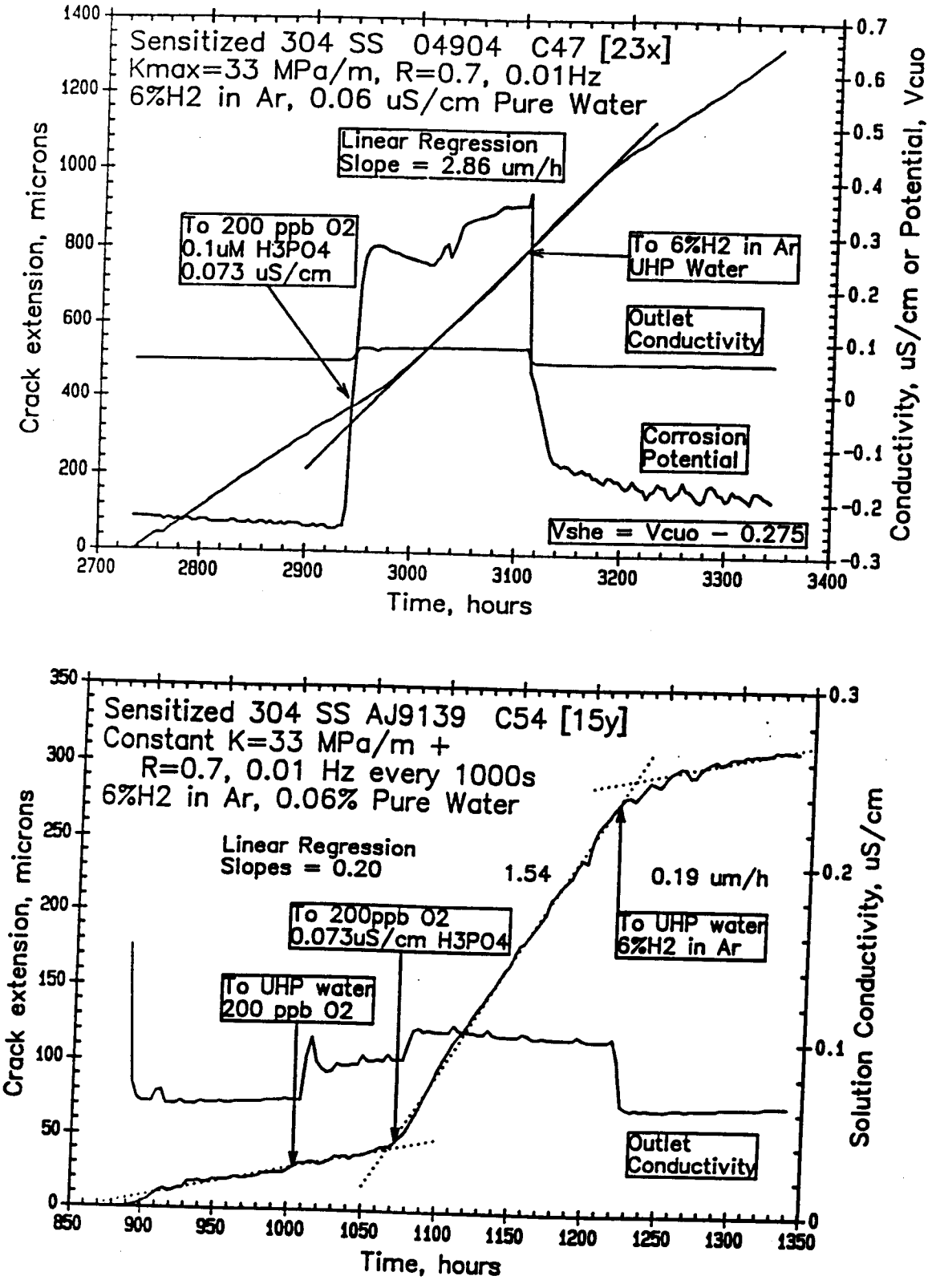

Figure 31. Crack length vs. time for CT specimens of sensitized type 304 stainless steel showing the effect of phosphate (as H_3PO_4) on the crack growth rate in 288°C water.

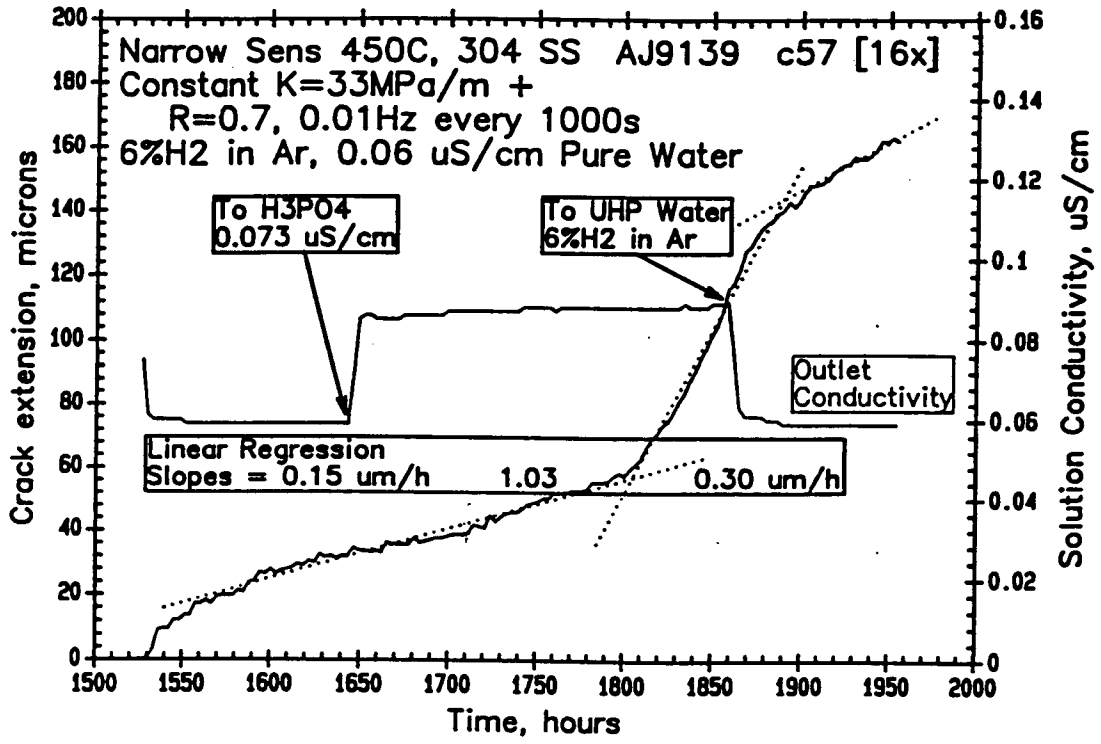

Figure 31 continued.

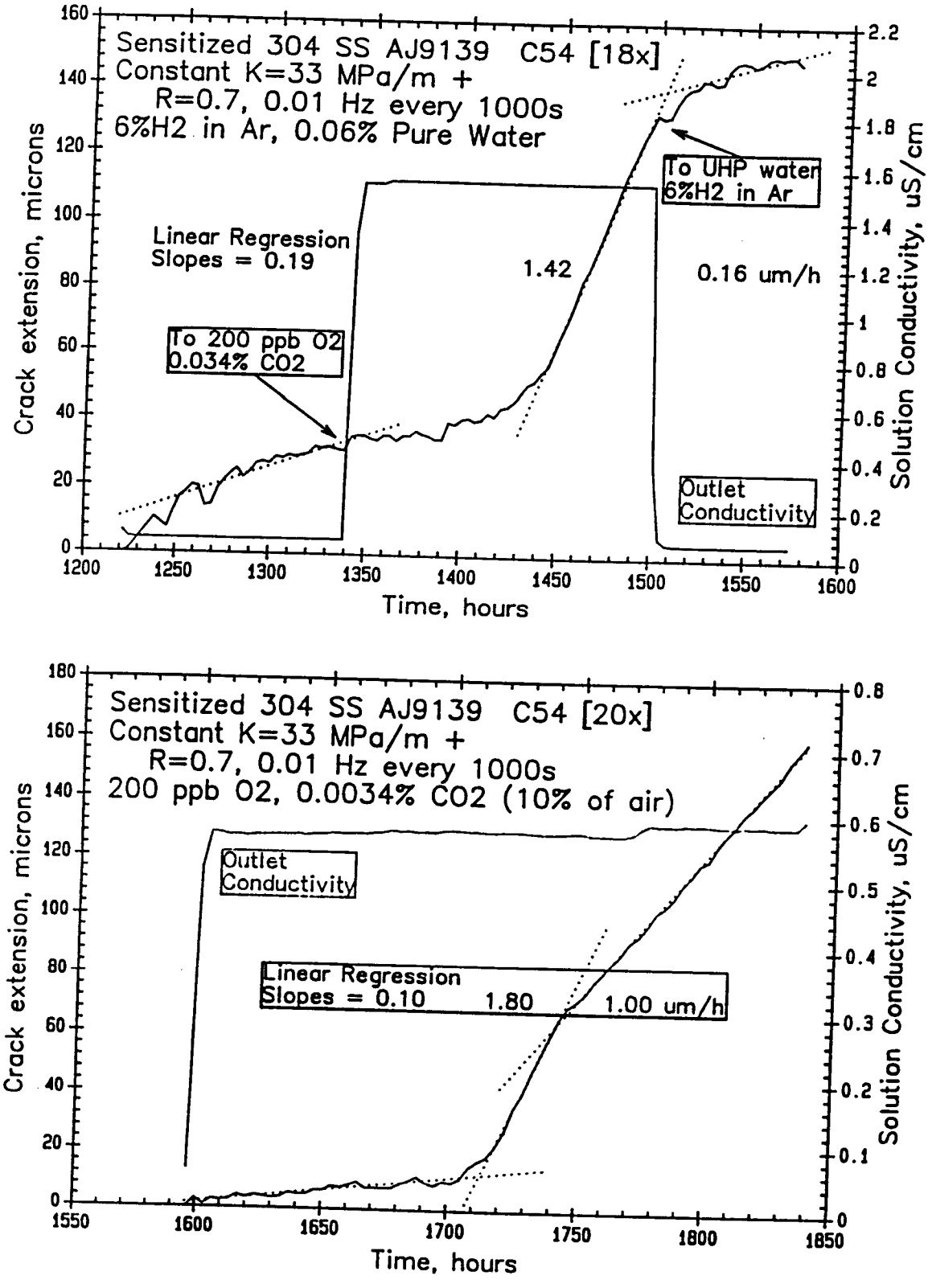

Figure 32. Crack length vs. time for CT specimens of sensitized type 304 stainless steel showing the effect of carbonate (as dissolved CO_2) on the crack growth rate in 288°C water.

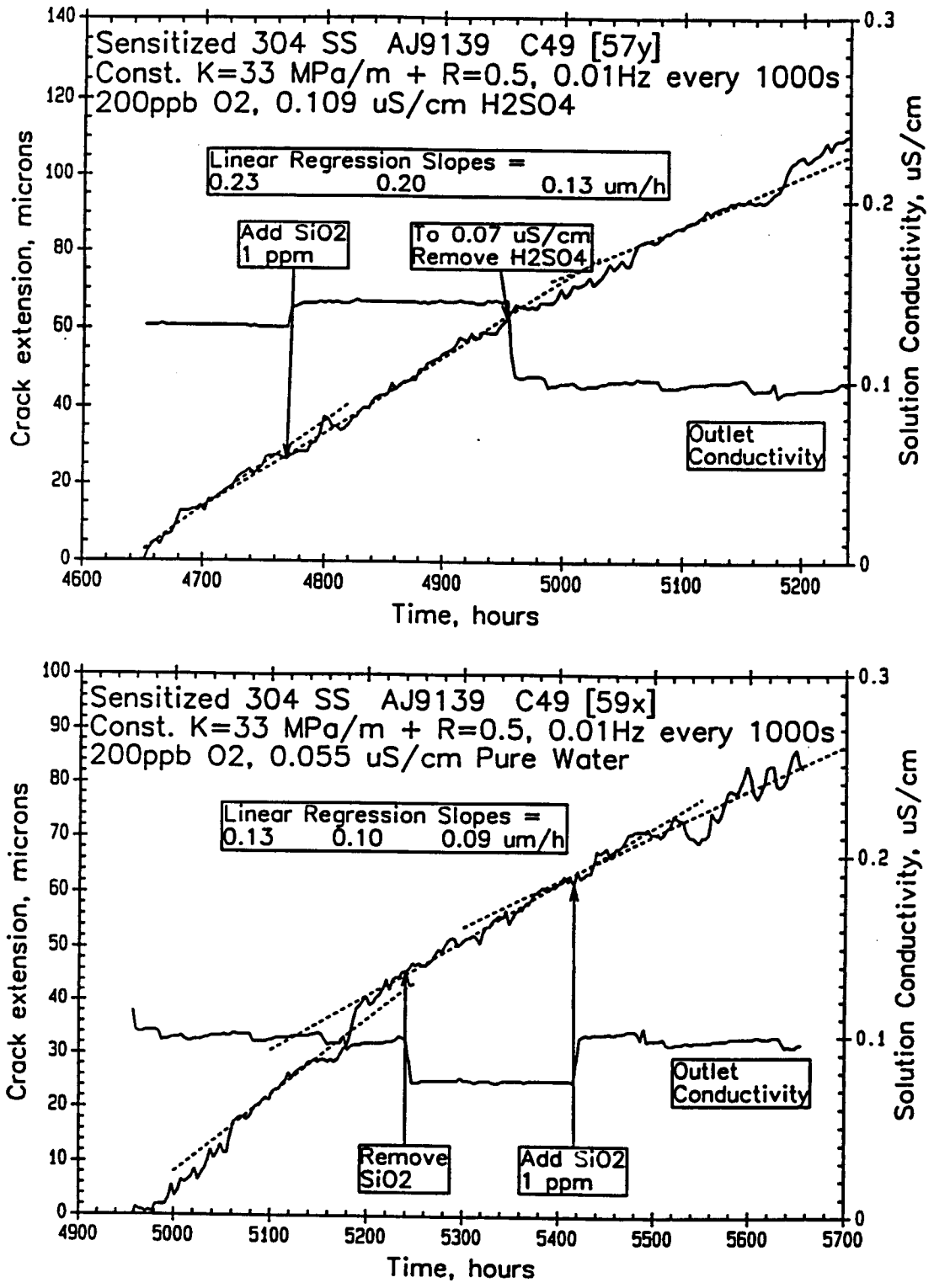

Figure 33. Crack length vs. time for CT specimens of sensitized type 304 stainless steel showing the effect of silica on the crack growth rate in 288°C water. High purity fumed silica was dissolved in water, where a very large fraction does not dissociate nor, therefore, contribute to conductivity.

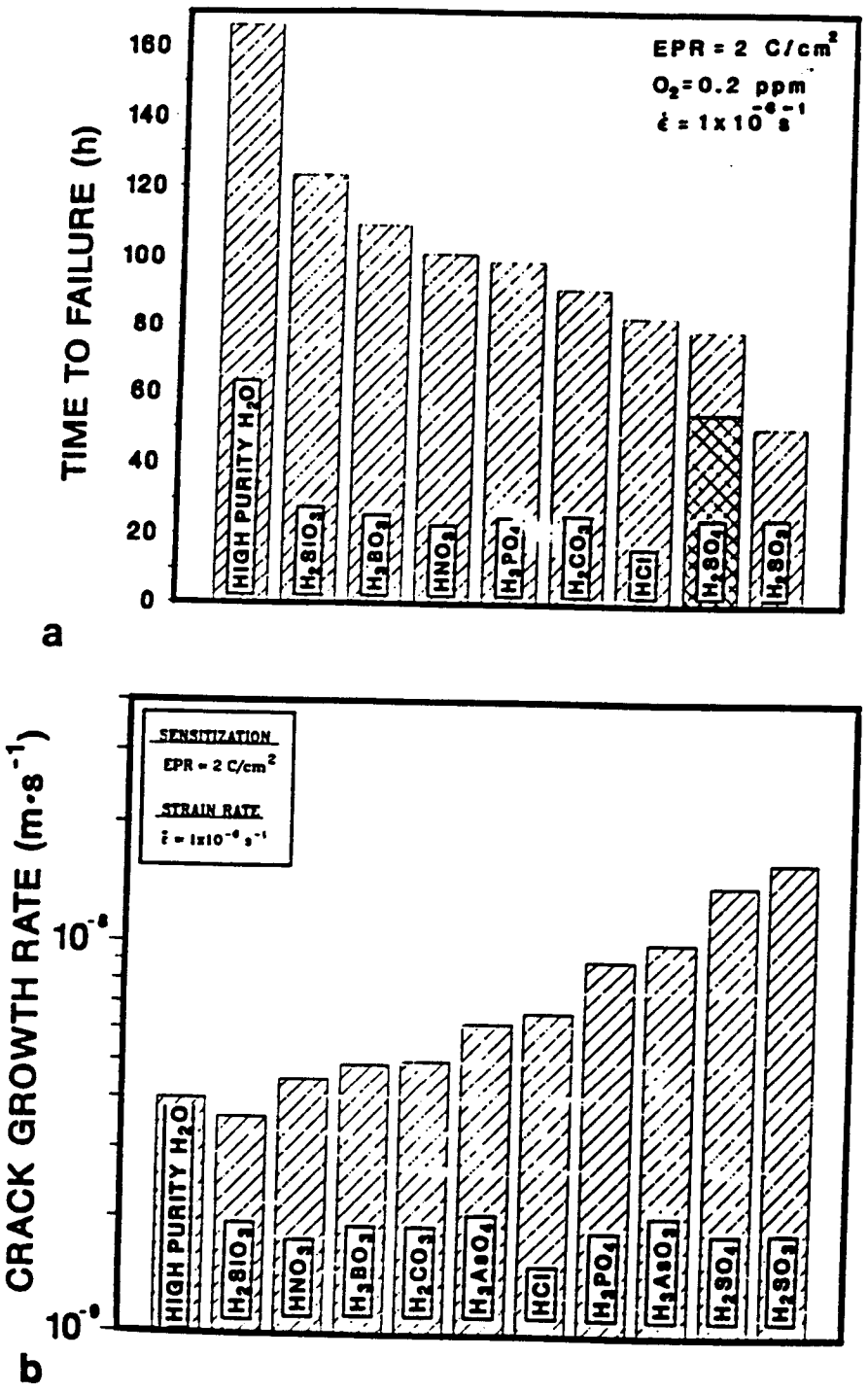

Figure 34. Effect of various impurities on stress corrosion cracking of sensitized type 304 stainless steel in 288°C water in slow strain rate tests performed at 10^{-6}/s.

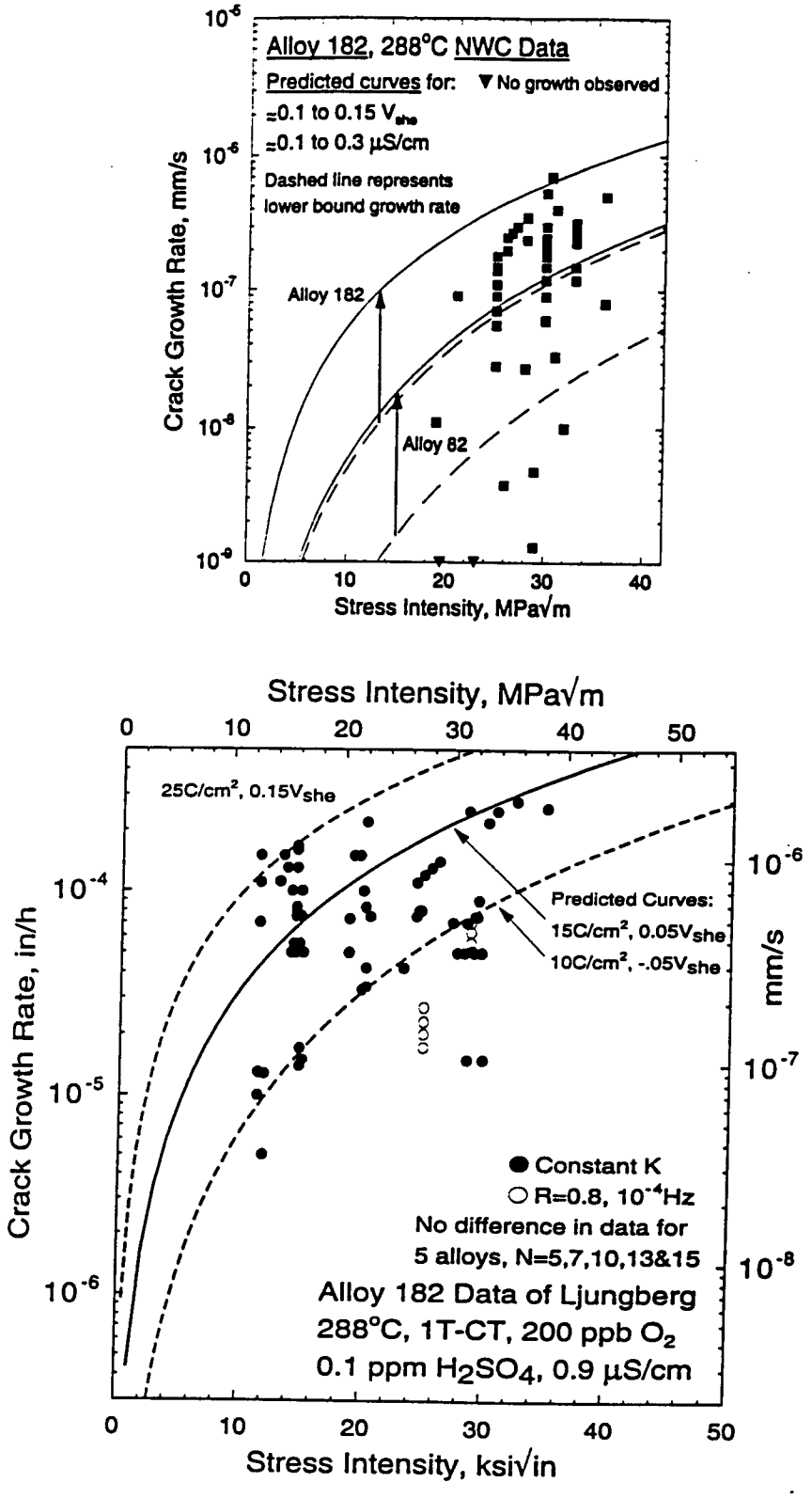

Figure 35. Effect of sulfate on stress corrosion crack growth rates of sensitized Alloy 182 weld metal in 288°C water.

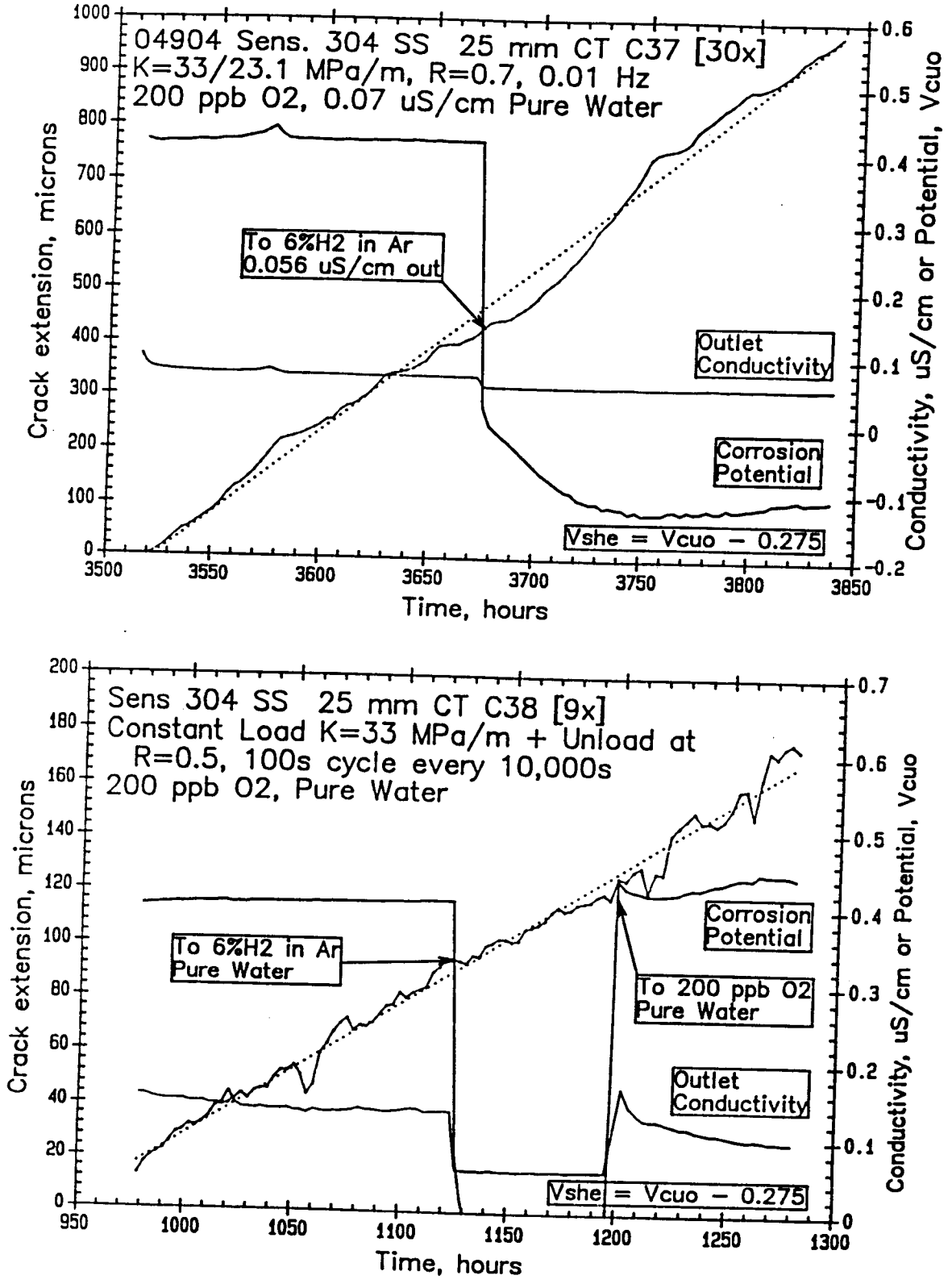

Figure 36. Crack length vs. time for CT specimens of sensitized type 304 stainless steel where *no effect* of corrosion potential shifts associated with a change from 0 to 200 ppb oxygen (≈ –0.5 to ≈ 0.1 V_{she}) on the crack growth rate was observed in 288°C water.

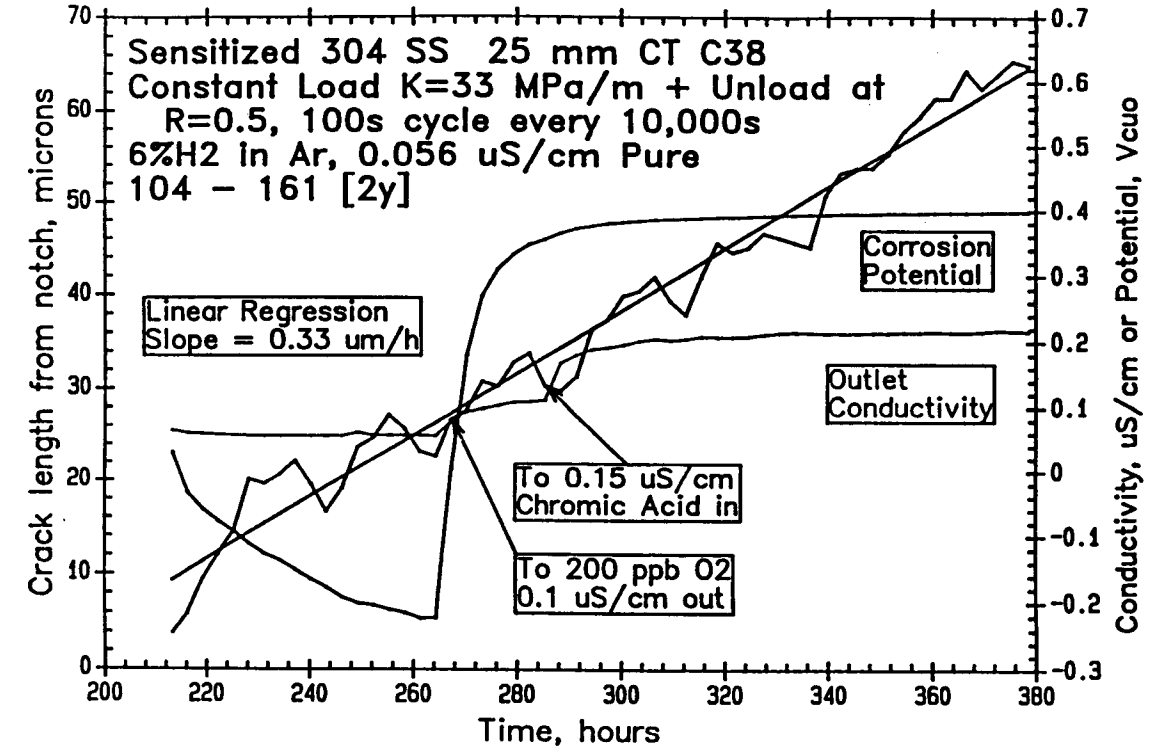

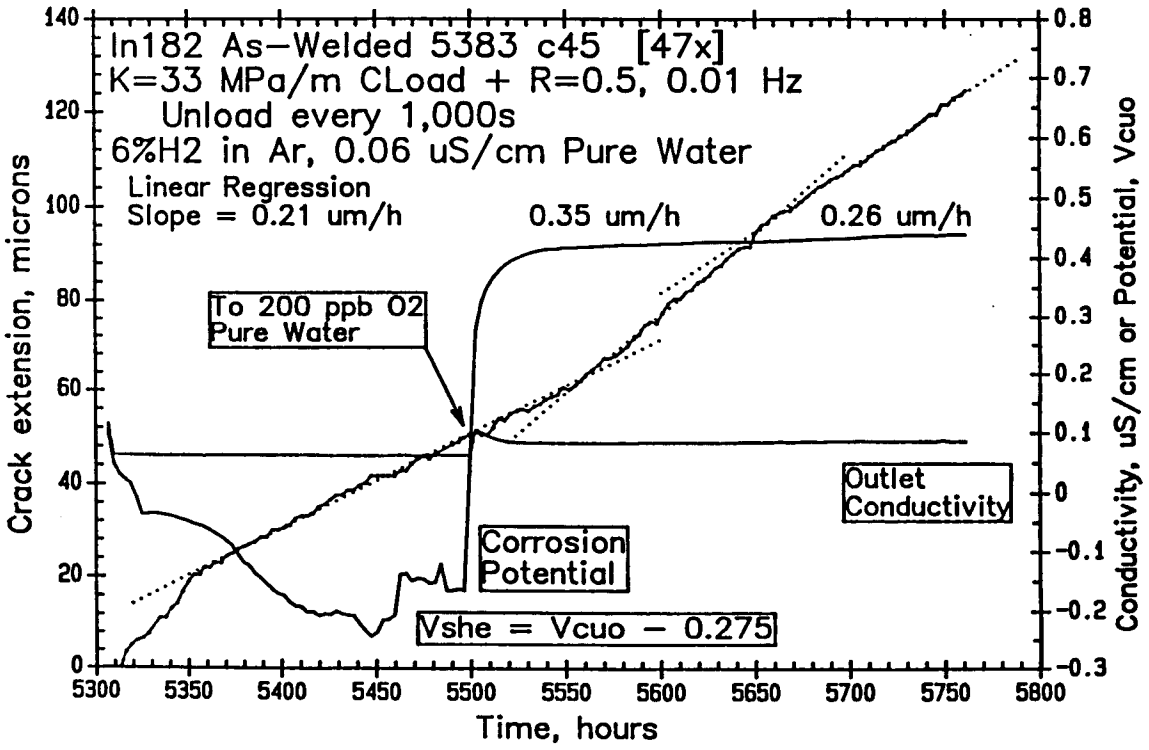

Figure 36 continued.

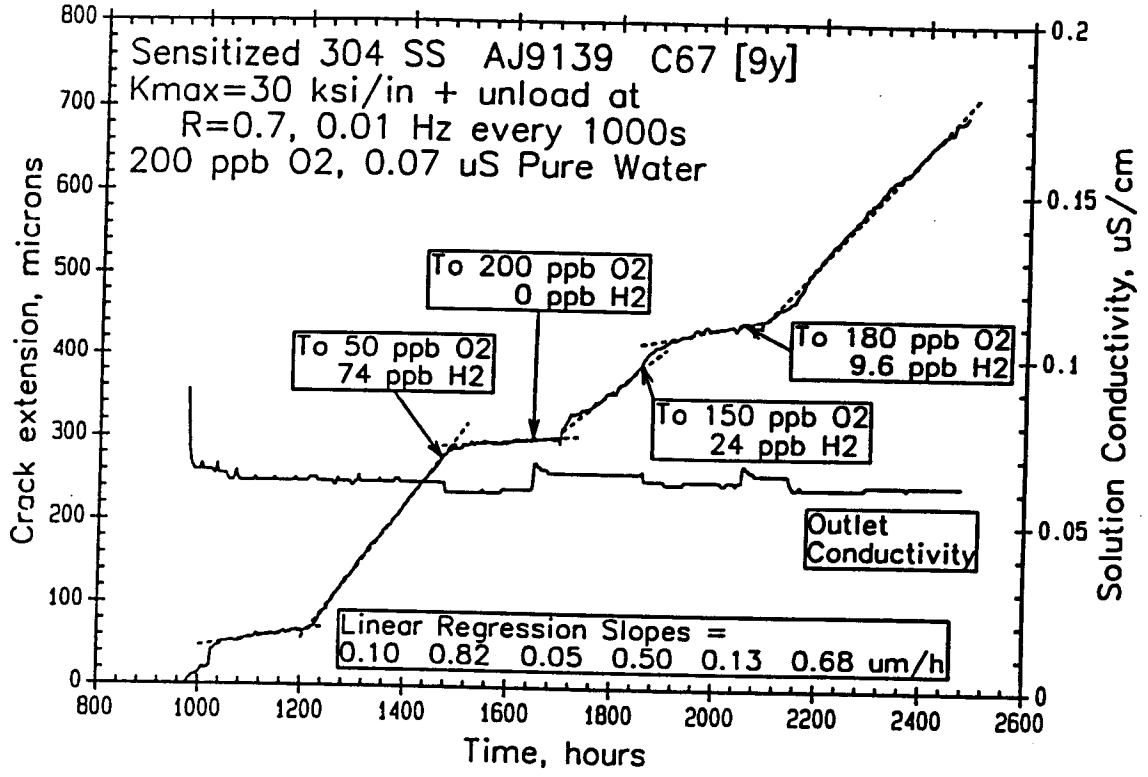

Figure 37. Crack length vs. time for CT specimens of sensitized type 304 stainless steel where *an effect was observed* of corrosion potential shifts associated with a change from 0 to 200 ppb oxygen (≈ -0.5 to ≈ 0.1 V_{she}) on the crack growth rate in 288°C water.

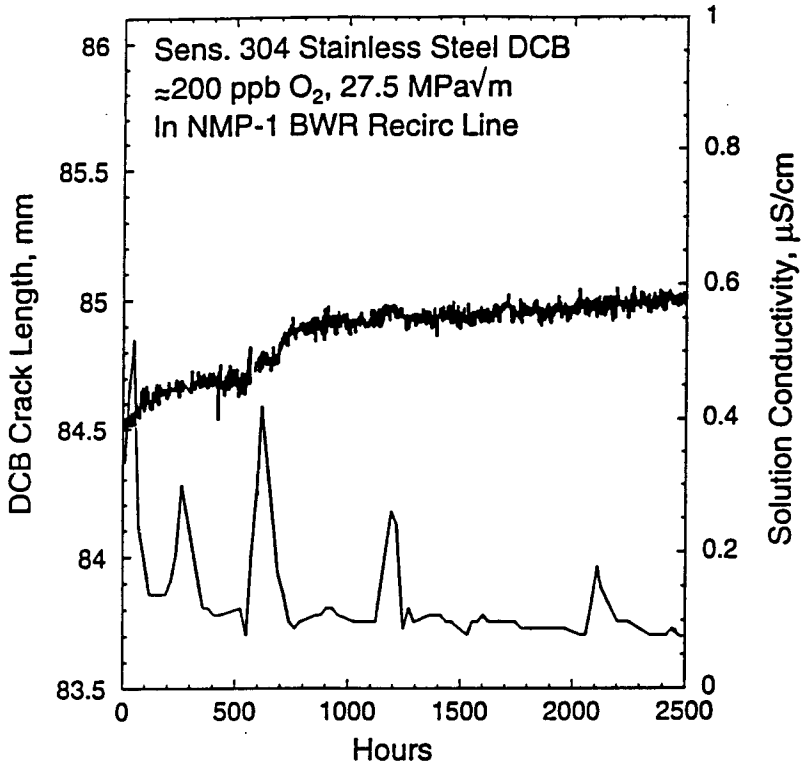

Figure 38. The crack length vs. time response for a double cantilever beam specimen of sensitized type 304 stainless steel wedge loaded to 27.5 MPa$\sqrt{m}$ and exposed in a flange to BWR recirculation water. Under otherwise constant conditions, the crack growth response during the first 1000 hours is sensitive to solution conductivity transients. While these transients have short term effects, the crack growth rate returns to a low level within ≈100 - 200 hours after the transient.

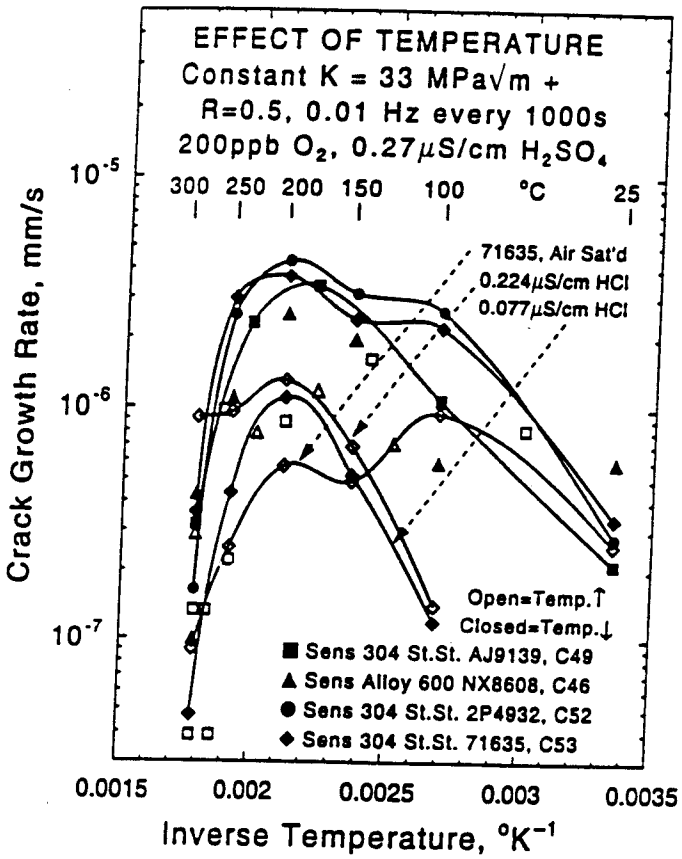

Figure 39. The effect of temperature on crack growth rate of sensitized type 304 stainless steel and sensitized Alloy 600 in pure water with moderate impurity levels. In relatively pure water, the crack growth rate decreases rapidly above ≈200°C, and this is the regime where water chemistry effects are particularly pronounced. While some differences among materials may exist, scatter in the data and differences between data obtained under decreasing vs. increasing temperature appear to dominate over difference heat-to-heat variations of sensitized stainless steel vs. sensitized Alloy 600.

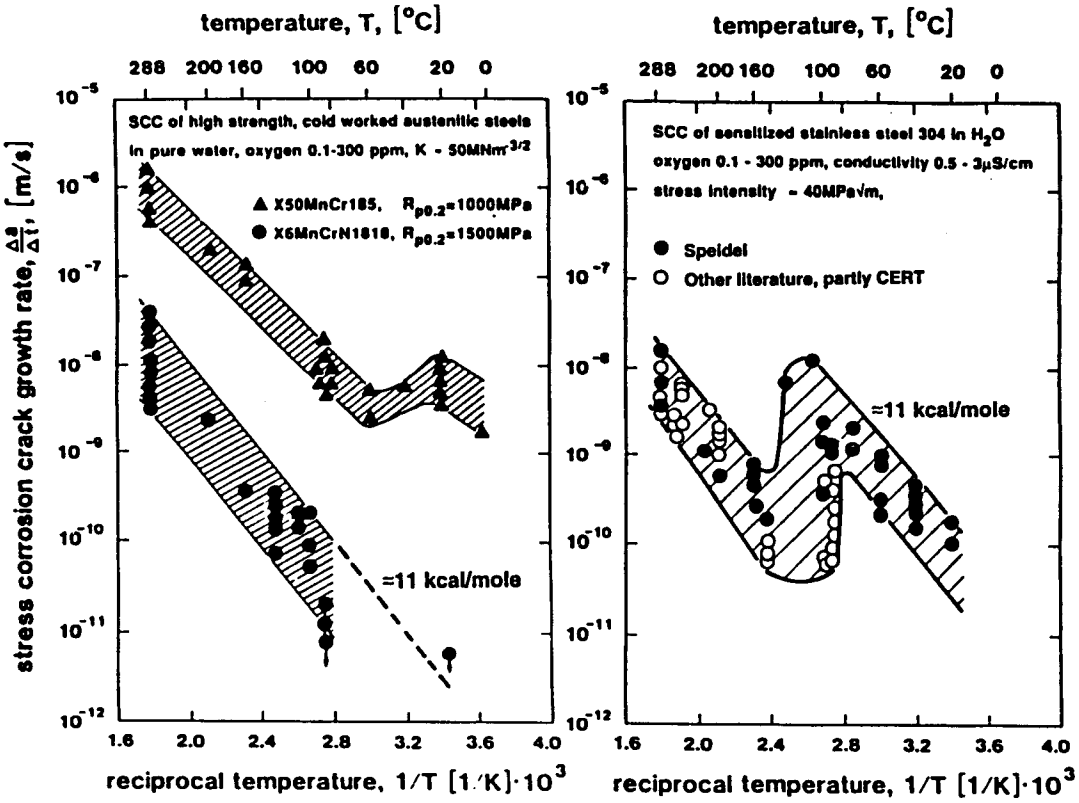

Figure 40. The effect of temperature on average crack growth rate in pre-cracked, wedge loaded, double cantilever beam specimens of (a) cold worked, high Mn "stainless steels" (X50MnCr185 is 18Mn-5.1Cr-1Ni-0.54C, intergranular cracking; X6MnCrN1818 is 19Mn-18%Cr-0.7Ni-0.6N-0.06C, transgranular cracking), and (b) sensitized type 304 stainless steel (intergranular cracking). In this more aggressive water chemistry, the crack growth rate tends to increase monotonically with temperature, in contrast to Figure 39. Interpretation is complicated by the range in dissolved oxygen (0.1 to 300 ppm), the effects of initiation on average growth rate obtained by post-fracture visual examination, and the variation in corrosion potential and pH in this activation energy plot.

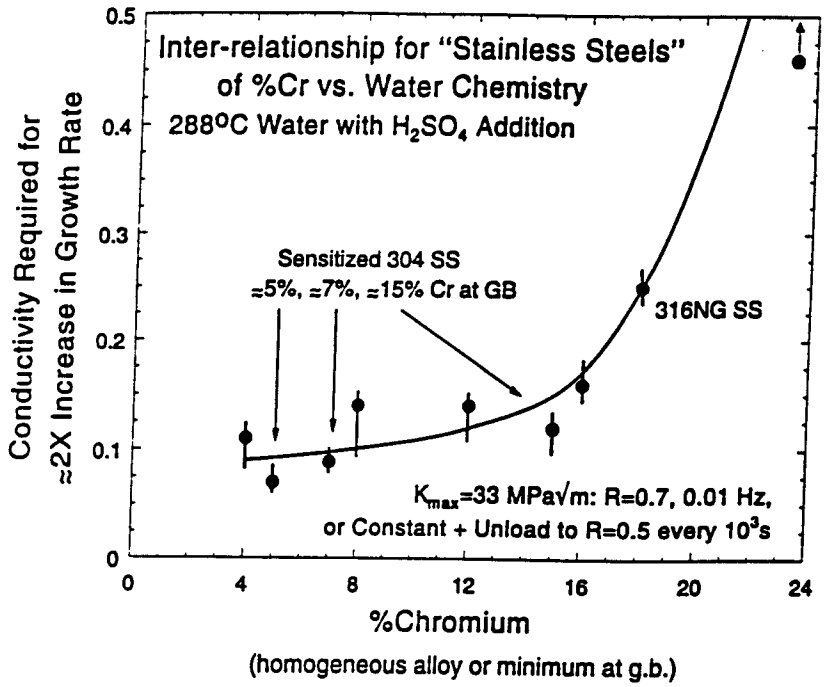

Figure 41. The relationship between the chromium content in "stainless steel" and the solution conductivity (as H_2SO_4) required to cause a 2X increase in crack growth rate above that observed in high purity water. Variations in chromium content were achieved by using custom melted, homogeneous alloys as well as by heat treating commercial type 304 stainless steel and measuring the grain boundary chromium profile by analytical electron microscopy.

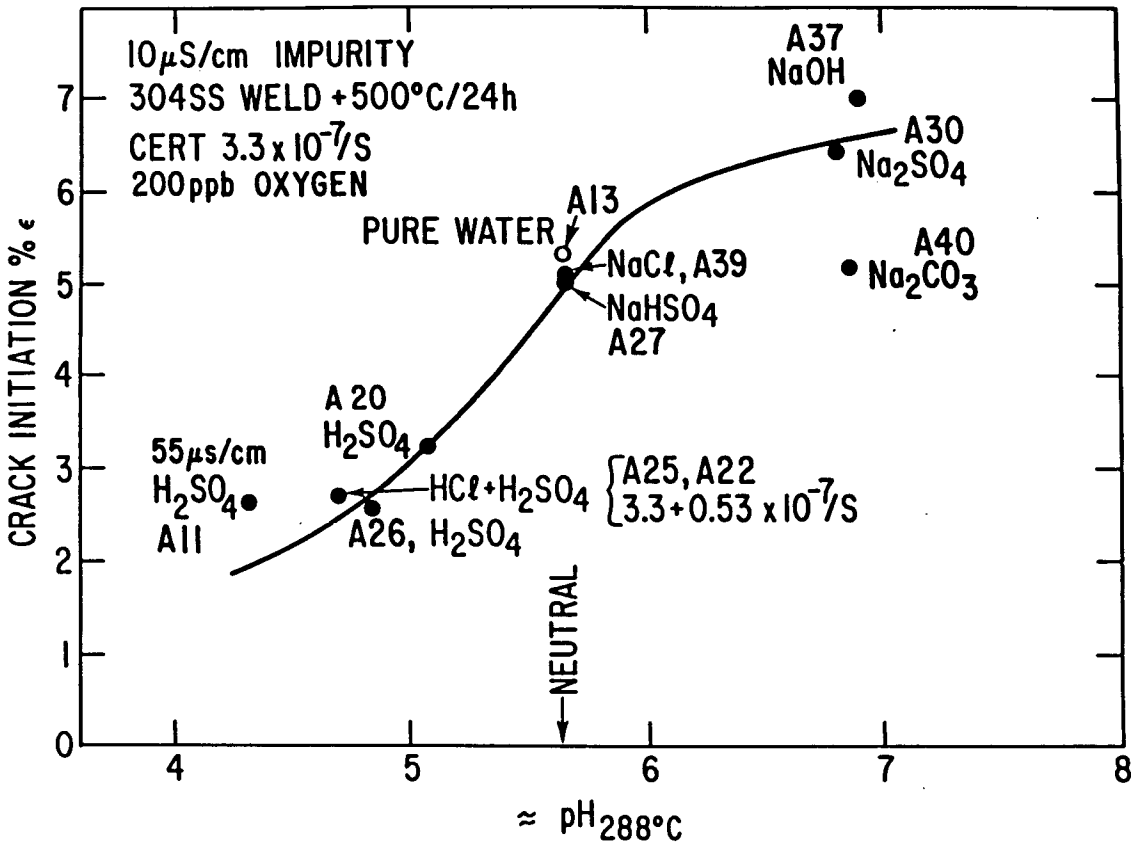

Figure 42. The effect of impurities on crack initiation as measured by repeated interruption during slow strain rate testing of sensitized stainless steel in 288°C water. Results correlated poorly with impurity level (or solution conductivity), but show good correlation with (approximate) pH at temperature.

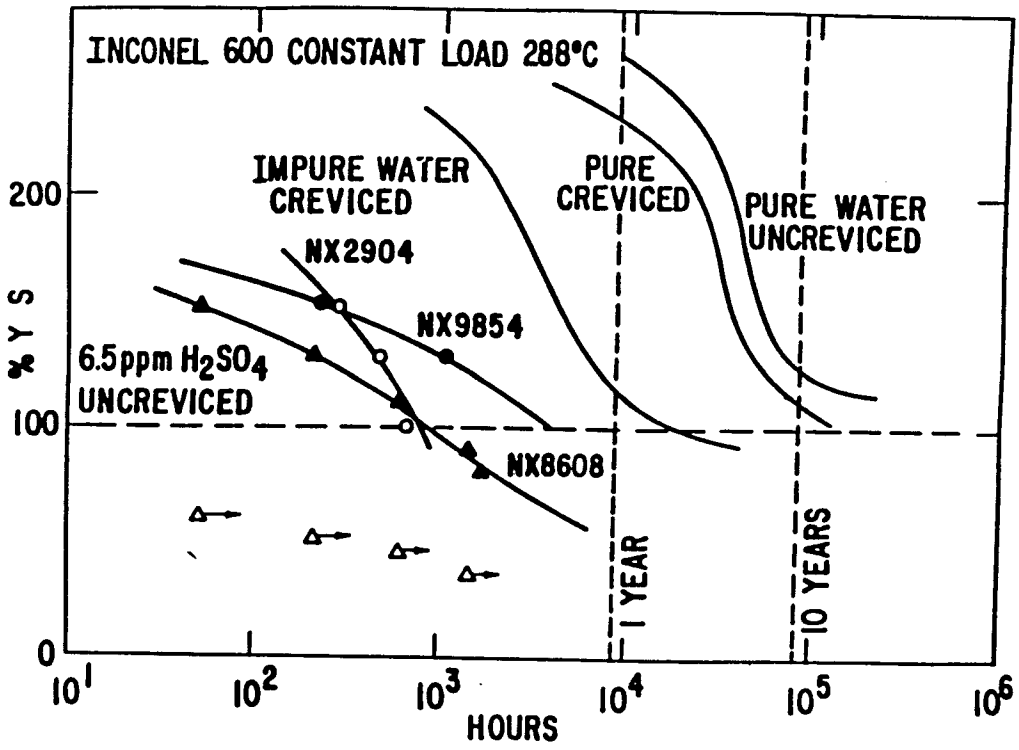

Figure 43. Effect of applied stress on intergranular stress corrosion cracking of creviced and uncreviced sensitized Alloy 600 under constant load conditions in 288°C water. The curves marked *"Impure Water Creviced"*, *"Pure Creviced"*, and *"Pure Water Uncreviced"* represent long-term laboratory and in-reactor specimen data. The curves with data represent laboratory data on several heats of sensitized Alloy 600 under a simulated, severe resin intrusion.

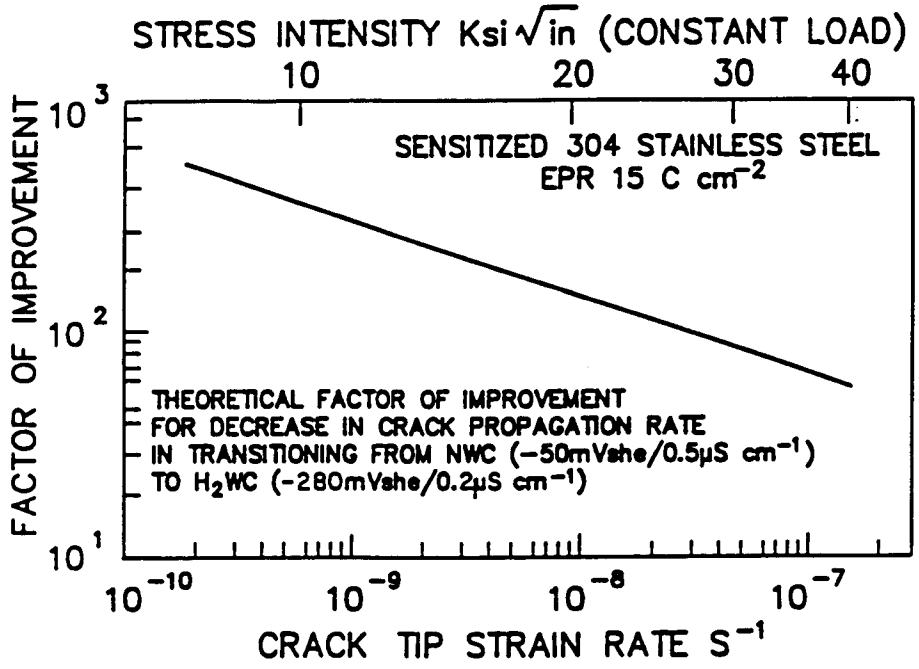

Figure 44. Factor of improvement (ratio of crack growth rates in NWC to HWC) for sensitized type 304 stainless steel as a function of the stress intensity and corresponding crack tip strain rate [1-3].

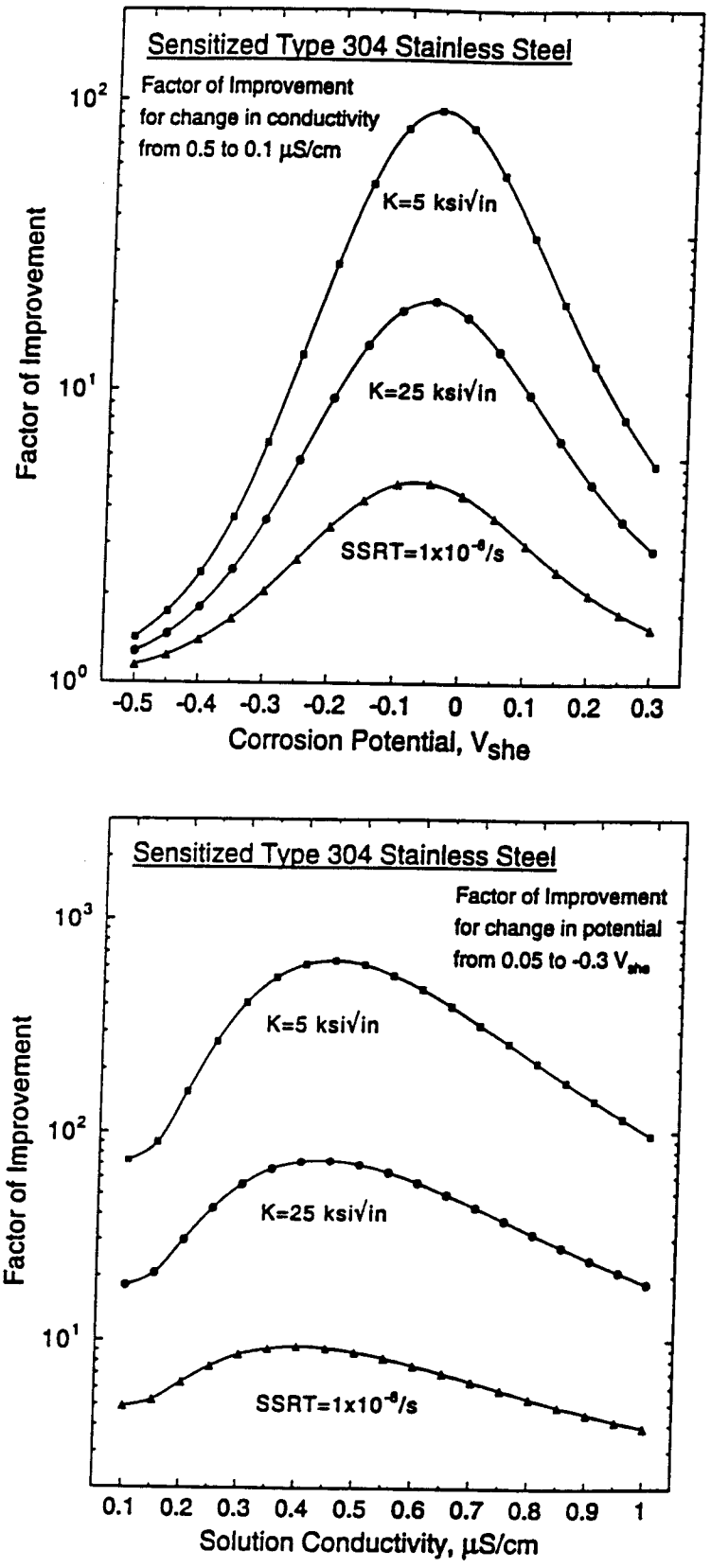

Figure 45. Factors of improvement associated with specific changes in (a) water purity or (b) corrosion potential for specific loading conditions.

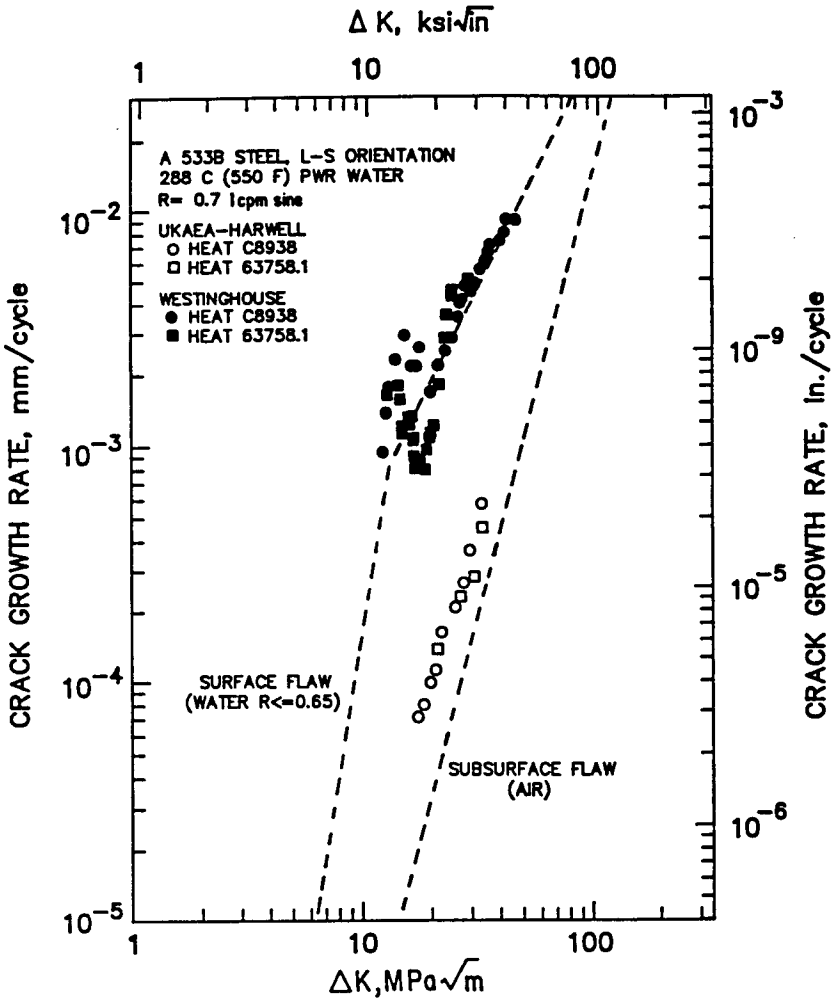

Figure 46. The effect of solution flow rate on the crack growth rate of a CT specimen of a medium sulfur low alloy steel tested in deaerated, 288°C water [32]. High flow rate causes "flushing out" of the crack tip sulfur content resulting from dissolution of MnS in the crack.

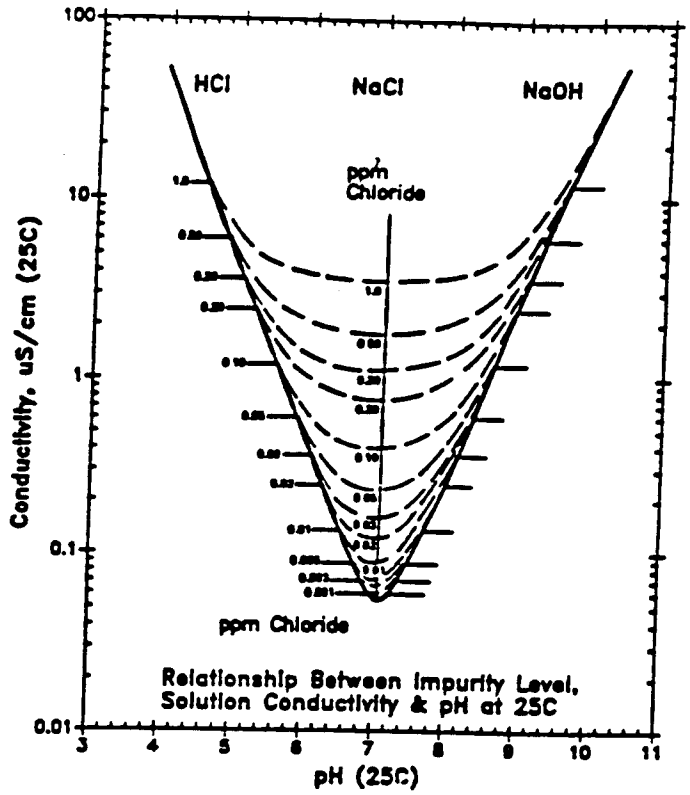

Figure 47. Relationships between ppm impurity addition, room temperature pH, and solution conductivity.

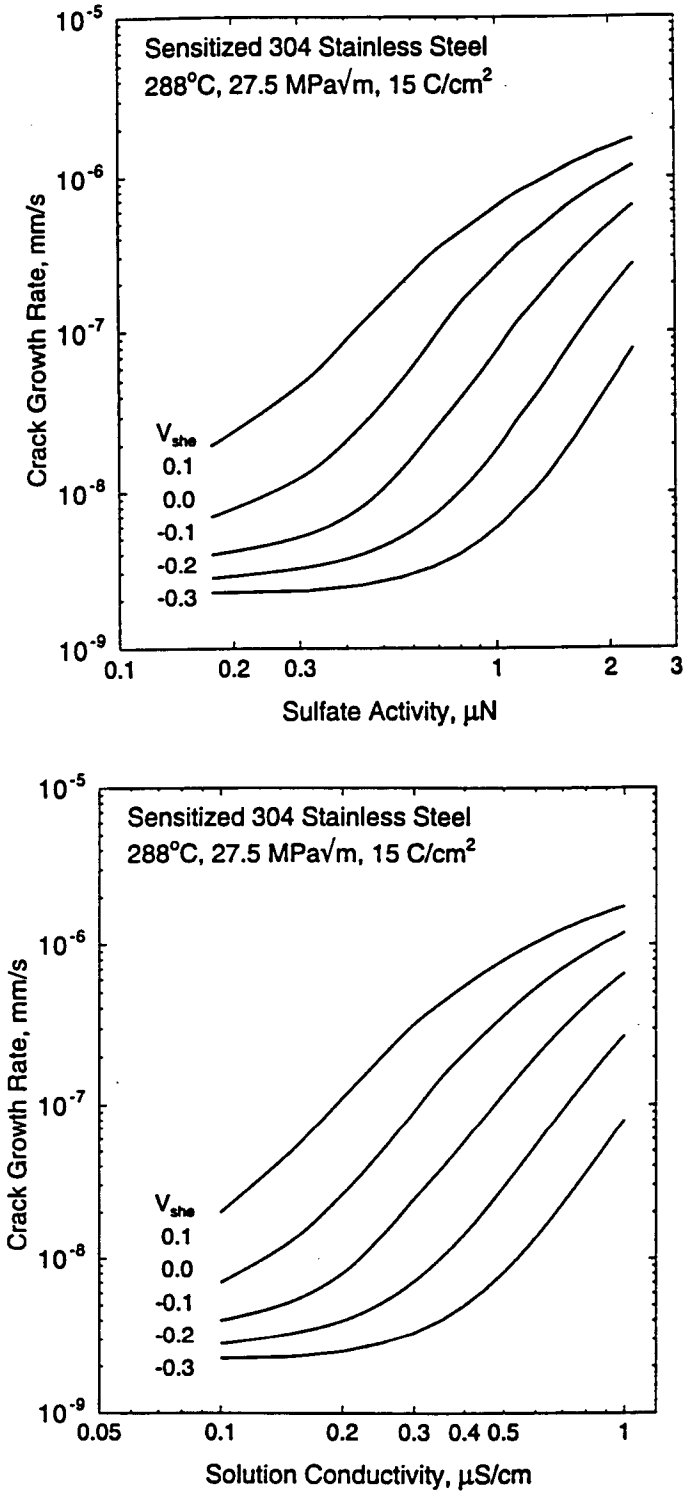

Figure 48. The approximate response of sensitized type 304 stainless steel to impurities in 288°C water based on crack growth rate predictions. This provide some guidelines for the interplay between corrosion potential and impurity level, and show the continuum in crack growth response.